Galileo dust data from the jovian system: 2000 to 2003

H. Krüger[a,b,1], D. Bindschadler[c], S. F. Dermott[d], A. L. Graps[e], E. Grün[b,f], B. A. Gustafson[d], D. P. Hamilton[g], M. S. Hanner[h], M. Horányi[f], J. Kissel[a], D. Linkert[b], G. Linkert[b], I. Mann[i], J. A. M. McDonnell[j], R. Moissl[a], G. E. Morfill[k], C. Polanskey[c], M. Roy[c], G. Schwehm[l] and R. Srama[b,m]

a) Max-Planck-Institut für Sonnensystemforschung, 37191 Katlenburg-Lindau, Germany
b) Max-Planck-Institut für Kernphysik, 69029 Heidelberg, Germany
c) Jet Propulsion Laboratory, Pasadena, California 91109, USA
d) University of Florida, 211 SSRB, Campus, Gainesville, FL 32609, USA
e) Department of Space Studies, Southwest Research Institute, 1050 Walnut Street, Suite 300, Boulder, Colorado, 80302, USA
f) Laboratory for Atmospheric and Space Physics, Univ. of Colorado, Boulder, CO 80309, USA
g) University of Maryland, College Park, MD 20742-2421, USA
h) Astronomy Dept. 619 LGRT, University of Massachusetts, Amherst MA 01003, USA
i) School of Science and Engineering, Kindai University, Kowakae 3-4-1, Higashi-Osaka, Osaka, 577-8502, Japan
j) Planetary and Space Science Research Institute, The Open University, Milton Keynes, MK7 6AA, UK
k) Max-Planck-Institut für Extraterrestrische Physik, 85748 Garching, Germany
l) ESAC, PO Box 78, 28691 Villanueva de la Cañada, Spain
m) Universität Stuttgart, Institut für Raumfahrtsysteme, Pfaffenwaldring 31, 70569 Stuttgart, Germany

[1] *Correspondence to:* Harald Krüger, krueger@mps.mpg.de

Abstract

The Galileo spacecraft was the first man-made satellite of Jupiter, orbiting the planet between December 1995 and September 2003. The spacecraft was equipped with a highly sensitive dust detector that monitored the jovian dust environment between approximately 2 and 370 R_J (jovian radius $R_J = 71492\,km$). The Galileo dust detector was a twin of the one flying on board the Ulysses spacecraft. This is the tenth in a series of papers dedicated to presenting Galileo and Ulysses dust data. Here we present data from the Galileo dust instrument for the period January 2000 to September 2003 until Galileo was destroyed in a planned impact with Jupiter. The previous Galileo dust data set contains data of 2883 particles detected during Galileo's interplanetary cruise and 12978 particles detected in the jovian system between 1996 and 1999. In this paper we report on the data of additional 5389 particles measured between 2000 and the end of the mission in 2003. The majority of the 21250 particles for which the full set of measured impact parameters (impact time, impact direction, charge rise times, charge amplitudes, etc.) was transmitted to Earth were tiny grains (about 10 nm in radius), most of them originating from Jupiter's innermost Galilean moon Io. They were detected throughout the jovian system and the impact rates frequently exceeded $10\,min^{-1}$. Surprisingly large impact rates up to $100\,min^{-1}$ occurred in August/September 2000 when Galileo was far away ($\approx 280\,R_J$) from Jupiter, implying dust ejection rates in excess of $100\,kg\,s^{-1}$. This peak in dust emission appears to coincide with strong changes in the release of neutral gas from the Io torus. Strong variability in the Io dust flux was measured on timescales of days to weeks, indicating large variations in the dust release from Io or the Io torus or both on such short timescales. Galileo has detected a large number of bigger micron-sized particles mostly in the region between the Galilean moons. A surprisingly large number of such bigger grains was measured in March 2003 within a 4-day interval when Galileo was outside Jupiter's magnetosphere at approximately $350\,R_J$ jovicentric distance. Two passages of Jupiter's gossamer rings in 2002 and 2003 provided the first actual comparison of in-situ dust data from a planetary ring with the results inferred from inverting optical images. Strong electronics degradation of the dust instrument due to the harsh radiation environment of Jupiter led to increased calibration uncertainties of the dust data.

1 Introduction

The Galileo spacecraft was the first artifical satellite orbiting Jupiter. Galileo had a highly sensitive impact ionization dust detector on board which was identical with the dust detector of the Ulysses spacecraft (Grün et al., 1992a,b, 1995c). Dust data from both spacecraft were used for the analysis of e. g. the interplanetary dust complex, dust related to asteroids and comets, interstellar dust grains sweeping through the solar system, and various dust phenomena in the environment of Jupiter. References can be found in Krüger et al. (1999a,c).

In Section 1.1 we summarize results that are related to dust in the Jupiter system. A comprehensive overview of the investigation of dust in the jovian system was given by Krüger (2003) and Krüger et al. (2004).

1.1 Summary of results from the Galileo dust investigations at Jupiter

The Jupiter system was found to be a strong source of dust when in 1992 Ulysses flew by the planet and discovered streams of dust particles emanating from the giant planet's magnetosphere (Grün et al., 1993). These were later confirmed by Galileo (Grün et al., 1996a,b) and measured again by Ulysses in 2003-05 during its second flyby at the planet (Krüger et al., 2006c; Flandes and Krüger, 2007; Flandes et al., 2009). At least four dust populations were identified in the Jupiter system with Galileo (Grün et al., 1997a, 1998):

i) Streams of dust particles with high and variable impact rates throughout Jupiter's magnetosphere. They are the extension of streams discovered with Ulysses outside Jupiter's magnetosphere. The particles are about 10 nm in radius (Zook et al., 1996) and they mostly originate from the innermost Galilean moon Io (Graps et al., 2000). Because of their small sizes the charged grains strongly interact with Jupiter's magnetosphere (Horányi et al., 1997; Grün et al., 1998; Heck, 1998), and they are a natural laboratory to study dust-plasma interactions. The dust streams mostly show a dust-in-plasma behavior while only some portions of those Galileo orbits displaying the highest dust stream fluxes (Galileo orbits E4, G7, G8, C21) satisfy the minimum requirements for a dusty plasma (Graps, 2006). The dust streams served as a monitor of Io's volcanic plume activity (Krüger et al., 2003a) and as probes of the Io plasma torus (Krüger et al., 2003b). Dust charging mechanisms in Io's plumes and in the jovian magnetosphere were investigated by Graps (2001) and Flandes (2005). Dust measurements of the Cassini spacecraft at its Jupiter flyby in 2000 showed that the grains are mostly composed of sodium chloride (NaCl) formed by condensation in Io's volcanic plumes (Postberg et al., 2006).

ii) Dust clouds surrounding the Galilean moons which consist of mostly sub-micron grains (Krüger et al., 1999d, 2000, 2003c). These grains were ejected from the moons' surfaces by hypervelocity impacts of interplanetary dust particles (Krivov et al., 2003; Sremčević et al., 2003, 2005).

iii) Bigger micron-sized grains forming a tenuous dust ring between the Galilean moons. This group is composed of two sub-populations, one orbiting Jupiter on prograde orbits and a second one on retrograde orbits (Colwell et al., 1998; Thiessenhusen et al., 2000). Most of the prograde population is maintained by grains escaping from the clouds that surround the Galilean moons (Krivov et al., 2002a,b).

iv) On 5 November 2002 and 21 September 2003 – before Galileo was destroyed in a planned impact with Jupiter – the spacecraft traversed Jupiter's gossamer ring twice and provided the first in-situ measurements of a dusty planetary ring (Krüger, 2003; Moissl, 2005; Hamilton and Krüger, 2008; Krüger et al., 2009) which is also accessible with astronomical imaging techniques. These fly-throughs revealed previously unknown structures in the gossamer rings: a drop in the dust density between the moons Amalthea and Thebe, grains orbiting Jupiter on highly inclined orbits and an increase in the number of small grains in the inner regions of the rings as compared to the regions further away from the planet. All these features can nicely be explained by electromagnetic forces on the grains that shape the gossamer rings (Hamilton and Krüger, 2008).

1.2 The Galileo and Ulysses dust data papers

This is the tenth paper in a series dedicated to presenting both raw and reduced data from the Galileo and Ulysses dust instruments. Grün et al. (1995c, hereafter Paper I) described the reduction process of Galileo and Ulysses dust data. In the even-numbered Papers II, IV, VI and VIII (Grün et al., 1995a; Krüger et al., 1999a, 2001a, 2006b) we presented the Galileo data set spanning the ten year time period from October 1989 to December 1999. The present paper extends the Galileo data set from January 2000 to September 2003, which covers the Galileo Millenium mission and two traverses of Jupiter's gossamer ring until the spacecraft impacted Jupiter on 21 September 2003. Companion odd-numbered Papers III, V, VII, IX and XI (Grün et al., 1995b; Krüger et al., 1999c, 2001b, 2006a, 2010) provide the entire dust data set measured with Ulysses between 1990 and 2007. An overview of our Galileo dust data papers and mission highlights is given in Table 1.

Insert Table 1

The main data products are a table of the number of all impacts determined from the particle accumulators and a table of both raw and reduced data of all "big" impacts received on the ground. The information presented in these papers is similar to data which we are submitting to the various data archiving centres (Planetary Data System, NSSDC, etc.). The only difference is that the paper version does not contain the full data set of the large number of "small" particles, and the numbers of impacts deduced from the accumulators are typically averaged over several days. Electronic access to the complete data set including the numbers of impacts deduced from the accumulators in full time resolution is also possible via the world wide web: http://www.mpi-hd.mpg.de/dustgroup/.

This paper is organised similarly to our previous papers. Section 2 gives a brief overview of the Galileo mission with particular emphasis on the time period 2000-2003, the dust instrument operation and lists important mission events in the time interval 2000-2003 considered in this paper. A description of the new Galileo dust data set for 2000-2003 together with a discussion of the detected noise and dust impact rates is given in Section 3. Section 4 analyses and discusses various characteristics of the new data set. Finally, in Section 5 we discuss results on jovian dust achieved with this new data set, and in Section 6 we summarise our results.

2 Mission and instrument operations

2.1 Galileo mission

Galileo was launched on 18 October 1989. Two flybys at Earth and one at Venus between 1990 and 1992 gave the spacecraft enough energy to leave the inner solar system. During its interplanetary voyage Galileo had close encounters with the asteroids Gaspra and Ida. On 7 December 1995 the spacecraft arrived at Jupiter and was injected into a highly elliptical orbit about the planet, becoming the first spacecraft orbiting a planet of the outer solar system. Galileo performed 34 revolutions about Jupiter until 21 September 2003 when the spacecraft was destroyed in a planned impact with Jupiter.

Galileo's trajectory during its orbital tour about Jupiter from January 2000 to September 2003 is shown in Figure 1. Galileo had regular close flybys at Jupiter's Galilean moons. Eight such encounters occurred in the 2000-2003 interval (1 at Europa, 4 at Io, 2 at Ganymede, 1 at Callisto) plus one at Amalthea (Table 2). Galileo orbits are labelled with the first letter of the Galilean moon which was the encounter target during that orbit, followed by the orbit number. For example, "G29" refers to a Ganymede flyby in orbit 29. Satellite flybys always occurred within two days of Jupiter closest approach (pericentre passage). Detailed descriptions of the Galileo mission and the spacecraft were given by Johnson et al. (1992) and D'Amario et al. (1992).

Insert Table 2

Insert Figure 1

Galileo was a dual spinning spacecraft with an antenna that pointed antiparallel to the positive spin axis. During most of the initial 3 years of the mission the antenna pointed towards the Sun (Paper II). Since 1993 the antenna was usually pointed towards Earth. Deviations from the Earth pointing direction in 2000-2003, the time period considered in this paper, are shown in Figure 2. Sharp spikes in the pointing deviation occurred when the spacecraft was turned away from the nominal Earth direction for dedicated imaging observations with Galileo's cameras or for orbit trim maneuvers with the spacecraft thrusters. These spikes lasted typically several hours. From January to September 2003, the Galileo pointing deviated significantly from the Earth pointing direction for a long time interval. Table 2 lists significant mission and dust instrument events for 2000-2003. Comprehensive lists of earlier events can be found in Papers II, IV, VI and VIII.

Insert Figure 2

2.2 Dust detection geometry

The Dust Detector System (DDS) was mounted on the spinning section of Galileo and the sensor axis was offset by 60° from the positive spin axis (an angle of 55° was erroneously stated in publications before). A schematic view of the Galileo spacecraft and the geometry of dust detection is shown in the inset in Figure 1.

The rotation angle measured the viewing direction of the dust sensor at the time of a dust impact. During one spin revolution of the spacecraft the rotation angle scanned through a complete circle of 360°. At rotation angles of 90° and 270° the sensor axis lay nearly in the ecliptic plane, and at 0° it was close to the ecliptic north direction. DDS rotation angles are taken positive around the negative spin axis of the spacecraft which pointed towards Earth. This is done to facilitate comparison of the Galileo spin angle data with those taken by Ulysses, which, unlike Galileo, had its positive spin axis pointed towards Earth (Grün et al., 1995c).

The nominal field-of-view (FOV) of the DDS sensor target was 140°. A smaller FOV applies to a subset of jovian dust stream particle impacts – the so-called class 3 impacts in amplitude range AR1 (Krüger et al., 1999b, *cf.* Paper I and Section 3 for a definition of these parameters) while the nominal target size should be applied to class 2 jovian dust stream impacts. For all impacts which are not due to jovian dust stream particles a larger FOV of 180° should be applied because the inner sensor side wall turned out to be almost as sensitive to larger dust impacts as the target itself (Altobelli et al., 2004; Willis et al., 2004, 2005). These different sensor fields-of-view and the corresponding target sizes are summarised in Table 3.

Insert Table 3

During one spin revolution of the spacecraft the sensor axis scanned a cone with 120° opening angle towards the anti-Earth direction. Dust particles that arrived from within 10° of the positive spin axis (anti-Earth direction) could be detected at all rotation angles, whereas those that arrived at angles from 10° to 130° from the positive spin axis could be detected over only a limited range of rotation angles. Note that these angles refer to the nominal sensor field-of-view of 140°.

2.3 Data transmission

In June 1990 the dust instrument was reprogrammed for the first time after launch and since then the instrument memory could store 46 instrument data frames (with each frame comprising the complete data set of an impact or noise event, consisting of 128 bits, plus ancillary and engineering data; *cf.* Papers I and II). The dust instrument time-tagged each impact event with an 8 bit word allowing for the identification of 256 unique steps. In 1990 the step size of this time word was set to 4.3 hours. Hence, the total accumulation time after which the time word was reset and the time labels of older impact events became ambiguous was $256 \times 4.3\,\mathrm{h} \simeq 46\,\mathrm{days}$.

During a large fraction of Galileo's orbital mission about Jupiter dust detector data were transmitted to Earth in the so-called realtime science mode (RTS). In RTS mode, dust data were read out either every 7.1 or every 21.2 minutes – depending on the spacecraft data transmission rate – and directly transmitted to Earth with a rate of 3.4 or 1.1 bits per second, respectively. Additionally, Galileo had the so-called record mode. In this mode data were read out from the dust instrument memory with 24 bits per second, recorded on Galileo's tape recorder and transmitted to Earth up to several weeks later. Recorded data were received during three satellite flybys in 2000 during short periods of $\sim \pm 1/2$ hour around closest approach to the satellite, and for ~ 3.8 hours during Galileo's gossamer ring passage on 5 November 2002 (Table 2). Details of the various data transmission modes of Galileo are also given in Table 4.

Insert Table 4

In RTS and record mode the time between two readouts of the instrument memory determined the number of events in a given time period for which their complete information could be transmitted. Thus, the complete information on each impact was transmitted to Earth when the impact rate was below one impact per either 7.1 or 21.2 minutes in RTS mode or one impact per minute in record mode, respectively (Table 4). If the impact rate exceeded these values, the detailed information of older events was lost because the full data set of only the latest event was stored in the dust instrument memory.

Furthermore, in RTS and record mode the time between two readouts also defined the accuracy with which the impact time is known. Hence, the uncertainty in the impact time is 7.1 or 21.2 minutes in RTS mode and about one minute in record mode, respectively.

In RTS and record mode only seven instrument data frames were read out at a time and transmitted to Earth rather than the complete instrument memory. Six of the frames contained the information of the six most recent events in each amplitude range. The seventh frame belonged to an older event read out from the instrument memory (FN=7) and was transmitted in addition to the six new events. The position in the instrument memory from which this seventh frame was read changed for each readout so that after 40 readouts the complete instrument memory was transmitted (note that the contents of the memory may have changed significantly during the time period of 40 readouts if high event rates occurred).

RTS data were usually obtained when Galileo was in the inner jovian system where relatively high dust impact rates occurred. During time intervals when Galileo was in the outer jovian magnetosphere dust data were usually received as instrument memory-readouts (MROs). MROs returned event data which had accumulated in the instrument memory over time. The contents of all 46 instrument data frames of the dust instrument was read out during an MRO and transmitted to Earth. If too many events occurred between two MROs, the data sets of the oldest events became overwritten in the memory and were lost. Although the entire memory was read out during an MRO, the number of data sets of new events that could be transmitted to Earth in a given time period was much smaller than with RTS data because MROs occurred much less frequently (Table 4). During times when only MROs occurred, the accuracy of the impact time was defined by the increment of the instrument's internal clock, i.e. 4.3 hours.

In 2000-2003, RTS and record data were obtained during a period of 570 days (Figure 1) which amounts to about 40% of the total almost 4-year period. During the remaining times when the dust instrument was operated in neither RTS nor record mode, a total of 59 MROs occurred at approximately 2 to 3 week intervals. Until the end of 2002, MROs were frequent enough so that usually no ambiguities in the time-tagging occurred (i.e. MROs occurred at intervals smaller than 46 days).

The last MRO for the entire Galileo mission occurred at the end of 2002 on day 02-363. In 2003 we received dust data neither as MROs nor as record data. Only RTS data were received during rather short time intervals: about one week from 03-063 to 03-070 and a total of about two days between 03-255 and 03-264 before the spacecraft hit Jupiter (Table 2). No dust data were obtained outside these intervals in 2003.

Several resets of the dust instrument's internal clock occurred during the long periods without data transmission in 2003, leading to ambiguities in the impact time of some dust impacts. One clock reset occurred during the first data gap between 02-363 and 03-063 and four resets in the second gap between 03-070 and 03-255. Furthermore, due to data transmission problems, the time tagging was lost for the events transmitted in the interval 03-063 to 03-070. Consequently, the impact time of two events which occurred between 02-363 and 03-063 is completely unknown. We have therefore set their impact time to 03-030 (these grains are indicated by horizontal bars in Figure 9). For seven data sets transmitted between 03-063 and 03-070 the impact time could be determined with an accuracy of approximately one day from the time tagging of test pulses that were routinely performed by the dust instrument (see also Section 5.4).

2.4 Dust instrument operation

During Galileo's earlier orbital mission about Jupiter strong channeltron noise was usually recorded while Galileo was within about $20 R_J$ distance from Jupiter (Jupiter radius, $R_J = 71,492\,\mathrm{km}$). The details are described in Papers VI and VIII and not repeated here. Furthermore, due to degradation of the channeltron, the high voltage setting (HV) had to be raised two times in 1999 (Paper VIII). At the beginning of the year 2000, i.e. at the beginning of the time period considered in this paper, the dust instrument was operated in the following nominal configuration: the channeltron high voltage was set to 1250 V (HV = 4), the event definition status was set such that only the ion-collector channel could initiate a measurement cycle (EVD = I) and the detection thresholds for the charges on the ion-collector, channeltron, electron-channel and entrance grid were set (SSEN = 0, 1, 1, 1).

This configuration effectively prevented dead time of the instrument due to channeltron noise (serious channeltron noise rates with CN > 10 occurred only during seven short time intervals in orbit A34 on day 02-309 when Galileo was inside Io's orbit and lasted only between several seconds and less than a minute. The resulting dead time is negligible because of its random occurrence and short duration). Due to degradation of the channeltron (Section 2.5) the channeltron high voltage was raised two additional times on days 00-309 and 01-352 in order to maintain a rather constant instrument sensitivity for dust impacts (Table 2).

During the Jupiter orbital tour of Galileo, orbit trim maneuvers (OTMs) were executed around perijove and apojove passages to target the spacecraft to close encounters with the Galilean moons. Many of these maneuvers required changes in the spacecraft attitude off the nominal Earth pointing direction (Figure 2). Additionally, dedicated spacecraft turns occurred typically in the inner jovian system within a few days around perijove passage to allow for imaging observations with Galileo's cameras or to maintain the nominal Earth pointing direction.

In the time interval considered in this paper a total of five spacecraft anomalies (safings) occurred on days 00-055, 02-017, 02-047, 02-274, and 02-309 (Table 2). Three of these anomalies occurred in the inner jovian system in the region where the highest radiation levels were collected by the spacecraft, and recovery usually took several days. Although the dust instrument continued to measure dust impacts, the collected data could not be transmitted to Earth during the recovery and most of them were lost.

No reprogramming of the instrument's onboard computer was necessary in the 2000-2003 time interval. In fact, the last reprogramming for the entire Galileo mission took place on 4 December 1996 when two overflow counters were added for the so-called AR1 impacts in classes 2 and 3 (Paper VI). With these overflow counters, all accumulator overflows could be recognized in these two channels in the 2000-2003 interval. It is very unlikely that unrecognized overflows occurred in the higher amplitude ranges. The only exception is day 02-309 when Galileo was in the gossamer ring region and the instrument continued to collect data after the spacecraft anomaly (see also Section 5.5). Here unrecognized overflows have likely occurred in amplitude range AR1, class 1 (channel AC11) and amplitude range AR2 (except channel AC32), while the higher amplitude ranges AR3 and AR4 were most likely free of overflows. See Section 3.1 for a description of the amplitude ranges and quality classes of dust impacts.

2.5 Dust instrument electronics degradation

Analysis of the impact charges and rise times measured by the dust instrument revealed strong degradation of the instrument electronics which was most likely caused by the harsh radiation environment in the inner jovian magnetosphere. A detailed analysis was published by Krüger et al. (2005). Here we recall the most significant results: a) the sensitivity of the instrument for dust impacts and noise had dropped. b) the amplification of the charge amplifiers had degraded, leading to reduced impact charge values Q_{I} and Q_{E}. c) drifts in the target and ion collector rise time signals lead to prolonged rise times t_I and t_E. d) degradation of the channeltron required increases in the channeltron high voltage (Table 2). In particular, a) requires a time-dependent correction when comparing dust fluxes early in the Galileo Jupiter mission with later measurements; b) and c) affect the mass and speed calibration of the dust instrument. After 2000, masses and speeds derived from the instrument calibration have to be taken with caution because the electronics degradation was very severe. Only in cases where impact speeds are known from other arguments can corrected masses of particles be derived (e.g. the dust cloud measurements in the vicinity of the Galilean moons or Galileo's gossamer ring passages). On the other hand, given the uncertainty in the impact calibration of a factor of two in the speed and that of a factor of ten in the mass, the increased uncertainty due to the electronics degradation was comparatively small before 2000 (it should be noted that the dust data until end 1999 published earlier – Papers II, IV, VI and VIII – remain unchanged). In particular, no corrections for dust fluxes, grain speeds and masses are necessary until end 1999 and results obtained with this data set in earlier publications remain valid. Beginning in 2000, however, the degradation became so severe that the calibrated speeds and masses have to be considered as lower and upper limits, respectively (see also Section 3.3).

3 Impact events

3.1 Event classification and noise

The dust instrument classified all events – real dust impacts and noise events – into one of 24 different categories (6 amplitude ranges for the charge measured on the ion collector grid and 4 event classes) and counted them in 24 corresponding 8 bit accumulators (Paper I). In interplanetary space most of the 24 categories were relatively free from noise and only sensitive to real dust impacts. The details of the noise behaviour in interplanetary space can be found in Papers II and IV.

In the extreme radiation environment of the jovian system, a different noise response of the instrument was recognized: especially within about 20 R_J from Jupiter class 1 and class 2 were contaminated with noise while class 3 was almost always noise-free (Krüger et al., 1999b). Analysis of the dust data set from Galileo's entire Jupiter mission showed that noise events could reliably be eliminated from class 2 (Krüger et al., 2005) while most class 1 events detected in the jovian environment showed signatures of being noise events. For most of Galileo's Jupiter mission we therefore consider the class 3 and the noise-removed class 2 impacts as the complete set of dust data. Apart from a missing third charge signal – class 3 has three charge signals and class 2 only two – there is no physical difference between dust impacts categorized into class 2 or class 3. In particular, we usually classify all class 1 and class 0 events detected in the jovian environment as noise.

The only exceptions are the passages through Jupiter's gossamer rings in 2002 and 2003 where a somewhat different noise response of the instrument was recognized (Moissl, 2005). Here, good dust impacts could also be identified in class 1. In Table 5 we show the noise identification scheme applied to the data from the gossamer ring passages obtained while Galileo was within Io’s orbit.

Insert Table 5

To summarise, noise was removed from the data set we present here with two different criteria: data obtained outside Io’s orbit were processed according to the criteria derived by Krüger et al. (2005), while data obtained inside Io’s orbit were noise-removed with the criteria of Moissl (2005) (Table 5). Degradation of the instrument electronics was taken into account beginning in 1997 (Paper VIII). The derivation of the noise contamination factor $f_{\rm noi}$ for class 2 was described in Paper VI and is not repeated here.

In this paper the terms ”small“ and ”big“ have the same meaning as in Papers IV, VI and VIII (which is different from the terminology of Paper II). Here, we call all particles in the amplitude ranges 2 and higher (AR2-6) ”big“. Particles in the lowest amplitude range (AR1) are called ”small“. This distinction separates the small jovian dust stream particles from bigger grains which are mostly detected between the Galilean moons (see also Section 3.2).

Table 6 lists the number of all dust impacts and noise events identified with the dust instrument in the 2000-2003 interval as deduced from the accumulators of classes 2 and 3. Depending on the event rate the numbers are given in intervals from half a day to a few weeks (the numbers with the highest time resolution are available in electronic form only and are provided to the data archiving centres). For impacts in these two classes in the lowest amplitude range AR1 the complete data sets for only 2% of all detected events were transmitted, the remaining 98% of events were only counted. About 32% of all data sets for events in the higher amplitude ranges were transmitted. We give only the number of events in classes 2 and 3 because they have been shown to contain real dust impacts during the entire Jupiter mission: class 3 is almost always noise free (although Krüger et al. (1999b) found indications for a very small number of noise events in class 3, AR1, in the inner jovian system). Class 2 is strongly contaminated by noise events in the inner jovian system (within about $15\,\mathrm{R_J}$ from Jupiter).

Insert Table 6

In the 2000-2003 interval Galileo had a total of eight targeted flybys at the Galilean moons plus one at Amalthea (Table 2). During the flybys at the Galilean moons no ejecta particles from the moons could be detected because of unfavourable detection geometry. During the Amalthea flyby in A34, however, the dust instrument had the right detection geometry. Taking the recently determined mass of Amalthea (Anderson et al., 2005), its Hill radius is $r_{\rm Hill} \sim 130\,\mathrm{km}$, only slightly larger than the moon itself. Galileo’s closest approach distance was 244 km from the moon’s centre so that the spacecraft did not cross the Hill sphere where an increased dust density was expected. In fact, no increase in the dust impact rate could be identified, consistent with our expectations (Krüger et al., 2009).

3.2 Dust impact rates

Figure 3 shows the dust impact rate recorded by the dust instrument in 2000-2003 as deduced from the class 2 and 3 accumulators. The impact rate measured in the lowest amplitude range (AR1) and the one measured in the higher amplitude ranges (AR2-6) are shown separately because they reflect two distinct populations of dust. Until early 2002 AR1 contains mostly stream particles which were measured throughout the jovian system. Bigger particles (AR2-6) were mostly detected in the region between the Galilean moons.

Between the perijove passages I33 and A34 in 2002 a low background rate of a few times $10^{-4}\,\mathrm{min}^{-1}$ was measured in AR1 which is at least an order of magnitude higher than dust impact rates measured with Galileo and Ulysses in interplanetary space (Grün et al., 1997b). These impacts show a broad distribution over all rotation angles (Figure 9) while stream particles were expected to approach from rotation angles around 90° most of the time in 2002, similar to the earlier Galileo orbits in 2000 and 2001. These grains could be stream particles approaching from a much broader range of directions as was reported from the dust measurements with Cassini during Jupiter flyby (Sascha Kempf, personal communication).

During the gossamer ring passages impacts were measured in all amplitude ranges AR1-4 (Section 5.5). Note that the impact rate in AR1 was usually at least one to two orders of magnitude higher than that for the big particles. Diagrams showing the AR1 impact rate with a much higher time resolution in the inner jovian system are given in Figure 4, and Galileo's gossamer ring passages are discussed in detail by Krüger et al. (2009).

Insert Figure 3

Insert Figure 4

In the inner jovian system the impact rates of AR1 particles frequently exceeded $10\,\mathrm{min}^{-1}$. An exceptionally large dust impact rate was recorded during the orbit G28 in the outer jovian system when Galileo was approximately $280\,\mathrm{R_J}$ away from Jupiter (Section 5.2 and Figure 12). This represents one of the highest dust ejection rates of Io recorded during the entire Galileo Jupiter mission and is likely connected with a single strong volcanic eruption on Io (Krüger et al., 2003a; Geissler et al., 2004).

3.3 Event tables

Table 7 lists the data sets for all 224 big particles detected between 1 January 2000 and 21 September 2003 for which the complete information exists. Class 1 and class 2 particles were separated from noise by applying the criteria developed by Krüger et al. (1999b, 2005) and Moissl (2005) (Section 3.1). We do not list the small stream particles (AR1) in Table 7 because their masses and velocities are outside the calibrated range of the dust instrument and they are by far too numerous to be listed here. The complete information of a total of 5165 small (AR1) dust particles was transmitted in 2000-2003. These are mostly stream particles which are believed to be about 10 nm in size and their velocities exceed $200\,\mathrm{km\,s^{-1}}$ (Zook et al., 1996). Any masses and velocities derived for these particles with existing calibration algorithms would be unreliable. The full data set for all 5389 particles is submitted to the data archiving centres and is available in electronic form. A total number of 7566 events (dust plus noise in all amplitude ranges and classes) were transmitted in 2000-2003, each with a complete data set.

Insert Table 7

In Table 7 dust particles are identified by their sequence number and their impact time. Gaps in the sequence number are due to the omission of the small particles. The time error value (TEV) which was introduced for the data set from the Jupiter mission because of the large differences in the timing accuracy of the dust instrumnet in the various data readout modes is listed next (see Table 4 and Paper VI for details). Then the event category – class (CLN) and amplitude range (AR) – are given. Raw data as transmitted to Earth are displayed in the next columns: sector value (SEC) which is the spacecraft spin orientation at the time of impact, impact charge numbers (IA, EA, CA) and rise times (IT, ET), time difference and coincidence of electron and ion signals (EIT, EIC), coincidence of ion and channeltron signal (IIC), charge reading at the entrance grid (PA) and time (PET) between this signal and the impact. Then the instrument configuration is given: event definition (EVD), charge sensing thresholds (ICP, ECP, CCP, PCP) and channeltron high voltage step (HV). See Paper I for further explanation of the instrument parameters, except TEV which was introduced in Paper VI.

The next four columns in Table 7 give information about Galileo's orbit: ecliptic longitude and latitude (LON, LAT) and distance from Jupiter (D_{Jup}, in R_J). The next column gives the rotation angle (ROT) as described in Section 2. Whenever this value is unknown, ROT is arbitrarily set to 999. This occurs 71 times in the full data set that includes the small particles. Then follows the pointing direction of the instrument at the time of particle impact in ecliptic longitude and latitude (S_{LON}, S_{LAT}). When ROT is not valid, S_{LON} and S_{LAT} are also useless and set to 999. Mean impact velocity (v) and velocity error factor (VEF, i.e. multiply or divide stated velocity by VEF to obtain upper or lower limits) as well as mean particle mass (m) and mass error factor (MEF) are given in the last columns. For VEF > 6, both velocity and mass estimates are invalid and should be discarded.

Beginning in 2000 the degradation of the dust instrument electronics became very severe, leading to artificially too long rise times and reduced charge amplitudes. The calibrated mass and speed values for VEF < 6 listed in Table 7 should thus be considered as lower limits for the impact velocity and upper limits for the particle mass throughout the 2000-2003 interval.

No intrinsic dust charge values are given (Svestka et al., 1996). Even though the charge carried by the dust grains is expected to be larger in the jovian magnetosphere than in interplanetary space the charge measured on the entrance grid of the dust instrument did not give any convincing results yet. Reliable charge measurements for interplanetary dust grains and for dust in Saturn's E ring were recently reported for the Cassini dust detector (Kempf et al., 2004, 2006). These measurements may lead to an improved unterstanding of the charge measurements of Ulysses and Galileo in the future.

Entries for the parameter PA in Table 7 sometimes have values between 49 and 63 although the highest possible value allowed by the instrument electronics is 48 (Paper I). This is also inherent in all Galileo and Ulysses data sets published earlier (Papers II to IX) and it is due to a bit flip. According to our present understanding the correct PA values are obtained by subtracting 32 from all entries which have values between 49 and 63. Values of 48 and lower should remain unchanged.

4 Analysis

The positive charge measured on the ion collector, Q_{I}, is the most important impact parameter determined by the dust instrument because it is rather insensitive to noise. Figure 5 shows the distribution of Q_{I} for the full 2000-2003 data set (small and big particles together). Ion impact charges were only detected over four orders of magnitude instead of the entire range of six orders of magnitude the instrument could measure. Note that the saturation limit of the instrument was at about $\sim 10^{-8}$ C but the maximum measured charge was $Q_{\mathrm{I}} = 9.7 \times 10^{-11}$ C, well below the saturation limit. This is most likely due to instrument degradation (Section 2.5 and Krüger et al., 2005).

The impact charge distribution of the big particles ($Q_{\mathrm{I}} > 10^{-13}$ C) follows a power law with index -0.15 and is shown as a dashed line in Figure 5 (if we exclude the particles from the region inside Io's orbit the slope is reduced somewhat to -0.04). This slope is flatter than the values of approximately $-1/3$ derived for the jovian system from the 1996-1999 Galileo data set (Papers VI and VIII). Whether this flattening is due to changes in the particle properties or due to electronics degradation remains unclear. Note that the jovian stream particles (AR1) were excluded from the power law fit.

Insert Figure 5

In Figure 5 the small stream particles ($Q_{\mathrm{I}} < 10^{-13}$ C) are squeezed into the two leftmost histogram bins. In order to investigate their behaviour in more detail we show their number per individual digital step separately in Figure 6. The distribution flattens for impact charges below 2×10^{-14} C. Such a flattening was also evident in the earlier data sets (Papers II, IV, VI and VIII), indicating the sensitivity threshold of the dust instrument may not be sharp. The impact charge distribution for small particles with $Q_{\mathrm{I}} > 2 \times 10^{-14}$ C follows a power law with index -4.7. It is very close to the slope found from the 1996 Galileo data set (-4.5, Paper VI) and somewhat steeper than the value measured in 1997-1999 (-3.6, Paper VIII). The charge distibution strongly increases towards smaller impact charges. Note that the distribution of the stream particles is much steeper than that of the big particles shown in Figure 5. Interestingly, if we restrict the time interval to the period between 00-220 and 00-250 when Galileo was outside the jovian magnetosphere in orbit G28 the stream particles show a somewhat steeper slope of -5.9 (not shown here).

Insert Figure 6

The ratio of the channeltron charge Q_{C} and the ion collector charge Q_{I} is a measure of the channeltron amplification A which is an important parameter for dust impact identification (Paper I). The in-flight channeltron amplification was monitored in Papers II, IV, VI and VIII for the initial ten years of the Galileo mission to identify possible degrading of the channeltron. In the earlier mission the amplification $A = Q_{\mathrm{C}}/Q_{\mathrm{I}}$ for a channeltron high voltage setting of 1020 V (HV = 2) determined from impacts with $10^{-12}\,\mathrm{C} \leq Q_{\mathrm{I}} \leq 10^{-10}\,\mathrm{C}$ was in the range $1.4 \lesssim A \lesssim 1.8$. No significant channeltron degradation was evident until the end of 1996. In the 1997-1999 interval (Paper VIII) a value of $A \simeq 0.7$ was found which indicated serious channeltron degradation. As a consequence, the channeltron high voltage was raised two times (on days 99-305 and 99-345) to return to the original amplification factor.

Here we repeat the same analysis for the 2000-2003 interval. Figure 7 shows the charge ratio $Q_{\mathrm{C}}/Q_{\mathrm{I}}$ as a function of Q_{I} for a constant high voltage, HV, as in the previous papers. Here we show data for HV = 6. The charge ratio $Q_{\mathrm{C}}/Q_{\mathrm{I}}$ determined for $10^{-12}\,\mathrm{C} \leq Q_{\mathrm{I}} \leq 10^{-10}\,\mathrm{C}$ is $A \simeq 1.6$ and is obtained from 65 impacts. The data for HV = 4 and HV = 5 (time intervals 00-001 to 00-209 and 00-209 to 01-352) give $A \simeq 1.3$ and $A \simeq 0.5$, respectively. These values, however, are derived from only 9 and 15 impacts, respectively, and therefore have a much lower statistical significance. The amplification for HV = 6 is close to the value from the interplanetary cruise and the early Jupiter mission, showing that the original channeltron amplification could be roughly reestablished. Details of the dust instrument degradation due to the harsh radiation environment in the jovian magnetosphere are described by Krüger et al. (2005, see also Section 2.5). It should be noted that the ratio $Q_{\mathrm{C}}/Q_{\mathrm{I}}$ is entirely determined by the instrument performance. It does not depend upon the properties of the detected particles.

Insert Figure 7

Figure 8 displays the calibrated masses and velocities of all 5389 dust grains detected in the 2000-2003 interval. Although the range of impact velocities calibrated in the laboratory extended from 2 to $70\,\mathrm{km\,s^{-1}}$, the measured impact speeds ranged only up to about $20\,\mathrm{km\,s^{-1}}$. This is caused by the degradation of the dust instrument electronics which lead to extended rise time measurements and, hence, impact velocities which are artificially too low, and calibrated grain masses artificially too large. This becomes apparent when comparing Figure 8 with the corresponding figures in the earlier Papers II, IV, VI and VIII where the measured range of impact speeds extends up to $70\,\mathrm{km\,s^{-1}}$. *Therefore, due to the* *strong electronics degradation, all calibrated impact speeds and masses in the time interval considered in this paper should be considered as lower and upper limits, respectively.* Any clustering of the velocity values is due to discrete steps in the rise time measurement but this quantization is much smaller than the velocity uncertainty. For further details of the mass and velocity calibration the reader is referred to the description of the mass-velocity diagrams in our earlier papers.

Insert Figure 8

The impact direction of the dust particles detected in the 2000-2003 interval is shown in Figures 9 and 10. On the inbound trajectory, when Galileo approached Jupiter, the dust stream particles (AR1) were mainly detected from rotation angles $270 \pm 70°$ while on the outbound trajectory the streams were detectable from $90 \pm 70°$. Before 2000 the detection geometry of the streams was such that the grains could only be detected during a very limited period of time around perijove passage (Paper VIII, Table 4 therein). This changed in 2000 when the streams became detectable from rotation angles $90 \pm 70°$ during almost the entire orbit of Galileo. This is best seen in orbits G28 to C30 in 2000 and 2001. Big particles were, as in the earlier periods, mostly detected in the inner jovian system when Galileo was close to Jupiter with the exception of several impacts recorded in March 2003 at about $350\,R_J$ from Jupiter (Section 5.4). Note that an error occurred in our earlier rotation angle plots in Paper VIII (Figure 9 in that paper). The corrected figure is shown in the Appendix.

Insert Figure 9

Insert Figure 10

5 Discussion

The dust data set from Galileo's entire Jupiter mission is a unique set of dust measurements from the jovian system for many years to come. Various jovian dust populations were investigated during the last 15 years which we have summarised in Section 1. The present paper finalises our series of Galileo dust data papers and we discuss some particular aspects of the 2000-2003 data set.

5.1 Variability of Io's dust emission

Imaging observations of Io with Voyager, Galileo, Cassini and New Horizons detected at least 17 volcanic centres with related plumes (Porco et al., 2003; McEwen et al., 2004; Spencer et al., 2007; Geissler and McMillan, 2008). Most of the plumes were sensed through the scattering of sunlight by dust particles entrained within the plumes, and ring-shaped surface deposits on Io suggest that other plumes have been recently active as well. The dust data from the entire Galileo Jupiter mission are a unique record of the dust ejected from Io. In particular, as the plumes are the most plausible sources of the grains (Graps et al., 2000), the dust measurements monitor plume activity (Krüger et al., 2003a).

The Galileo dust data show a large orbit-to-orbit variation due to both systematic and stochastic changes. Systematic effects include Io's orbital motion, changes in the geometry of Galileo's orbit and in the magnetic field configuration due to the rotation of Jupiter. Stochastic variations include fluctuations of Io's volcanic activity, changes of the particle charging in the Io torus, variations in grain release from the torus, and the deformation of the outer magnetosphere in response to the variable solar wind conditions. It should be emphasized that the mechanisms acting on the grains in the Io torus and in particular the connected temporal variability are presently not well understood. By combining the entire Galileo dust data set, the variability due to stochastic processes could be removed and a strong flux variation with jovian local time showed up (Krüger et al., 2003b), confirming earlier predictions (Horányi et al., 1997).

Dust emission rates of Io were derived by Krüger et al. (2003a). After removal of the systematic variations, the total dust emission rate of Io turned out to be between 10^{-3} and $10\,\mathrm{kg\,s^{-1}}$, with typical values in the range 0.1 to $1\,\mathrm{kg\,s^{-1}}$. Exceptionally high dust emission rates occurred during orbits E4 (1996), C21 (1999), G28, and, to a lesser extent, also during G29 and C30. Some of these peaks in the dust emission could be related to specific plume sightings or other markers of volcanic activity on Io: The Pele plume is one of the most powerful plumes and the most steady high-temperature volcanic centre on Io. Surface changes at the Pele site were detected frequently, whereas detections of the Pele plume are relatively rare. Two detections of the Pele plume are coincident with our measurements of high dust fluxes in E4 and G29, while a low dust flux in E6 may be explained by the absence of the Pele plume (McEwen et al., 1998; Porco et al., 2003). In August/September 2000 (orbit G28; Section 5.2) when Galileo was far away from Jupiter, a large dust flux was observed which is likely connected with surface changes observed at the site of the Tvashtar plume (Krüger et al., 2003a).

Here we investigate the orbit-to-orbit variability of the dust emission pattern on much shorter timescales of days to weeks. As in earlier works (Krüger et al., 2003a) we assume a particle radius $s = 10\,\mathrm{nm}$, grain density $\rho = 1.5\,\mathrm{g\,cm^{-3}}$, dust grain charging to +5V in the Io torus, and calculate the effective dust sensor area from the particle dynamics based on the model of Horányi et al. (1997). We divide the measured dust impact rate by the effective sensor area to obtain the dust flux f ($\mathrm{m^{-2}\,s^{-1}}$) as a function of distance d from Jupiter. If we assume that Io's dust emission, the dust charging, ejection conditions from the plasma torus and the grain speed remain constant over the time interval considered, we expect a "dilution" of the dust with d^{-2}. Dynamical modelling implies that – after the grains are released from the Io torus – the major acceleration occurs within approximately $10\,\mathrm{R_J}$ from Jupiter so that their speed remains basically unchanged further away from the planet. Finally, the variation of the dust flux with jovian local time is usually below a factor of five (Krüger et al., 2003b) and thus of minor significance here. With all these assumptions, we expect a variation of the dust flux with d^{-2}. It should be emphasized that here we use exactly the same assumptions for calculating dust emission rates as Krüger et al. (2003a).

Insert Figure 11

In Table 6 we list the slopes of power law fits $f \propto d^{\alpha}$ to the derived dust flux profiles. We only considered Galileo orbits where sufficiently long data sets for at least two days are available so that meaningful flux profiles could be obtained. Large variations in the flux profiles are obvious from Table 6. Given the overall uncertainties we believe that slopes in the range $-3 \lesssim \alpha \lesssim -1$ are still compatible with a rather constant dust ejection rate from Io and the Io torus ($\alpha = -2$). In Figure 11 we show the dust flux during the G29 orbit as an example. Here the power law fit to the data gives a slope $\alpha \approx -2$, indicating that the dust release from the Io torus stayed remarkably constant for a rather long period of more than two months.

Large deviations from this simple and ideal case with constant dust ejection are also obvious in the table. For example, orbits E4, E19, I32 and A34 show very flat profiles in the range $-1 \lesssim \alpha \lesssim 0$, implying that during these orbits stronger dust emissions occurred when Galileo was far away from Jupiter than when the spacecraft was closer to the planet. On the other hand, during orbits G2, G8, E14, E16, E18 and E26 Galileo experienced a stronger dust ejection when the spacecraft was in the inner jovian system (power law slopes $-4 \lesssim \alpha \lesssim -7$). Note that the time coverage of these data sets usually ranges from days to a few weeks, indicating that Io's plume activity or the dust charging and release from the Io torus, or both frequently changed on such rather short timescales.

Insert Table 6

Dust production rates of Io calculated with the method described above are also listed in Table 6. It should be emphasized that within less than a week the dust release frequently changed by approximately a factor of 10, and the absolute levels of the dust emission may have been vastly different from one Galileo orbit to the next. For a detailed discussion of the total dust ejection rates from Io and correlations with individual plume sightings the reader is referred to Krüger et al. (2003a) who showed that all intervals with elevated dust emission exceeding $\sim 1\,\mathrm{kg\,s^{-1}}$ (six intervals in total) can be connected with giant plume eruptions or large area surface changes on Io or both. See also Section 5.2.

5.2 Io's dust emission in August/September 2000

In summer 2000 (orbit G28) Galileo left the jovian magnetosphere for the first time since it was injected into the jovian system in 1995 and reached a jovicentric distance of $\sim 280\,\mathrm{R_J}$

(0.13 AU). In August/September 2000, around Galileo's apojove, the dust instrument measured a surprisingly large dust impact rate exceeding $10\,\mathrm{min}^{-1}$ for about two months (Figure 12). Similarly high fluxes were also recorded with the Cassini dust instrument at $\sim 0.3\,\mathrm{AU}$ from Jupiter when the spacecraft was approaching the planet in September 2000 (Sascha Kempf, personal communication). The dust emission from Io derived from the Galileo measurements by Krüger et al. (2003a) in this time period exceeds $\sim 100\,\mathrm{kg\,s}^{-1}$. Later, when Galileo approached Jupiter again, the dust flux profile showed a surprisingly steep drop (slope $\alpha \approx 10$), implying a huge decrease in Io's dust emission.

Insert Figure 12

Frequency analysis of the Galileo dust data from the first three years of the Galileo Jupiter mission (1996-1998) revealed strong 5 and 10 hour periodicities which were due to Jupiter's rotation (Graps et al., 2000). A weak "Io footprint" with approximately 42 hour frequency caused by this moon's orbital motion about Jupiter and harmonics with Jupiter's rotation frequencies were also revealed. These data were collected mostly in the inner jovian magnetosphere between 10 and $60\,\mathrm{R_J}$. In the data obtained during the later Galileo orbits in 1999 and 2000 the Io footprint became more prominent and was evident during most Galileo orbits from E19 to G29 (Graps, 2001).

In the data from a total of 26 Galileo orbits measured between 1996 and 2000, a total of 11 orbits showed a clear modulation with Io's frequency, 3 showed a weak Io modulation, while the remaining 12 orbits showed no Io signature at all (Graps, 2001). In many, but not all, cases the missing Io signature coincided with time periods when a rather weak dust flux was measured.

In the data set from August/September 2000, collected between days 00-220 and 00-250 at much larger jovicentric distances, Io's signature dominated all other frequency signatures including the 5 and 10 hour periods caused by Jupiter's rotation (Graps et al., 2001). These data provide direct evidence for Io being the source for the majority of the jovian dust stream particles during this time period. The presence of Io's orbital frequency implies that Io is a localised source of charged dust particles because charged dust from diffuse sources would couple to Jupiter's magnetic field and appear in frequency space with Jupiter's rotation frequency and its harmonics.

The period of strong dust emission seen in August/September 2000 coincided with enhanced neutral gas production from the Io torus, suggesting a coupling mechanism between gas and dust ejection, although the relation between the dust emissions and the production of neutral gas is not known (Delamere et al., 2004). Furthermore, there was a significant reduction in the neutral source beginning in October 2000, again coinciding with the strong drop in the dust emission as derived from our Galileo dust data.

5.3 Galileo-Cassini joint dust stream measurements

On 30 December 2000 the Cassini spacecraft flew by Jupiter, providing a unique opportunity for a two-spacecraft time-of-flight measurement (Cassini-Galileo) of particles from one collimated stream from the jovian dust streams. The goal was to detect particles in a stream first with Galileo when the spacecraft was inside the jovian magnetosphere close to the orbit of Europa (about $12\,R_J$), and particles in potentially the same stream later by Cassini outside the magnetosphere (at $140\,R_J$) (see Graps et al., 2001, for a preliminary analysis).

The Cassini data from the Jupiter flyby imply that particles of different sizes have different phases with respect to Jupiter's rotation (Sascha Kempf, personal communication), a result which is also seen in earlier Galileo data (Grün et al., 1998). Comparison of the measurements from both dust instruments, however, is hampered by the higher detection sensitivity of the Cassini detector with respect to the Galileo sensor. Both instruments have detected stream particles with different sizes and, hence likely different phases. The analysis is ongoing (Hsiang-Wen Hsu, personal communication), and more detailed modelling to describe the phase relation of different-sized particles taking into account the 3-dimensional structure of the dust emission pattern from the jovian system is necessary. Our present preliminary analysis indicates particle speeds of about $400\,\mathrm{km\,s^{-1}}$. This value is in agreement with speeds for 10 nm particles as derived from dynamical modelling (Hamilton and Burns, 1993; Horányi et al., 1993), and earlier studies of the jovian dust stream dynamics (Zook et al., 1996).

5.4 Large dust grains far from Jupiter

On 29 December 2002 (day 02-363) the last MRO of the dust instrument memory occurred for the remainder of the Galileo mission. The next time we received dust data was during the time interval 4 to 11 March 2003 (days 03-063 to 03-070). These data were obtained as RTS data. We identified a total number of nine large dust impacts in amplitude ranges AR2-4 which occurred between 29 December 2002 and 11 March 2003. Due to corruption of the readings from the instrument's internal clock and one clock reset in this time interval, two of these impacts have an exceptionally large uncertainty in the impact time of 66 days. We could reconstruct the impact time of the remaining seven impacts with a higher accuracy from accumulator readings obtained with test pulses which were routinely performed by the dust instrument (see Krüger et al., 2005, for more details). This gave impact times for five impacts with about one day uncertainty and for two impacts with 4.3 hour uncertainty (Table 7).

The reconstruction of these partially corrupted data implies that at least seven impacts occurred during a period of only four days when Galileo was outside Jupiter's magnetosphere in interplanetary space at approximately $350\,R_J$ from Jupiter. This is a surprisingly large number of impacts at such a large distance from Jupiter given the Galileo measurements from the earlier Jupiter mission (Papers VI and VIII) and from Galileo's interplanetary cruise. Potential sources for these grains are, for example, collisional ejecta from an (unknown) small jovian satellite or a cometary trail crossed by the spacecraft. Judging from the impact charge distribution of the measured grains, jovian stream particles (Figure 6) can be most likely ruled out because a much larger number of impacts should have occurred in the lower amplitude range AR1. In fact, only few impacts were recognized in AR1 during this time. A more detailed analysis of these impacts has to be postponed to a future investigation.

5.5 Galileo's gossamer ring passages

On 5 November 2002 (orbit A34, day 02-309) Galileo traversed Jupiter's gossamer rings for the first time and approached the planet to $2\,R_J$. During this ring passage the spacecraft had a close flyby at Amalthea at 244 km distance from the moon's centre, well outside Amaltheas's Hill sphere. During approach to Jupiter dust data were collected with the highest possible rate (record mode; Section 2.3) while Galileo was within Io's orbit (i.e. within $\sim 5.9\,R_J$). Shortly after Amalthea flyby a spacecraft anomaly at $2.33\,R_J$ jovicentric distance prevented the collection of further Galileo dust data. Although the dust instrument continued to measure dust impacts after the anomaly, the data were not written to the tape recorder on board and, hence, the majority of them were lost. Only the data sets of a few dust impacts were received from an MRO on day 02-322. These events could be located to have happened during the gossamer ring passage but their impact time is uncertain by a few hours (Table 7). The traverse of the optically visible ring from its outer edge at $\sim 3.75\,R_J$ until the spacecraft anomaly occurred lasted about 100 min, and the total gossamer ring traverse from $\sim 3.75\,R_J$ inbound to $\sim 3.75\,R_J$ outbound took approximately six hours.

During the A34 ring passage the lowest amplitude range in class 2 (AC21) was strongly contaminated with noise, while the higher amplitude ranges showed little or no noise contamination. In addition, many class 1 events recognised within Io's orbit showed signatures of being true dust impacts as well. The noise identification scheme applied to the dust data from both Galileo gossamer ring passages is described in Section 3.1 and given in Table 5.

With the new noise identification scheme, complete data sets of 90 dust impacts were identified in the Galileo recorded data from the gossamer ring region. Several hundred more events were counted only and their data sets were lost, in particular in AR1. The completeness of the transmitted ring data varied between 100% in the highest amplitude ranges (AR2-4) in the faint ring extension beyond Thebe's orbit down to only 4% for the lowest amplitude range (AR1) in the more populated Amalthea ring.

In record mode, the dust instrument memory was read out once per minute, and this readout frequency determined the spatial resolution of the measurements: within one minute Galileo moved about 1,800 km through the ring which corresponds to about 1,100 km (or $0.015\,R_J$) in radial direction. This is the highest spatial resolution achievable in the ring with the Galileo in-situ measurements.

Dust measurements in the gossamer rings were also obtained during Galileo's second ring traverse on 21 September 2003 (orbit J35) a few hours before Galileo impacted Jupiter. The data sets of about 20 dust impacts were successfully transmitted to Earth as RTS data. This time the spatial resolution was only about 14,000 km (or $0.2\,R_J$).

The data from both gossamer ring traverses allowed for the first actual comparison of in-situ measurements with the properties inferred from inverting optical images. A detailed analysis of this data was published by Krüger et al. (2009). Below we summarise the most important results.

Images of the rings imply inclinations of the grain orbits of $i \approx 1^\circ$ for the visible 5 to 10μm grains (Showalter et al., 2008). The expected rotation angle for ring particles on circular prograde uninclined jovicentric orbits was $\simeq 90^\circ$. The rotation angles measured within Io's orbit and in particular during the ring passages were – to a first approximation – consistent with these expectations. However, the width of the rotation angle distribution was much wider than the expected width for the geometry conditions during both gossamer ring passages.

What was the reason for such a broad distribution in impact directions? One possibility was the sensor side wall which was very sensitive to dust impacts (Altobelli et al., 2004; Willis et al., 2005). Taking the sensor side wall into account (Table 3), the expected width in rotation angle was still significantly smaller than the observed width. Another potential explanation was impacts onto nearby spacecraft structures like the magnetometer boom, the EPD and PLS instruments which masquerade as particles with high inclinations. We are convinced that such an explanation can be ruled out for two reasons (Moissl, 2005): First, the impact parameters (charge rise times, charge signal coincidences, etc.) of grains measured with rotation angles outside the nominal field-of-view for low-inclination particles do not show significant differences compared to gains inside the nominal field-of-view. Second, the data from both Galileo ring traverses show similarly broad rotation angle patterns although they had different detection geometries. During the first flyby the magnetometer boom obscured the field-of-view while during the second flyby this was not the case (Krüger et al., 2009).

The most likely explanation for the observed structure in the rotation angle pattern is the particle dynamics: The wide range in impact directions as well as a drop measured in the impact rate profile immediately interior to Thebe's orbit and a gradual increase in the relative abundance of small particles closer to Jupiter can best be explained by a shadow resonance caused by varying particle charge on the day and night side of Jupiter, driving particles onto high inclination orbits (Hamilton and Krüger, 2008). In fact, inclinations up to 20° nicely explain the measured impact directions for most grains.

Comparison of our in-situ measurements with imaging observations showed that the in-situ measurements preferentially probe the large population of small sub-micron particles while the images are sensitive to larger grains with radii of at least several microns. The grains form a halo of material faint enough to be invisible to imaging, but populated enough to be detectable with the Galileo sensor. The faint gossamer ring extension previously imaged to about $3.75\,\mathrm{R_J}$ was detected out to at least $5\,\mathrm{R_J}$, indicating that ejecta from Thebe spread much further and particle orbits get higher eccentricities than previously known. Both the gap in the ring and the faint ring extension indicate that the grain dynamics is strongly influenced by electromagnetic forces. For a more detailed discussion of the ring particle dynamics the reader is referred to Hamilton and Krüger (2008).

6 Conclusions

In this paper, which is the tenth in a series of Galileo and Ulysses dust data papers, we present data from the Galileo dust instrument for the period January 2000 to September 2003. In this time interval the spacecraft completed nine revolutions about Jupiter in the jovicentric distance range between 2 and $370\,\mathrm{R_J}$ (Jupiter radius, $\mathrm{R_J} = 71,492\,\mathrm{km}$). On 21 September 2003 Galileo was destroyed in a planned impact with Jupiter.

The data sets of a total of 5389 (or 2% of the total) recorded dust impacts were transmitted to Earth in this period. Many more impacts (98%) were counted with the accumulators of the instrument but their complete information was lost because of the low data transmission capability of the Galileo spacecraft. Together with 15861 impacts recorded in interplanetary space and in the Jupiter system between Galileo's launch in October 1989 and December 1999 published earlier (Grün et al., 1995a; Krüger et al., 1999a, 2001a, 2006b), the complete data set of dust impacts measured with the dust detector during Galileo's entire mission contains 21250 impacts.

Galileo has been an extremely successful dust detector, measuring dust streams flowing away from Jupiter, a tenuous dust ring throughout the jovian magnetosphere and Jupiter's gossamer rings over the almost four year timespan of data considered in this paper.

Most of the time the jovian dust streams dominated the overall impact rate, reaching maxima of more than $10\,\mathrm{min}^{-1}$ in the inner jovian system. A surprisingly large impact rate up to $100\,\mathrm{min}^{-1}$ was measured in August/September 2000 (G28 orbit) when the spacecraft was at about $280\,\mathrm{R_J}$ distance from Jupiter. This strong dust emission was most likely connected with a heavy volcanic eruption on Io (Krüger et al., 2003a; Geissler, 2003; Geissler et al., 2004). A strong variation in the release of neutral gas from the Io torus in this time interval was also reported by Delamere et al. (2004).

Io's dust emission as derived from the measured dust fluxes varied by many orders of magnitude, with typical values ranging between 0.01 to $1\,\mathrm{kg\,s^{-1}}$ of dust ejected. In August/September 2000 the derived dust emission exceeded $100\,\mathrm{kg\,s^{-1}}$. The investigation of the dust impact rate profiles measured for the jovian stream particles as a function of radial distance from Jupiter revealed large orbit-to-orbit variations and variability by a factor of 10 or more on timescales of days to a few weeks. This implies strong variability of the dust release from Io or the Io torus or variability of the jovian magnetosphere on such short timescales.

A surprisingly large number of impacts of bigger micron-sized dust grains was detected within a 4-day time interval far away from Jupiter in March 2003 when Galileo was in interplanetary space. The source of these grains remains unclear.

Finally, in November 2002 and September 2003 Galileo traversed Jupiter's gossamer rings twice, providing the first actual opportunity to compare in-situ dust measurements with the results obtained from remote imaging. These flybys revealed previously unknown structures in the gossamer rings (Krüger et al., 2009): a drop in the dust density between the moons Amalthea and Thebe, grains orbiting Jupiter on highly inclined orbits and an increase in the number of small grains in the inner regions of the rings as compared to the regions further away from the planet. All these features can nicely be explained by electromagnetic forces on the grains that shape the gossamer rings (Hamilton and Krüger, 2008).

Strong degradation of the dust instrument electronics was recognised in the Galileo dust data (Krüger et al., 2005). It was most likely caused by the harsh radiation environment in the jovian magnetosphere and lead to a degradation of the instrument sensitivity for noise and dust detection during the Galileo mission. The Galileo data set obtained until the end of 1999 (Papers VI and VIII) was not seriously affected by this degradation. In the time interval 2000 to 2003 which is the subject of this paper, however, the electronics degradation became so severe that the instrument calibration does not give reliable impact speeds and masses of the dust particles anymore. Instead, only lower limits for the impact speed and upper limits for the grain mass, respectively, can be given. The only exception are dust impacts for which their impact speeds can be derived from other means (e.g. impacts in the gossamer rings; Krüger et al., 2009). On the other hand, a reduction of the channeltron amplification was counterbalanced by four increases of the channeltron high voltage during the entire Jupiter mission (two in 1999, one each in 2000 and 2001) to maintain stable instrument operation.

Even though this is the final paper in our serious of Galileo dust data papers published during the last 15 years, the evaluation of this unique data set is continuing. A list of specific open questions raised in this and earlier data papers includes:

- *Electromagnetic interaction and phase relation of different sized stream particles:* Dust grains with different sizes have a different susceptibility to electromagnetic interaction with the jovian magnetosphere. Different-sized grains released from a source in the inner jovian system at the same time are expected to arrive at Galileo at a different phase of Jupiter's rotation (Grün et al., 1998). This rather simple picture is further complicated by the grains' charging history. Studies of the phase relation may lead to better constraints of the grain size distribution and may give new insights into the grains' electromagnetic interaction. The phase relation may turn out to be essential to understand the Galileo-Cassini joint dust streams measurements.

- *Galileo-Cassini joint dust streams measurements:* Being originally designed as a two-spacecraft time-of-flight measurement of one collimated stream from the jovian dust streams, the analysis of this data set turned out to be more complicated than anticipated. More detailed modelling of the 3-dimensional structure of the dust stream emission pattern from the jovian system is necessary to describe the phase relation of different-sized particles and to understand these unique measurements.

- *"Big" micron-sized particles:* Impacts of micron-sized dust grains were preferentially detected in the inner jovian system between the Galilean moons. Two subpopulations – one orbiting Jupiter on prograde and one on retrograde orbits – were identified in earlier analyses (Thiessenhusen et al., 2000). The derived ratio in number density was approximately 4:1 with the majority of grains being on prograde orbits. At the time, however, only about half of the entire Galileo dust data set from Jupiter was available. Given that the detection geometry of the dust instrument changed with time during the mission, re-evaluation of the full data set from the entire Galileo Jupiter mission would be worthwhile to verify the abundance of grains on retrograde orbits.

- *Dust-plasma interaction:* Very preliminary comparison of the Galileo dust measurements from the gossamer ring passages with energetic particle data from the same period has revealed some interesting correlations between both data sets (Norbert Krupp, personal communication). New insights into the dust-plasma interaction and particle dynamics can be expected from combined studies of the dust data and other Galileo particles and fields data.

Acknowledgements. We dedicate this work to the memory of Dietmar Linkert who passed away in spring 2009. He was Principal Engineer for space instruments at MPI für Kernphysik including the dust instruments flown on the HEOS-2, Helios, Galileo, Ulysses and Cassini missions. His friends and colleagues around the world appreciated his experience and sought his professional advice. The authors wish to thank the Galileo project at NASA/JPL for effective and successful mission operations. This research was supported by the German Bundesministerium für Bildung und Forschung through Deutsches Zentrum für Luft- und Raumfahrt e.V. (DLR, grant 50 QJ 9503 3). Support by MPI für Kernphysik and MPI für Sonnensystemforschung is also gratefully acknowledged.

ERRATUM

Due to an error in Paper VIII, all panels of Figure 9 in that paper have wrong labels on the vertical axis. Furthermore, the third panel (data of 1999) erroneously shows the dataset of 1997. We apologize for this error and show the corrected plots in Figure 13.

Insert Figure 13

References

Altobelli, N., Moissl, R., Krüger, H., Landgraf, M., and Grün, E. (2004). Influence of wall impacts on the Ulysses dust detector in modelling the interstellar dust flux. *Planetary and Space Science*, 52:1287–1295.

Anderson, J. D., Johnson, T. V., Schubert, G., Asmar, S., Jacobson, R. A., Johnston, D., Lau, E. L., Lewis, G., Moore, W. B., Taylor, A., Thomas, P. C., and Weinwurm, G. (2005). Amalthea's Density Is Less Than That of Water. *Science*, 308:1291–1293.

Colwell, J. E., Horányi, M., and Grün, E. (1998). Capture of interplanetary and interstellar dust by the Jovian magnetosphere. *Science*, 280:88–91.

D'Amario, L. A., Bright, L. E., and Wolf, A. A. (1992). Galileo trajectory design. *Space Science Reviews*, 60:23–78.

Delamere, P. A., Steffl, A., and Bagenal, F. (2004). Modeling temporal variability of plasma conditions in the Io torus during the Cassini era. *Journal of Geophysical Research (Space Physics)*, 109:10216–10224.

Flandes, A. (2005). *Dust dynamics in the jovian system*. PhD thesis, Universidad Nacional Autonoma de Mexico.

Flandes, A. and Krüger, H. (2007). Solar wind modulation of Jupiter dust stream detection. In H. Krüger and A. L. Graps, editor, *Dust in planetary systems*, pages 87–90. ESA SP-643.

Flandes, A., Krüger, H., Hamilton, D. P., and Valdés-Galicia, J. F. (2009). Magnetic field modulated dust streams from Jupiter in interplanetary space. *Icarus*. in preparation.

Geissler, P. E. (2003). Volcanic Activity on Io During the Galileo Era. *Annual Reviews of Earth and Planetary Sciences*, 31:175–211.

Geissler, P. E., McEwen, A., Phillips, C., Kesthelyi, L., and Spencer, J. (2004). Surface Changes on Io during the Galileo Mission. *Icarus*, 169:29–64.

Geissler, P. E. and McMillan, M. T. (2008). Galileo observations of volcanic plumes on Io. *Icarus*, 197:505–518.

Graps, A. L. (2001). *Io revealed in the Jovian dust streams*. PhD thesis, Ruprecht-Karls-Universität Heidelberg.

Graps, A. L. (2006). Characterization of Jovian plasma-embedded dust particles. *Planetary and Space Science*, 54:911–918.

Graps, A. L., Grün, E., Krüger, H., Horányi, M., and Svedhem, H. (2001). Io revealed in the jovian dust streams. In *Proceedings of the Meteoroids 2001 Conference, ESA SP-495*, pages 601–608.

Graps, A. L., Grün, E., Svedhem, H., Krüger, H., Horányi, M., Heck, A., and Lammers, S. (2000). Io as a source of the Jovian dust streams. *Nature*, 405:48–50.

Grün, E., Baguhl, M., Divine, N., Fechtig, H., Hamilton, D. P., Hanner, M. S., Kissel, J., Lindblad, B. A., Linkert, D., Linkert, G., Mann, I., McDonnell, J. A. M., Morfill, G. E., Polanskey, C., Riemann, R., Schwehm, G. H., Siddique, N., Staubach, P., and Zook, H. A. (1995a). Three years of Galileo dust data. *Planetary and Space Science*, 43:953–969. Paper II.

Grün, E., Baguhl, M., Divine, N., Fechtig, H., Hamilton, D. P., Hanner, M. S., Kissel, J., Lindblad, B. A., Linkert, D., Linkert, G., Mann, I., McDonnell, J. A. M., Morfill, G. E., Polanskey, C., Riemann, R., Schwehm, G. H., Siddique, N., Staubach, P., and Zook, H. A. (1995b). Two years of Ulysses dust data. *Planetary and Space Science*, 43:971–999. Paper III.

Grün, E., Baguhl, M., Hamilton, D. P., Kissel, J., Linkert, D., Linkert, G., and Riemann, R. (1995c). Reduction of Galileo and Ulysses dust data. *Planetary and Space Science*, 43:941–951. Paper I.

Grün, E., Baguhl, M., Hamilton, D. P., Riemann, R., Zook, H. A., Dermott, S. F., Fechtig, H., Gustafson, B. A., Hanner, M. S., Horányi, M., Khurana, K. K., Kissel, J., Kivelson, M., Lindblad, B. A., Linkert, D., Linkert, G., Mann, I., McDonnell, J. A. M., Morfill, G. E., Polanskey, C., Schwehm, G. H., and Srama, R. (1996a). Constraints from Galileo observations on the origin of Jovian dust streams. *Nature*, 381:395–398.

Grün, E., Fechtig, H., Hanner, M. S., Kissel, J., Lindblad, B. A., Linkert, D., Maas, D., Morfill, G. E., and Zook, H. A. (1992a). The Galileo dust detector. *Space Science Reviews*, 60:317–340.

Grün, E., Fechtig, H., Kissel, J., Linkert, D., Maas, D., McDonnell, J. A. M., Morfill, G. E., Schwehm, G. H., Zook, H. A., and Giese, R. H. (1992b). The Ulysses dust experiment. *Astronomy and Astrophysics, Supplement*, 92:411–423.

Grün, E., Hamilton, D. P., Riemann, R., Dermott, S. F., Fechtig, H., Gustafson, B. A., Hanner, M. S., Heck, A., Horányi, M., Kissel, J., Kivelson, M., Krüger, H., Lindblad, B. A., Linkert, D., Linkert, G., Mann, I., McDonnell, J. A. M., Morfill, G. E., Polanskey, C., Schwehm, G. H., Srama, R., and Zook, H. A. (1996b). Dust measurements during Galileo's approach to Jupiter and Io encounter. *Science*, 274:399–401.

Grün, E., Krüger, H., Graps, A., Hamilton, D. P., Heck, A., Linkert, G., Zook, H., Dermott, S. F., Fechtig, H., Gustafson, B., Hanner, M., Horányi, M., Kissel, J., Lindblad, B., Linkert, G., Mann, I., McDonnell, J. A. M., Morfill, G. E., Polanskey, C., Schwehm, G. H., and Srama, R. (1998). Galileo observes electromagnetically coupled dust in the Jovian magnetosphere. *Journal of Geophysical Research*, 103:20011–20022.

Grün, E., Krüger, P., Dermott, S. F., Fechtig, H., Graps, A. L., Gustafson, B. A., Hamilton, D. P., Heck, A., Horányi, M., Kissel, J., Lindblad, B. A., Linkert, D., Linkert, G., Mann, I., McDonnell, J. A. M., Morfill, G. E., Polanskey, C., Schwehm, G. H., Srama, R., and Zook, H. A. (1997a). Dust measurements in the Jovian magnetosphere. *Geophysical Research Letters*, 24:2171–2174.

Grün, E., Staubach, P., Baguhl, M., Hamilton, D. P., Zook, H. A., Dermott, S. F., Gustafson, B. A., Fechtig, H., Kissel, J., Linkert, D., Linkert, G., Srama, R., Hanner, M. S., Polanskey, C., Horányi, M., Lindblad, B. A., Mann, I., McDonnell, J. A. M., Morfill, G. E., and Schwehm, G. H. (1997b). South-North and Radial Traverses through the Interplanetary Dust Cloud. *Icarus*, 129:270–288.

Grün, E., Zook, H. A., Baguhl, M., Balogh, A., Bame, S. J., Fechtig, H., Forsyth, R., Hanner, M. S., Horányi, M., Kissel, J., Lindblad, B. A., Linkert, D., Linkert, G., Mann, I., McDonnell, J. A. M., Morfill, G. E., Phillips, J. L., Polanskey, C., Schwehm, G. H., Siddique, N., Staubach, P., Svestka, J., and Taylor, A. (1993). Discovery of Jovian dust streams and interstellar grains by the Ulysses spacecraft. *Nature*, 362:428–430.

Hamilton, D. P. and Burns, J. A. (1993). Ejection of dust from Jupiter's gossamer ring. *Nature*, 364:695–699.

Hamilton, D. P. and Krüger, H. (2008). Jupiter's shadow sculpts its gossamer rings. *Nature*, 453:72–75.

Heck, A. (1998). *Modellierung und Analyse der von der Raumsonde Galileo im Jupitersystem vorgefundenen Mikrometeoroiden-Populationen*. PhD thesis, Ruprecht-Karls-Universität Heidelberg.

Horányi, M., Grün, E., and Heck, A. (1997). Modeling the Galileo dust measurements at Jupiter. *Geophysical Research Letters*, 24:2175–2178.

Horányi, M., Morfill, G. E., and Grün, E. (1993). Mechanism for the acceleration and ejection of dust grains from Jupiter's magnetosphere. *Nature*, 363:144–146.

Johnson, T. V., Yeates, C., and Young, R. (1992). Galileo Mission Overview. *Space Science Reviews*, 60:3–21.

Kempf, S., Beckmann, U., Srama, R., Horanyi, M., Auer, S., and Grün, E. (2006). The electrostatic potential of E ring particles. *Planetary and Space Science*, 54:999–1006.

Kempf, S., Srama, R., Altobelli, N., Auer, S., Tschernjawski, V., Bradley, J., Burton, M. E., Helfert, S., Johnson, T. V., Krüger, H., Moragas-Klostermeyer, G., and Grün, E. (2004). Cassini between Earth and asteroid belt: first in-situ charge measurements of interplanetary grains. *Icarus*, 171:317–335.

Krivov, A. V., Krüger, H., Grün, E., Thiessenhusen, K.-U., and Hamilton, D. P. (2002a). A tenuous dust ring of Jupiter formed by escaping ejecta from the Galilean satellites. *Journal of Geophysical Research*, 107:E1, 10.1029/2000JE001434.

Krivov, A. V., Sremčević, M., Spahn, F., Dikarev, V. V., and Kholshevnikov, K. V. (2003). Impact-generated dust clouds around planetary satellites: Spherically-symmetric case. *Planetary and Space Science*, 51:251–269.

Krivov, A. V., Wardinski, I., Spahn, F., Krüger, H., and Grün, E. (2002b). Dust on the outskirts of the Jovian system. *Icarus*, 157:436–455.

Krüger, H. Hamilton, D. P., Moissl, R., and Grün, E. (2009). Galileo in-situ dust measurements in Jupiter's gossamer rings. *Icarus*. in press.

Krüger, H. (2003). *Jupiter's Dust Disc, An Astrophysical Laboratory*. Shaker Verlag Aachen, ISBN 3-8322-2224-3. Habilitation Thesis Ruprecht-Karls-Universität Heidelberg.

Krüger, H., Altobelli, N., Anweiler, B., Dermott, S. F., Dikarev, V., Graps, A. L., Grün, E., Gustafson, B. A., Hamilton, D. P., Hanner, M. S., Horányi, M., Kissel, J., Landgraf, M., Lindblad, B., Linkert, D., Linkert, G., Mann, I., McDonnell, J. A. M., Morfill, G. E., Polanskey, C., Schwehm, G. H., Srama, R., and Zook, H. A. (2006a). Five years of Ulysses dust data: 2000 to 2004. *Planetary and Space Science*, 54:932–956. Paper IX.

Krüger, H., Bindschadler, D., Dermott, S. F., Graps, A. L., Grün, E., Gustafson, B. A., Hamilton, D. P., Hanner, M. S., Horányi, M., Kissel, J., Lindblad, B., Linkert, D., Linkert, G., Mann, I., McDonnell, J. A. M., Moissl, R., Morfill, G. E., Polanskey, C., Schwehm, G. H., Srama, R., and Zook, H. A. (2006b). Galileo dust data from the jovian system: 1997 to 1999. *Planetary and Space Science*, 54:879–910. Paper VIII.

Krüger, H., Dikarev, V., Anweiler, B., Dermott, S. F., Graps, A. L., Grün, E., Gustafson, B. A., Hamilton, D. P., Hanner, M. M. S., Horányi, M., Kissel, J., Linkert, D., Linkert, G., Mann, I., McDonnell, J. A. M., Morfill, G. E., Polanskey, C., Schwehm, G. H., and Srama, R. (2010). Three years of Ulysses dust data: 2005 to 2007. *Planetary and Space Science*. Paper XI, submitted.

Krüger, H., Geissler, P., Horányi, M., Graps, A. L., Kempf, S., Srama, R., Moragas-Klostermeyer, G., Moissl, R., Johnson, T. V., and Grün, E. (2003a). Jovian dust streams: A Monitor of Io's volcanic plume activity. *Geophysical Research Letters*, 30:2101–2105.

Krüger, H., Graps, A. L., Hamilton, D. P., Flandes, A., Forsyth, R. J., Horányi, M., and Grün, E. (2006c). Ulysses jovian latitude scan of high-velocity dust streams originating from the jovian system. *Planetary and Space Science*, 54:919–931.

Krüger, H., Grün, E., Graps, A. L., Bindschadler, D. L., Dermott, S. F., Fechtig, H., Gustafson, B. A., Hamilton, D. P., Hanner, M. S., Horányi, M., Kissel, J., Lindblad, B., Linkert, D., Linkert, G., Mann, I., McDonnell, J. A. M., Morfill, G. E., Polanskey, C., Schwehm, G. H., Srama, R., and Zook, H. A. (2001a). One year of Galileo dust data from the jovian system: 1996. *Planetary and Space Science*, 49:1285–1301. Paper VI.

Krüger, H., Grün, E., Hamilton, D. P., Baguhl, M., Dermott, S. F., Fechtig, H., Gustafson, B. A., Hanner, M. S., Horányi, M., Kissel, J., Lindblad, B. A., Linkert, D., Linkert, G., Mann, I., McDonnell, J. A. M., Morfill, G. E., Polanskey, C., Riemann, R., Schwehm, G. H., Srama, R., and Zook, H. A. (1999a). Three years of Galileo dust data: II. 1993 to 1995. *Planetary and Space Science*, 47:85–106. Paper IV.

Krüger, H., Grün, E., Heck, A., and Lammers, S. (1999b). Analysis of the sensor characteristics of the Galileo dust detector with collimated Jovian dust stream particles. *Planetary and Space Science*, 47:1015–1028.

Krüger, H., Grün, E., Landgraf, M., Baguhl, M., Dermott, S. F., Fechtig, H., Gustafson, B. A., Hamilton, D. P., Hanner, M. S., Horányi, M., Kissel, J., Lindblad, B., Linkert, D., Linkert, G., Mann, I., McDonnell, J. A. M., Morfill, G. E., Polanskey, C., Schwehm, G. H., Srama, R., and Zook, H. A. (1999c). Three years of Ulysses dust data: 1993 to 1995. *Planetary and Space Science*, 47:363–383. Paper V.

Krüger, H., Grün, E., Landgraf, M., Dermott, S. F., Fechtig, H., Gustafson, B. A., Hamilton, D. P., Hanner, M. S., Horányi, M., Kissel, J., Lindblad, B., Linkert, D., Linkert, G., Mann, I., McDonnell, J. A. M., Morfill, G. E., Polanskey, C., Schwehm, G. H., Srama, R., and Zook, H. A. (2001b). Four years of Ulysses dust data: 1996 to 1999. *Planetary and Space Science*, 49:1303–1324. Paper VII.

Krüger, H., Grün, E., Linkert, D., Linkert, G., and Moissl, R. (2005). Galileo long-term dust monitoring in the jovian magnetosphere. *Planetary and Space Science*, 53:1109–1120.

Krüger, H., Horányi, M., and Grün, E. (2003b). Jovian dust streams: Probes of the Io plasma torus. *Geophysical Research Letters*, 30:1058–1061.

Krüger, H., Horányi, M., Krivov, A. V., and Graps, A. L. (2004). *Jovian dust: streams, clouds and rings*, pages 219–240. Jupiter. The planet, satellites and magnetosphere. Edited by Fran Bagenal, Timothy E. Dowling, William B. McKinnon. Cambridge planetary science, Vol. 1, Cambridge, UK: Cambridge University Press, ISBN 0-521-81808-7, 2004.

Krüger, H., Krivov, A. V., and Grün, E. (2000). A dust cloud of Ganymede maintained by hypervelocity impacts of interplanetary micrometeoroids. *Planetary and Space Science*, 48:1457–1471.

Krüger, H., Krivov, A. V., Hamilton, D. P., and Grün, E. (1999d). Detection of an impact-generated dust cloud around Ganymede. *Nature*, 399:558–560.

Krüger, H., Krivov, A. V., Sremčević, M., and Grün, E. (2003c). Galileo measurements of impact-generated dust clouds surrounding the Galilean satellites. *Icarus*, 164:170–187.

McEwen, A., Keszthelyi, L., Lopes, R., Schenk, P., and Spencer, J. (2004). The Lithosphere and Surface of Io. In Bagenal, F., McKinnon, B., and Dowling, T., editors, *Jupiter: Planet, Satellites & Magnetosphere*, pages 307–328. Cambridge University Press.

McEwen, A. S., Keszthelyi, L., Geissler, P., Simonelli, D. P., Carr, M. H., Johnson, T. V., Klaasen, K. P., Breneman, H. H., Jones, T. J., Kaufman, J. M., Magee, K. P., Senske, D. A., Belton, M. J. S., and Schubert, G. (1998). Active volcanism on Io as seen by Galileo SSI. *Icarus*, 135:181–219.

Moissl, R. (2005). *Galileos Staubmessungen in Jupiters Gossamer-Ringen*. Ruprecht-Karls-Universität Heidelberg. Diplom thesis.

Porco, C. C., West, R. A., McEwen, A., Del Genio, A. D., Ingersoll, A. P., Thomas, P., Squyres, S., Dones, L., Murray, C. D., Johnson, T. V., Burns, J. A., Brahic, A., Neukum, G., Veverka, J., Barbara, J. M., Denk, T., Evans, M., Ferrier, J. J., Geissler, P., Helfenstein, P., Roatsch, T., Throop, H., Tiscareno, M., and Vasavada, A. R. (2003). Cassini Imaging of Jupiter's Atmosphere, Satellites, and Rings. *Science*, 299:1541–1547.

Postberg, F., Kempf, S., Green, S. F., Hillier, J. K., McBride, N., and Grün, E. (2006). Composition of jovian dust stream particles. *Icarus*, 183:122–134.

Showalter, M. R., de Pater, I., Verbanac, G., Hamilton, D. P., and Burns, J. A. (2008). Properties and Dynamics of Jupiter's Gossamer Rings from Galileo, Voyager, Hubble and Keck Images. *Icarus*, 195:361–377.

Spencer, J. R., Stern, S. A., Cheng, A. F., Weaver, H. A., Reuter, D. C., Retherford, K., Lunsford, A., Moore, J. M., Abramov, O., Lopes, R. M. C., Perry, J. E., Kamp, L., Showalter, M., Jessup, K. L., Marchis, F., Schenk, P. M., and Dumas, C. (2007). Io Volcanism Seen by New Horizons: A Major Eruption of the Tvashtar Volcano. *Science*, 318:240–243.

Sremčević, M., Krivov, A. V., Krüger, H., and Spahn, F. (2005). Impact-generated dust clouds around planetary satellites: model versus Galileo data. *Planetary and Space Science*, 53:625–641.

Sremčević, M., Krivov, A. V., and Spahn, F. (2003). Impact-generated dust clouds around planetary satellites: Asymmetry effects. *Planetary and Space Science*, 51:455–471.

Svestka, J., Auer, S., Baguhl, M., and Grün, E. (1996). Measurements of dust electric charges by the Ulysses and Galileo dust detectors. In Gustafson, B. A. and Hanner, M. S., editors, *Physics, Chemistry and Dynamics of Interplanetary Dust, ASP Conference Series*, volume 104, pages 481–484.

Thiessenhusen, K.-U., Krüger, H., Spahn, F., and Grün, E. (2000). Dust grains around Jupiter – The observations of the Galileo Dust Detector. *Icarus*, 144:89–98.

Willis, M. J., Burchell, M., Ahrens, T. J., Krüger, H., and Grün, E. (2005). Decreased values of cosmic dust number density estimates in the solar system. *Icarus*, 176:440–452.

Willis, M. J., Burchell, M., Cole, M., and McDonnell, J. A. M. (2004). Influence of impact ionization detection methods on determination of dust particle flux in space. *Planetary and Space Science*, 52:711–725.

Zook, H. A., Grün, E., Baguhl, M., Hamilton, D. P., Linkert, G., Linkert, D., Liou, J.-C., Forsyth, R., and Phillips, J. L. (1996). Solar wind magnetic field bending of Jovian dust trajectories. *Science*, 274:1501–1503.

Table 1: Summary of Galileo dust data papers and significant mission events.

Time Interval	Significant Mission Events	Paper Number
1989 – 1992	Galileo launch (18 Oct 1989)	II (Grün et al., 1995a)
1993 – 1995	Jupiter orbit insertion (7 Dec 1995)	IV (Krüger et al., 1999a)
1996	Galileo orbits G1 – E4	VI (Krüger et al., 2001a)
1997 – 1999	Galileo orbits J5 – I25	VIII (Krüger et al., 2006b)
2000 – 2003	Galileo orbits E26 – J35, First gossamer ring passage (5 Nov 2002), second gossamer ring passage and Galileo Jupiter impact (21 Sep 2003)	X (this paper)

Table 2: Galileo mission and dust detector (DDS) configuration, tests and other events (2000-2003). See text for details.

Yr-day	Date	Time	Event
89-291	18 Oct 1989	16:52	Galileo launch
95-341	07 Dec 1995	21:54	Galileo Jupiter closest approach, distance: 4.0 R_J
99-345	11 Dec 1999	02:07	DDS configuration: HV=4, EVD=I, SSEN=0,1,1,1
00-001	01 Jan 2000	00:00	DDS begin RTS data
00-003	03 Jan 2000	17:28	DDS end RTS data, begin record data
00-003	03 Jan 2000	18:00	**Galileo Europa 26 (E26) closest approach**, altitude 351 km
00-003	03 Jan 2000	18:30	DDS end record data, begin RTS data
00-004	04 Jan 2000	03:33	Galileo Jupiter closest approach, distance 5.8R_J
00-006	06 Jan 2000	02:00	Galileo turn 5°, duration 3 h, return to nominal attitude
00-007	07 Jan 2000	19:00	Galileo OTM-82, size of turn 3°, duration 5 h, return to nominal attitude
00-009	09 Jan 2000	11:49	DDS end RTS data
00-029	29 Jan 2000	04:00	Galileo OTM-83, size of turn 3°, duration 3 h, return to nominal attitude
00-033	02 Feb 2000	18:00	Galileo turn 4°, new nominal attitude
00-038	07 Feb 2000	23:00	Galileo turn 7°, duration 3 h, return to nominal attitude
00-049	18 Feb 2000	16:36	Galileo OTM-84, no attitude change
00-050	19 Feb 2000	12:00	DDS begin RTS data
00-053	22 Feb 2000	12:30	Galileo Jupiter closest approach, distance 5.9R_J
00-053	22 Feb 2000	13:02	DDS end RTS data, begin record data
00-053	22 Feb 2000	13:47	**Galileo Io 27 (I27) closest approach**, altitude 198 km
00-053	22 Feb 2000	14:25	DDS end record data, begin RTS data
00-054	23 Feb 2000	19:20	DDS last RTS data before spacecraft anomaly
00-055	24 Feb 2000	04:00	Galileo turn 15°, duration 30 h, return to nominal attitude
00-055	24 Feb 2000	21:00	Galileo spacecraft anomaly
00-056	25 Feb 2000	04:16	DDS begin RTS data after spacecraft anomaly
00-057	25 Feb 2000	14:00	Galileo OTM-85, size of turn 19°, duration 11 h, return to nominal attitude
00-059	28 Feb 2000	23:56	DDS end RTS data
00-070	10 Mar 2000	10:00	Galileo turn 8°, new nominal attitude
00-088	28 Mar 2000	00:00	Galileo turn 3°, duration 3 h, return to nominal attitude
00-098	07 Apr 2000	12:00	Galileo OTM-86, no attitude change
00-116	25 Apr 2000	20:00	Galileo turn 8°, new nominal attitude
00-117	26 Apr 2000	01:11	DDS last MRO before solar conjunction
00-118	27 Apr 2000		Start solar conjunction period
00-138	17 May 2000		End solar conjunction period
00-138	17 May 2000	09:30	DDS begin RTS data
00-139	18 May 2000	10:00	Galileo OTM-87, no attitude change
00-141	20 May 2000	09:39	DDS end RTS data, begin record data
00-141	20 May 2000	10:10	**Galileo Ganymede 28 (G28) closest approach**, altitude 808 km

Abbreviations used: MRO: DDS memory readout; HV: channeltron high voltage step; EVD: event definition, ion- (I), channeltron- (C), or electron-channel (E); SSEN: detection thresholds, ICP, CCP, ECP and PCP; OTM: orbit trim maneuver; RTS: Realtime science.

Table 2: Continued.

Yr-day	Date	Time	Event
00-141	20 May 2000	10:40	DDS end record data, begin RTS data
00-142	21 May 2000	04:52	Galileo Jupiter closest approach, distance $6.7R_J$
00-143	22 May 2000	08:00	Galileo turn 2°, duration 1 h, return to nominal attitude
00-146	25 May 2000	08:00	Galileo OTM-88, no attitude change
00-152	31 May 2000	07:00	Galileo turn 8°, new nominal attitude
00-170	18 Jun 2000	23:57	DDS end RTS data
00-176	23 Jun 2000	03:00	Galileo turn 7°, duration 2 h, return to nominal attitude
00-189	07 Jul 2000	19:00	Galileo turn 9°, new nominal attitude
00-209	27 Jul 2000	11:11	DDS configuration: HV = 5
00-216	03 Aug 2000	18:31	DDS begin RTS data
00-223	10 Aug 2000	02:00	Galileo turn 9°, new nominal attitude
00-244	31 Aug 2000	16:00	Galileo turn 2°, duration 2 h, return to nominal attitude
00-252	08 Sep 2000	18:00	Galileo OTM-89, size of turn 2°, duration 3 h, return to nominal attitude
00-253	09 Sep 2000	08:11	DDS end RTS data
00-300	26 Oct 2000	10:01	DDS begin RTS data
00-302	28 Oct 2000	01:00	Galileo OTM-90, no attitude change
00-342	07 Dec 2000	23:00	Galileo turn 2°, duration 1 h, return to nominal attitude
00-353	18 Dec 2000	05:00	Galileo turn 20°, new nominal attitude
00-356	21 Dec 2000	20:15	Galileo OTM-91, no attitude change
00-363	28 Dec 2000	08:25	**Galileo Ganymede 29 (G29) closest approach**, altitude 2,337 km
00-364	29 Dec 2000	03:27	Galileo Jupiter closest approach, distance $7.5R_J$
01-002	02 Jan 2001	20:00	Galileo OTM-92, no attitude change
01-004	04 Jan 2001	03:30	Galileo turn 10°, return to nominal attitude
01-086	27 Mar 2001	23:00	DDS end RTS data
01-094	04 Apr 2001	04:00	Galileo turn 8°, new nominal attitude
01-114	24 Apr 2001	03:00	Galileo turn 8°, duration 9 h, return to nominal attitude
01-130	10 May 2001	16:00	Galileo OTM-94, no attitude change
01-133	13 May 2001	01:00	Galileo turn 4°, new nominal attitude
01-142	22 May 2001	23:00	Galileo turn 6°, return to nominal attitude
01-143	23 May 2001	12:01	DDS begin RTS data
01-143	23 May 2001	17:33	Galileo Jupiter closest approach, distance $7.3R_J$
01-145	25 May 2001	11:24	**Galileo Callisto 30 (C30) closest approach**, altitude 138 km
01-146	26 May 2001	07:15	DDS end RTS data
01-146	26 May 2001	09:00	Galileo turn 5°, duration 2 h, return to nominal attitude
01-146	26 May 2001	22:00	Galileo turn 12°, duration 13 h, return to nominal attitude
01-148	28 May 2001	19:00	Galileo OTM-95, size of turn 1°
01-152	01 Jun 2001	11:00	Galileo turn 5°, new nominal attitude
01-154	03 Jun 2001	16:58	DDS last MRO before solar conjunction
01-155	04 Jun 2001		Start solar conjunction period
01-174	23 Jun 2001		End solar conjunction period

Table 2: Continued.

Yr-day	Date	Time	Event
01-177	26 Jun 2001	22:58	DDS fist MRO after solar conjunction
01-183	02 Jul 2001	21:00	Galileo turn 4°, new nominal attitude
01-186	05 Jul 2001	05:00	Galileo turn 5°, duration 5 h, return to nominal attitude
01-194	13 Jul 2001	06:00	Galileo OTM-97, size of turn 3°, duration 4 h, return to nominal attitude
01-201	20 Jul 2001	07:00	Galileo turn 4°, new nominal attitude
01-215	03 Aug 2001	23:00	Galileo OTM-98, no attitude change
01-217	05 Aug 2001	05:12	DDS begin RTS data
01-218	06 Aug 2001	04:52	Galileo Jupiter closest approach, distance 5.9R_J
01-218	06 Aug 2001	04:59	**Galileo Io 31 (I31) closest approach**, altitude 193 km
01-219	07 Aug 2001	16:08	DDS end RTS data
01-220	08 Aug 2001	03:00	Galileo turn 7°, duration 2 h, return to nominal attitude
01-222	10 Aug 2001	19:30	Galileo OTM-99, no attitude change
01-224	12 Aug 2001	08:00	Galileo turn 3°, new nominal attitude
01-236	24 Aug 2001	07:00	Galileo turn 3°, duration 2 h, return to nominal attitude
01-245	02 Sep 2001	03:00	Galileo OTM-100, no attitude change
01-246	03 Sep 2001	05:00	Galileo turn 4°, new nominal attitude
01-261	18 Sep 2001	12:00	Galileo OTM-101, no attitude change
01-270	27 Sep 2001	04:00	Galileo turn 3°, new nominal attitude
01-286	13 Oct 2001	18:00	Galileo OTM-102, no attitude change
01-287	14 Oct 2001	02:04	DDS begin RTS data
01-288	15 Oct 2001	23:56	Galileo Jupiter closest approach, distance 5.8R_J
01-289	16 Oct 2001	01:23	**Galileo Io 32 (I32) closest approach**, altitude 184 km
01-290	17 Oct 2001	12:00	Galileo turn 3°, duration 2 h, return to nominal attitude
01-293	20 Oct 2001	04:00	Galileo OTM-103, size of turn 1°, duration 2 h, return to nominal attitude
01-301	28 Oct 2001	23:30	DDS end RTS data
01-324	20 Nov 2001	00:00	Galileo turn 4°, duration 2 h, return to nominal attitude
01-335	01 Dec 2001	00:00	Galileo OTM-104, no attitude change
01-340	06 Dec 2001	15:00	Galileo turn 2°, new nominal attitude
01-352	18 Dec 2001	00:00	DDS configuration: HV = 6
01-357	23 Dec 2001	16:00	Galileo turn 2°, new nominal attitude
02-004	04 Jan 2002	12:25	DDS begin RTS data
02-010	10 Jan 2002	00:00	Galileo turn 5°, duration 2 h, new nominal attitude
02-017	17 Jan 2002	09:15	DDS end RTS data
02-017	17 Jan 2002	13:40	Galileo spacecraft anomaly
02-017	17 Jan 2002	14:08	**Galileo Io 33 (I33) closest approach**, altitude 102 km
02-017	17 Jan 2002	16:23	Galileo Jupiter closest approach, distance 5.5 R_J
02-017	17 Jan 2002	23:50	DDS begin RTS data after spacecraft anomaly
02-021	21 Jan 2002	12:00	Galileo OTM-106, no attitude change
02-029	29 Jan 2002	23:00	Galileo turn 2°, new nominal attitude
02-032	01 Feb 2002	01:00	Galileo turn 44°, duration 90 h, return to nominal attitude
02-047	16 Feb 2002	19:09	Galileo spacecraft anomaly
02-051	20 Feb 2002	17:54	DDS begin RTS data after spacecraft anomaly
02-094	04 Apr 2002	00:00	Galileo turn 3°, duration 3 h, return to nominal attitude

Table 2: Continued.

Yr-day	Date	Time	Event
02-102	12 Apr 2002	05:00	Galileo turn 3°, new nominal attitude
02-124	04 May 2002	23:00	Galileo turn 4°, new nominal attitude
02-131	11 May 2002	12:00	Galileo turn 1°, duration 2 h, return to nominal attitude
02-146	26 May 2002	02:00	Galileo turn 4°, new nominal attitude
02-157	06 Jun 2002	02:00	Galileo turn 6°, duration 3 h, return to nominal attitude
02-165	14 Jun 2002	16:00	Galileo OTM-107, size of turn 3°, duration 3 h, return to nominal attitude
02-182	01 Jul 2002	11:00	Galileo turn 12°, new nominal attitude
02-190	09 Jul 2002		Begin solar conjunction
02-209	28 Jul 2002		End solar conjunction
02-214	02 Aug 2002	08:00	Galileo turn 5°, new nominal attitude
02-232	20 Aug 2002	15:00	Galileo turn 4°, new nominal attitude
02-250	07 Sep 2002	12:00	Galileo turn 4°, new nominal attitude
02-274	01 Oct 2002	19:30	Galileo spacecraft anomaly
02-275	02 Oct 2002	23:54	DDS begin RTS after spacecraft anomaly
02-281	08 Oct 2002	02:00	Galileo turn 6°, duration 3 h, return to nominal attitude
02-285	12 Oct 2002	15:00	Galileo turn 9°, new nominal attitude
02-298	25 Oct 2002	03:00	Galileo turn 2°, duration 2 h, return to nominal attitude
02-309	05 Nov 2002	02:44	DDS end RTS data
02-309	05 Nov 2002	02:44	DDS begin record data
02-309	05 Nov 2002	06:19	**Galileo Amalthea 34 (A34) closest approach**, 244 km distance from moon's centre
02-309	05 Nov 2002	06:35	Galileo spacecraft anomaly, end record data
02-309	05 Nov 2002	07:25	Galileo Jupiter closest approach, distance 2.0 R_J
02-318	14 Nov 2002	08:00	Galileo turn 9°, duration 3 h, return to nominal attitude
02-322	18 Nov 2002	14:29	DDS first MRO after spacecraft anomaly
02-363	29 Dec 2002	07:53	DDS final MRO
03-003	03 Jan 2003	22:00	Galileo turn 20°, duration 6 h, return to nominal attitude
03-004	04 Jan 2003	21:00	Galileo turn 20°, duration 5 h, return to nominal attitude
03-008	08 Jan 2003	08:00	Galileo turn 17°, duration 2 h, return to nominal attitude
03-010	10 Jan 2003	22:00	Galileo turn 22°, duration 82 h, return to nominal attitude
03-015	15 Jan 2003	10:00	Galileo turn 22°, new nominal attitude
03-063	04 Mar 2003	15:00	DDS begin RTS data
03-070	11 Mar 2003	21:50	DDS end RTS data
03-255	12 Sep 2003	21:43	DDS begin RTS data
03-256	13 Sep 2003	18:57	DDS end RTS data
03-263	20 Sep 2003	13:44	DDS begin RTS data
03-263	20 Sep 2003	14:26	DDS end RTS data
03-264	21 Sep 2003	12:10	DDS begin RTS data
03-264	21 Sep 2003	17:59	DDS end RTS data
03-264	21 Sep 2003	18:57	**Galileo Jupiter impact, end of mission**

Table 3: Dust detector sensitive area and field-of-view (FOV) for different dust data sets.

Dust data set	FOV (°)	Sensor area (cm^2)	Comment
Stream particles class 2	140	1000	Nominal target FOV (Grün et al., 1992a)
Stream particles class 3	96	110	Reduced target FOV (Krüger et al., 1999b)
All other	180	1000	Target plus side wall FOV (Altobelli et al., 2004)

Table 4: Details of Galileo dust data transmission modes during the Jupiter mission. See text for details.

		Realtime Science (RTS)		Record	MROs
		Low rate	High rate		
Data rate (bits s^{-1})		1.1	3.4	24	$\sim 3 \times 10^{-3\,a)}$
Timing accuracy (min)		21.2	7.1	~ 1	259
Data frames per readout		7		7	46
Mission time coverage (%)		40		< 0.1	60
Maximum event rate recordable by accumulators ($\min^{-1}$)	AC21/AC31[b]	3000	9000	65000	$\approx 2^{a)}$
	All other	12	36	256	$\approx 0.01^{a)}$
Maximum event rate for full data set transmission ($\min^{-1}$)		$\frac{1}{21.2}$	$\frac{1}{7.1}$	~ 1	$\approx \frac{46}{20\,\mathrm{days}}$

[a] One MRO every 20 days assumed.

[b] Since 4 December 1996; the "All other" row was valid for all data before this time.

Table 5: Criteria for the separation of noise events in classes 1 and 2 from true dust impacts in the region within Io's orbit for Galileo orbits A34 and J35 (gossamer ring passages). Noise events in the lowest amplitude range (AR1) fulfill at least one of the criteria listed, whereas noise events in the higher ranges fulfill two criteria (from Moissl, 2005).

Class, AR	EA - IA		CA	EIC
Class 1, AR1	≤ 2 or ≥ 9	or	≤ 2	–
Class 1, AR2-6	≤ 2 or ≥ 9	and	≤ 2	–
Class 2, AR1	–		–	= 0
Class 2, AR2-6	≤ 1 or ≥ 7	and	≤ 2	–

Table 6: Overview of dust impacts accumulated with Galileo DDS between 1 January 2000 and 21 September 2003. The jovicentric distance D_{Jup}, the length of the time interval Δt (days) from the previous table entry, and the corresponding numbers of impacts are given for the class 2 and 3 accumulators. The accumulators are arranged with increasing signal amplitude ranges (AR), e.g. AC31 means counter for CLN = 3 and AR = 1. The determination of the noise contamination f_{noi} in class 2 is described in Paper VI. The Δt in the first line (day 00-002) is the time interval counted from the last entry in Table 2 in Paper VIII. The totals of counted impacts, of impacts with complete data, and of all events (noise plus impact events) for the entire period are given as well.

Date	Time	D_{Jup} [R_J]	Δt [d]	$f_{noi,AC21}$	AC 21*	AC 31*	$f_{noi,AC22}$	AC 22	AC 32	$f_{noi,AC23}$	AC 23	AC 33	$f_{noi,AC24}$	AC 24	AC 34
00-002	23:46	19.28	21.06	0.81	8	-	-	-	-	-	-	-	-	-	-
00-003	21:55	7.370	0.922	0.27	521	40	0.00	1	-	-	-	-	-	-	-
00-005	10:08	20.76	1.508	0.54	552	9	0.50	2	1	0.00	1	2	-	-	-
00-052	15:19	15.96	47.21	0.77	47	-	0.00	1	1	-	-	-	0.00	1	1
00-053	10:26	6.120	0.796	0.56	301	8	0.00	4	1	-	-	-	-	-	-
00-056	22:40	42.65	3.510	0.80	869	-	0.80	20	2	-	-	-	0.00	3	2
00-074	20:37	126.1	17.91	0.59	17	-	0.50	2	1	0.00	1	-	-	-	-
00-141	14:34	12.54	66.74	0.96	20	2	0.25	4	-	-	-	-	-	-	-
00-143	23:11	27.10	2.359	0.50	209	-	0.00	2	-	-	-	-	-	-	-
00-149	19:41	76.24	5.853	0.10	89	3	-	-	-	-	-	-	-	-	-
00-177	07:37	193.7	27.49	0.23	42	3	0.50	2	-	-	-	-	-	-	-
00-206	19:08	256.7	29.47	0.72	5383	160	-	-	-	-	-	1	-	-	-
00-216	23:50	270.0	10.19	0.00	4422	115	-	-	-	-	-	-	-	-	-
00-220	17:43	274.0	3.745	0.00	13922	522	1.00	1	-	-	-	-	-	-	-
00-222	23:09	276.2	2.226	0.00	3964	219	-	-	-	-	-	-	-	-	-
00-228	05:08	280.6	5.249	0.00	2648	203	-	-	-	-	-	-	-	-	-
00-231	18:47	283.1	3.568	0.00	5590	424	-	-	-	-	-	-	-	-	-
00-236	10:15	285.7	4.644	0.00	10750	842	-	-	-	-	-	-	-	-	-
00-246	03:28	289.1	9.717	0.00	33125	3489	0.00	2	-	-	-	-	-	-	-
00-256	11:57	289.6	10.35	0.01	49616	3149	0.00	1	-	-	-	-	-	-	-
00-266	13:29	287.1	10.06	0.00	47774	2768	-	-	1	-	-	-	-	-	-
00-276	00:28	281.8	9.457	0.00	17821	5196	-	-	-	-	-	-	-	-	-
00-300	11:26	254.7	24.45	0.00	3200	163	-	-	-	-	-	-	-	-	-
00-306	12:10	244.7	6.030	0.01	161	3	-	-	-	-	-	-	-	-	-
00-326	08:51	200.4	19.86	0.05	223	9	-	-	-	-	-	-	-	-	-
00-363	16:33	10.84	37.32	0.37	68	1	0.00	1	1	-	-	-	-	-	-
00-366	00:28	27.62	2.329	0.18	1014	41	0.00	3	-	-	-	-	-	-	-
00-366	23:49	37.39	0.973	0.04	345	19	-	-	-	0.00	1	-	-	-	-
01-002	14:24	51.27	0.607	0.09	513	47	-	-	-	-	-	-	-	-	-
01-006	08:59	77.49	3.774	0.00	661	47	-	-	-	-	-	-	-	-	-
01-010	13:29	100.5	4.187	0.05	312	15	-	-	-	-	-	-	-	-	-
01-015	12:45	122.8	4.969	0.02	373	17	-	-	-	-	-	-	-	-	-
01-026	00:22	158.6	10.48	0.07	365	24	-	-	-	-	-	-	-	-	-
01-040	21:05	191.8	14.86	0.09	87	4	-	-	-	-	-	-	-	-	-
01-096	14:04	198.7	55.70	0.11	59	3	0.33	3	-	-	-	1	-	-	-

Table 6 continued.

Date	Time	D_{Jup} [R_J]	Δt [d]	$f_{noi,AC21}$	AC 21*	AC 31*	$f_{noi,AC22}$	AC 22	AC 32	$f_{noi,AC23}$	AC 23	AC 33	$f_{noi,AC24}$	AC 24	AC 34
01-143	15:55	7.390	47.07	0.40	3245	45	0.44	9	2	-	-	-	-	-	-
01-146	06:32	34.34	2.609	0.60	2913	129	0.18	11	1	-	-	-	0.00	2	-
01-154	16:58	87.12	8.434	0.18	16888	756	0.00	1	-	-	-	-	-	-	-
01-177	20:07	136.1	23.13	0.00	38739	1940	0.00	1	-	-	-	-	-	-	-
01-194	13:03	124.8	16.70	0.00	4139	386	-	-	-	-	-	-	-	-	-
01-209	11:19	76.61	14.92	0.01	394	31	0.00	1	1	-	-	-	-	-	-
01-218	07:24	6.280	8.836	0.47	351	6	0.00	5	4	0.00	1	1	0.33	3	2
01-221	21:01	44.16	3.567	0.45	207	8	0.33	6	-	-	-	-	0.00	2	-
01-246	07:41	128.5	24.44	0.01	509	9	0.00	1	-	-	-	1	-	-	-
01-288	01:25	16.92	41.73	0.06	243	14	-	-	-	-	-	-	-	-	-
01-291	11:32	34.37	3.420	0.73	303	1	0.00	2	2	0.00	2	-	0.50	2	-
01-314	06:23	137.8	22.78	0.33	51	-	-	-	-	-	-	-	-	-	-
01-348	23:00	152.6	34.69	0.33	19	1	0.00	2	-	-	-	-	-	-	-
02-017	02:52	12.09	33.16	0.57	36	-	0.00	1	-	-	-	1	0.00	2	1
02-018	00:32	8.820	0.902	0.86	341	-	0.00	1	2	-	-	-	0.00	2	2
02-032	03:41	118.4	14.13	0.51	80	3	0.20	5	2	0.00	1	-	-	-	-
02-069	12:20	247.7	37.36	0.30	47	1	-	-	-	-	-	-	-	-	-
02-106	03:02	312.8	36.61	0.48	23	-	-	-	-	-	-	-	-	-	-
02-151	13:43	346.5	45.44	0.17	29	1	0.00	1	-	-	-	-	-	-	-
02-184	10:32	343.9	32.86	0.27	22	-	-	-	-	-	-	-	-	-	-
02-222	06:37	312.7	37.83	0.88	24	1	-	-	-	-	-	-	-	-	-
02-265	21:04	228.9	43.60	0.51	19	3	-	-	1	-	-	-	-	-	-
02-306	10:19	42.73	40.55	0.06	18	-	0.00	1	-	-	-	1	-	-	-
02-308	21:03	11.18	2.447	0.52	55	3	-	-	2	-	-	1	-	-	-
02-309	04:21	4.540	0.304	0.80	17	-	0.00	2	2	0.00	3	1	-	-	2
02-309	05:32	3.320	0.048	0.83	77	-	-	-	-	0.00	2	-	-	-	-
02-309	06:34	2.410	0.043	0.83	512	5	0.14	21	1	0.00	21	1	0.00	15	5
02-323	16:36	121.7	14.41	0.67	9841	80	0.00	191	2	0.00	46	-	0.00	62	2
02-357	20:16	245.2	34.15	0.04	92	6	-	-	-	-	-	-	-	-	1
03-066	18:08	357.0	73.91	0.86	11	1	-	-	-	-	-	-	-	-	2
03-262	11:23	38.06	195.7	0.00	28	1	0.00	2	5	0.00	1	-	-	-	1
03-264	14:11	7.190	2.117	0.00	36	-	0.00	14	1	-	-	-	0.00	1	1
03-264	15:43	5.500	0.063	0.53	41	-	-	-	1	0.00	1	2	-	-	1
03-264	17:59	2.540	0.094	0.53	124	-	0.00	45	8	0.42	26	10	0.12	68	36
Events (counted)				-	284545	20976	-	372	45	-	107	23	-	163	59
Impacts (complete data)				-	3291	1865	-	68	38	-	36	16	-	26	28
All events(complete data)				0.22	4229	1865	0.28	95	41	0.05	38	16	0.07	28	28

∗: AC21 and AC31: Overflows of the 8 bit accumulators were counted with overflow counters so that no unrecognized overflows occurred in these two channels.
f_{noi} has been estimated from the data sets transmitted.

Table 7: DPF data: No., impact time, TEV (in minutes) CLN, AR, SEC, IA, EA, CA, IT, ET, EIT, EIC, ICC, PA, PET, EVD, ICP, ECP, CCP, PCP, HV and evaluated data: LON, LAT, D_{Jup} (in R_J), rotation angle (ROT), instr. pointing (S_{LON}, S_{LAT}), speed v (in $km\,s^{-1}$), speed error factor (VEF), mass m (in g) and mass error factor (MEF). Velocity and mass should be considered as lower and upper limits for the true values, respectively, because of the strong degradation of the dust instrument electronics (see text for details).

No.	IMP. DATE	TEV	CLN	AR	SEC	IA	EA	CA	IT	ET	EIT	EIC	ICC	PA	PET	EVD	ICP	ECP	CCP	PCP	HV	LON	LAT	D_{Jup}	ROT	S_{LON}	S_{LAT}	V	VEF	M	MEF
15881	00-003 12:24:10	8	2	2	188	9	4	3	15	11	11	0	0	8	0	5	0	1	1	1	4	35.8	-1.2	12.631	186	17	-55	2.0	1.9	$3.9\cdot10^{-11}$	10.5
16010	00-004 02:52:43	8	3	3	133	20	23	22	11	10	8	0	1	41	0	5	0	1	1	1	4	35.9	-1.2	5.808	263	330	-5	5.2	1.9	$8.3\cdot10^{-11}$	10.3
16038	00-005 01:17:30	22	2	3	117	22	14	8	9	14	0	1	1	38	12	5	0	1	1	1	4	35.8	-1.2	16.274	285	331	12	7.2	1.9	$1.4\cdot10^{-11}$	10.5
16041	00-005 05:11:04	22	3	3	174	20	9	15	13	1	8	0	1	41	0	5	0	1	1	1	4	35.8	-1.2	18.306	205	353	-48	2.0	1.9	$3.8\cdot10^{-10}$	10.5
16042	00-005 05:48:29	259	3	2	111	8	27	9	14	15	8	0	1	47	1	5	0	1	1	1	4	35.8	-1.2	18.623	294	333	19	2.0	1.9	$9.6\cdot10^{-10}$	10.5
16047	00-006 06:18:37	22	3	2	153	13	21	19	12	11	8	0	1	38	0	5	0	1	1	1	4	35.9	-1.2	29.696	235	335	-28	4.5	1.9	$4.2\cdot10^{-11}$	10.5
16051	00-046 02:20:57	259	2	4	219	27	31	22	12	12	4	1	1	14	9	5	0	1	1	1	4	39.4	-1.1	65.806	142	71	-40	2.0	1.9	$2.6\cdot10^{-08}$	10.5
16052	00-050 01:15:31	259	3	4	21	30	50	4	13	12	9	0	1	27	0	5	0	1	1	1	4	39.9	-1.1	41.387	60	80	23	2.0	1.9	$8.6\cdot10^{-08}$	10.5
16066	00-052 19:13:01	22	3	2	196	10	49	4	12	12	7	0	1	25	1	5	0	1	1	1	4	40.3	-1.1	13.836	174	37	-55	4.5	1.9	$1.8\cdot10^{-10}$	10.5
16080	00-053 01:35:12	22	2	2	225	8	4	3	15	14	11	0	0	4	23	5	0	1	1	1	4	40.3	-1.1	10.244	134	76	-34	2.0	1.9	$3.3\cdot10^{-11}$	10.5
16082	00-053 01:56:26	22	2	2	236	9	21	5	15	15	12	0	0	9	28	5	0	1	1	1	4	40.3	-1.1	10.044	118	81	-22	2.0	1.9	$4.2\cdot10^{-10}$	10.5
16085	00-053 03:42:37	22	2	2	249	9	4	3	15	14	11	0	0	6	0	5	0	1	1	1	4	40.3	-1.1	9.055	100	84	-8	2.0	1.9	$3.9\cdot10^{-11}$	10.5
16103	00-053 17:01:24	8	2	2	149	9	11	5	14	15	0	1	1	47	31	5	0	1	1	1	4	40.4	-1.1	6.844	240	338	-23	2.1	1.6	$9.1\cdot10^{-11}$	6.0
16105	00-053 17:50:57	8	2	4	255	30	59	24	12	12	4	1	1	28	1	5	0	1	1	1	4	40.4	-1.1	7.202	91	84	-1	2.0	1.9	$5.0\cdot10^{-07}$	10.5
16107	00-053 18:33:25	8	3	4	143	30	30	28	12	10	5	0	1	46	0	5	0	1	1	1	4	40.4	-1.1	7.536	249	336	-17	2.0	1.9	$3.7\cdot10^{-08}$	10.5
16111	00-053 23:30:40	22	2	2	74	11	13	4	14	15	0	1	1	43	14	5	0	1	1	1	4	40.3	-1.1	10.247	346	10	52	2.1	1.6	$1.7\cdot10^{-10}$	6.0
16113	00-054 06:56:34	22	3	2	24	11	50	12	13	13	7	0	1	26	1	5	0	1	1	1	4	40.3	-1.1	14.540	56	79	26	2.3	1.9	$3.0\cdot10^{-09}$	10.5
16114	00-054 08:21:30	22	3	2	50	13	51	12	12	12	6	0	1	26	1	5	0	1	1	1	4	40.3	-1.1	15.337	20	54	49	4.5	1.9	$4.5\cdot10^{-10}$	10.5
16116	00-054 11:53:49	22	2	2	211	8	10	0	12	13	10	0	0	3	26	5	0	1	1	1	4	40.3	-1.1	17.284	153	62	-47	5.9	1.6	$2.0\cdot10^{-12}$	6.0
16117	00-054 13:18:45	22	3	4	157	30	54	25	13	12	5	0	1	46	0	5	0	1	1	1	4	40.3	-1.1	18.046	229	341	-32	2.0	1.9	$1.4\cdot10^{-07}$	10.5
16118	00-054 15:26:10	22	2	2	66	8	10	0	12	7	10	0	0	4	27	5	0	1	1	1	4	40.3	-1.1	19.167	357	25	54	15.9	3.7	$1.3\cdot10^{-13}$	106.8
16119	00-055 02:04:11	259	2	2	228	9	12	0	12	10	10	0	0	4	26	5	0	1	1	1	4	40.3	-1.1	24.470	129	79	-30	10.9	2.1	$5.5\cdot10^{-13}$	14.2
16121	00-058 01:55:34	22	3	2	45	11	15	15	14	15	6	0	1	42	8	5	0	1	1	1	4	40.5	-1.1	51.750	27	61	46	2.1	1.6	$2.3\cdot10^{-10}$	6.0
16123	00-063 04:11:32	259	2	2	167	8	10	0	12	11	11	0	0	2	22	5	0	1	1	1	4	40.8	-1.1	83.010	215	349	-42	9.5	1.7	$4.7\cdot10^{-13}$	7.6
16124	00-070 04:27:03	259	2	3	138	21	14	7	10	15	0	1	1	45	31	5	0	1	1	1	4	41.3	-1.1	112.177	256	335	-11	4.5	1.9	$5.1\cdot10^{-11}$	10.5
16125	00-109 08:54:08	259	2	2	68	8	14	0	13	14	7	0	0	38	1	5	0	1	1	1	4	44.7	-1.1	147.606	354	30	54	2.7	1.6	$4.8\cdot10^{-11}$	6.0
16127	00-121 09:56:42	259	2	2	178	13	22	14	14	15	15	0	1	17	1	5	0	1	1	1	4	46.0	-1.0	124.594	200	20	-50	2.0	1.9	$9.5\cdot10^{-10}$	10.5
16129	00-129 16:23:32	259	2	2	16	10	13	11	12	10	15	0	1	11	2	5	0	1	1	1	4	46.9	-1.0	96.258	68	98	18	10.9	2.1	$7.6\cdot10^{-13}$	14.2
16133	00-141 08:59:32	22	2	2	98	11	50	4	12	12	7	0	0	26	1	5	0	1	1	1	4	48.3	-1.0	15.647	312	360	33	4.5	1.9	$2.9\cdot10^{-10}$	10.5
16134	00-141 18:17:11	22	2	2	59	9	20	6	15	14	11	0	0	19	0	5	0	1	1	1	4	48.4	-1.0	10.473	7	56	54	2.0	1.9	$3.5\cdot10^{-10}$	10.5
16135	00-141 18:27:48	22	2	2	141	9	15	4	15	0	8	0	0	37	31	5	0	1	1	1	4	48.4	-1.0	10.377	252	352	-14	2.0	1.9	$2.3\cdot10^{-10}$	10.5
16283	00-195 19:58:14	259	3	3	69	20	21	11	10	11	6	0	1	13	1	5	0	1	1	1	5	51.9	-1.0	238.002	353	51	54	4.5	1.9	$9.3\cdot10^{-11}$	10.5
16366	00-219 15:53:18	22	2	2	194	8	4	10	13	14	11	0	0	6	31	5	0	1	1	1	5	53.9	-0.9	272.964	177	65	-55	2.3	1.9	$1.8\cdot10^{-11}$	10.5
18055	00-242 05:00:03	259	2	2	43	10	12	13	12	14	2	1	1	0	0	5	0	1	1	1	5	55.8	-0.9	288.137	30	104	45	3.8	1.6	$1.5\cdot10^{-11}$	6.0
18056	00-242 05:01:04	259	2	2	214	8	10	18	12	14	1	1	1	5	31	5	0	1	1	1	5	55.8	-0.9	288.137	149	106	-44	3.8	1.6	$7.9\cdot10^{-12}$	6.0
18880	00-253 17:06:45	259	2	2	39	8	3	14	12	10	0	1	1	3	31	5	0	1	1	1	5	56.8	-0.9	289.854	35	108	42	4.5	1.9	$1.5\cdot10^{-12}$	10.5
18897	00-260 04:24:34	259	3	2	75	8	14	7	13	14	6	0	1	37	0	5	0	1	1	1	5	57.4	-0.9	289.088	345	48	52	2.7	1.6	$4.8\cdot10^{-11}$	6.0
19332	00-363 15:50:50	22	3	2	61	10	49	7	13	13	7	0	1	26	1	5	0	1	1	1	5	68.2	-0.7	11.175	4	64	60	2.3	1.9	$1.8\cdot10^{-09}$	10.5
19344	00-364 01:45:21	22	2	2	166	9	12	3	15	14	13	0	0	8	7	5	0	1	1	1	5	68.2	-0.7	7.596	217	20	-36	2.5	1.6	$5.4\cdot10^{-11}$	6.0
19349	00-364 04:35:14	22	2	2	60	11	25	3	13	15	5	0	0	20	1	5	0	1	1	1	5	68.2	-0.7	7.539	6	67	60	2.3	1.9	$6.2\cdot10^{-10}$	10.5
19368	00-364 22:16:54	22	2	2	66	8	13	8	13	14	11	0	0	9	3	5	0	1	1	1	5	68.3	-0.7	14.891	357	53	60	2.7	1.6	$4.1\cdot10^{-11}$	6.0
19414	00-366 01:23:46	259	2	3	115	20	13	3	12	15	0	1	1	10	31	5	0	1	1	1	5	68.3	-0.7	28.040	288	2	18	2.0	1.9	$7.2\cdot10^{-10}$	10.5
20394	01-054 15:37:37	22	2	2	55	15	20	0	14	14	13	0	0	11	0	5	0	1	1	1	5	72.0	-0.6	209.299	13	78	52	2.5	1.6	$3.3\cdot10^{-10}$	6.0
20408	01-077 21:42:34	22	3	3	165	21	26	12	15	9	7	0	1	43	0	5	0	1	1	1	5	74.0	-0.5	215.070	218	19	-40	6.4	3.1	$8.2\cdot10^{-11}$	58.7
20415	01-092 19:28:24	259	2	2	242	8	4	4	10	14	11	0	0	3	31	5	0	1	1	1	5	75.4	-0.5	203.645	110	114	-15	9.7	1.9	$1.6\cdot10^{-13}$	10.5
20435	01-119 14:15:13	259	3	2	240	10	19	19	15	15	9	0	1	3	31	5	0	1	1	1	5	78.0	-0.5	147.493	113	125	-18	2.0	1.9	$3.4\cdot10^{-10}$	10.5
20451	01-143 07:42:40	259	3	2	132	11	49	3	12	13	7	0	1	26	1	5	0	1	1	1	5	80.9	-0.4	10.240	264	27	-2	4.5	1.9	$2.1\cdot10^{-10}$	10.5
20453	01-143 15:12:36	22	2	2	182	11	13	3	15	11	14	0	0	13	3	5	0	1	1	1	5	80.9	-0.4	7.491	194	63	-49	6.4	3.1	$4.1\cdot10^{-12}$	58.7
20455	01-143 16:58:47	64	2	2	238	10	30	5	12	11	7	0	1	26	1	5	0	1	1	1	5	81.0	-0.4	7.291	115	133	-18	4.5	1.9	$1.1\cdot10^{-10}$	10.5
20456	01-143 18:02:29	22	2	4	131	26	30	12	6	11	4	1	1	11	0	5	0	1	1	1	5	81.0	-0.4	7.287	266	27	-1	12.1	1.6	$5.9\cdot10^{-11}$	6.0

No.	IMP. DATE	TEV	CLN	AR	SEC	IA	EA	CA	IT	ET	EIT	EIC	ICC	PA	PET	EVD	ICP	ECP	CCP	PCP	HV	LON	LAT	D_{Jup}	ROT	S_{LON}	S_{LAT}	V	VEF	M	MEF
20458	01-143 18:23:43	22	2	2	136	8	21	3	13	11	6	0	0	10	1	5	0	1	1	1	5	81.0	-0.4	7.306	259	27	-7	2.3	1.9	$1.9\cdot10^{-10}$	10.5
20461	01-143 23:20:58	22	2	4	83	30	9	24	13	0	4	1	1	28	1	5	0	1	1	1	5	81.0	-0.4	8.473	333	47	49	2.0	1.9	$1.9\cdot10^{-09}$	10.5
20467	01-144 02:53:19	22	2	2	55	11	5	3	12	15	15	0	1	26	0	5	0	1	1	1	5	81.0	-0.4	9.998	13	100	55	4.5	1.9	$3.2\cdot10^{-12}$	10.5
20472	01-144 04:18:15	22	2	2	76	11	30	5	12	11	7	0	0	26	1	5	0	1	1	1	5	81.0	-0.4	10.687	343	58	54	4.5	1.9	$1.3\cdot10^{-10}$	10.5
20475	01-144 05:21:57	22	2	2	25	12	31	13	12	13	7	0	1	26	1	5	0	1	1	1	5	81.0	-0.4	11.220	55	132	30	4.5	1.9	$1.7\cdot10^{-10}$	10.5
20478	01-144 09:35:57	259	2	2	235	8	51	3	13	13	8	0	0	26	1	5	0	1	1	1	5	81.0	-0.4	13.423	120	132	-21	2.3	1.9	$2.1\cdot10^{-09}$	10.5
20482	01-144 22:32:29	259	3	2	55	10	22	3	12	15	5	0	1	5	0	5	0	1	1	1	5	81.0	-0.4	20.129	13	100	55	4.5	1.9	$3.0\cdot10^{-11}$	10.5
20487	01-145 07:11:10	22	2	2	187	8	30	3	13	12	7	0	0	25	8	5	0	1	1	1	5	81.0	-0.4	24.328	187	72	-51	2.3	1.9	$8.0\cdot10^{-10}$	10.5
20540	01-149 10:24:05	259	2	2	27	15	7	8	0	15	13	0	0	5	31	5	0	1	1	1	5	81.2	-0.4	58.949	52	131	32	11.8	11.8	$5.2\cdot10^{-13}$	5858.3
20624	01-196 12:40:34	259	3	2	252	13	22	18	13	11	8	0	1	40	0	5	0	1	1	1	5	84.9	-0.3	120.888	96	144	-4	2.3	1.9	$5.1\cdot10^{-10}$	10.5
20671	01-205 12:23:30	259	2	2	229	8	4	3	13	14	11	0	0	4	31	5	0	1	1	1	5	85.8	-0.3	94.336	128	141	-29	2.3	1.9	$1.8\cdot10^{-11}$	10.5
20688	01-212 21:15:24	259	3	3	212	23	10	5	14	3	10	0	1	26	3	5	0	1	1	1	5	86.6	-0.3	56.506	152	127	-45	2.0	1.9	$7.5\cdot10^{-10}$	10.5
20691	01-217 04:47:40	259	3	4	218	27	30	27	8	12	6	0	1	59	0	5	0	1	1	1	5	87.2	-0.3	17.719	143	133	-40	5.6	1.6	$6.1\cdot10^{-10}$	6.0
20692	01-217 06:09:54	259	3	2	208	8	26	12	14	15	7	0	1	47	1	5	0	1	1	1	5	87.2	-0.3	16.987	158	121	-48	2.0	1.9	$8.2\cdot10^{-10}$	10.5
20693	01-217 08:45:16	22	2	2	14	9	13	0	15	1	10	0	0	39	0	5	0	1	1	1	5	87.2	-0.3	15.577	70	146	16	11.8	9.5	$5.4\cdot10^{-13}$	2690.1
20694	01-217 13:21:19	22	3	4	228	27	30	24	8	11	5	0	1	47	0	5	0	1	1	1	5	87.2	-0.3	12.994	129	141	-30	8.6	1.6	$1.6\cdot10^{-10}$	6.0
20695	01-217 14:25:01	22	3	2	230	12	20	5	15	13	5	0	1	47	11	5	0	1	1	1	5	87.3	-0.3	12.386	127	142	-28	2.0	1.9	$5.7\cdot10^{-10}$	10.5
20696	01-217 15:28:43	22	2	2	40	8	31	4	13	14	8	0	0	26	1	5	0	1	1	1	5	87.3	-0.3	11.775	34	131	43	2.3	1.9	$9.2\cdot10^{-10}$	10.5
20697	01-217 17:57:20	22	2	3	130	22	25	14	15	15	0	1	1	17	29	5	0	1	1	1	5	87.3	-0.3	10.349	267	38	-1	2.5	1.6	$1.8\cdot10^{-09}$	6.0
20698	01-217 22:12:09	22	3	2	214	11	30	4	12	11	7	0	1	26	1	5	0	1	1	1	5	87.3	-0.3	8.007	149	129	-44	4.5	1.9	$1.3\cdot10^{-10}$	10.5
20701	01-217 22:54:37	22	3	2	63	11	22	4	12	15	6	0	1	7	0	5	0	1	1	1	5	87.3	-0.3	7.652	1	95	55	4.5	1.9	$3.5\cdot10^{-11}$	10.5
20714	01-218 06:41:45	22	2	4	143	30	60	24	13	13	4	1	1	28	1	5	0	1	1	1	5	87.4	-0.3	6.111	249	39	-16	2.0	1.9	$6.8\cdot10^{-07}$	10.5
20715	01-218 07:02:59	22	2	2	225	8	21	3	13	11	6	0	0	10	1	5	0	1	1	1	5	87.4	-0.3	6.187	134	139	-34	2.3	1.9	$1.9\cdot10^{-10}$	10.5
20716	01-218 07:24:13	22	2	4	215	30	4	24	13	15	15	0	1	27	0	5	0	1	1	1	5	87.4	-0.3	6.276	148	130	-43	2.0	1.9	$8.2\cdot10^{-10}$	10.5
20717	01-218 07:45:27	22	2	2	221	15	21	4	0	11	14	0	0	10	1	5	0	1	1	1	5	87.4	-0.3	6.377	139	136	-38	7.7	2.0	$1.0\cdot10^{-11}$	12.5
20727	01-219 00:02:10	22	2	2	248	8	6	3	15	12	10	0	0	3	0	5	0	1	1	1	5	87.4	-0.3	15.000	101	147	-8	2.0	1.9	$4.6\cdot10^{-11}$	10.5
20752	01-228 03:57:12	259	2	2	24	8	14	10	14	14	12	0	0	39	0	5	0	1	1	1	5	87.9	-0.3	82.021	56	146	27	2.5	1.6	$6.3\cdot10^{-11}$	6.0
20764	01-244 21:09:41	259	3	3	54	22	28	10	15	7	5	0	1	46	1	5	0	1	1	1	5	89.1	-0.2	126.938	14	116	52	7.9	4.6	$7.0\cdot10^{-11}$	211.2
20807	01-288 14:31:31	22	2	4	176	29	28	24	13	11	0	1	1	1	14	5	0	1	1	1	5	93.3	-0.1	9.456	203	75	-48	2.0	1.9	$2.4\cdot10^{-08}$	10.5
20808	01-288 15:56:27	22	2	3	28	23	24	23	15	12	0	1	1	43	10	5	0	1	1	1	5	93.3	-0.1	8.655	51	151	31	2.0	1.9	$4.9\cdot10^{-09}$	10.5
20809	01-288 15:56:27	22	2	4	47	30	29	24	13	10	0	1	1	11	10	5	0	1	1	1	5	93.3	-0.1	8.655	24	133	48	2.0	1.9	$3.3\cdot10^{-08}$	10.5
20821	01-289 15:39:06	22	3	2	167	9	49	7	14	13	9	0	1	26	1	5	0	1	1	1	5	93.5	-0.2	13.175	215	64	-41	2.0	1.9	$2.9\cdot10^{-09}$	10.5
20823	01-289 18:07:43	22	2	2	71	8	12	10	15	15	12	0	0	15	28	5	0	1	1	1	5	93.5	-0.2	14.603	350	90	54	2.1	1.6	$9.0\cdot10^{-11}$	6.0
20824	01-290 05:05:57	22	2	3	32	21	22	7	14	11	0	1	1	46	30	5	0	1	1	1	5	93.5	-0.2	20.551	45	149	35	2.0	1.9	$2.4\cdot10^{-09}$	10.5
20825	01-290 05:27:11	22	3	2	146	8	50	10	14	14	9	0	1	26	1	5	0	1	1	1	5	93.5	-0.2	20.733	245	51	-20	2.0	1.9	$3.4\cdot10^{-09}$	10.5
20826	01-290 05:48:25	22	2	2	183	8	12	2	13	14	9	0	0	11	4	5	0	1	1	1	5	93.5	-0.2	20.914	193	86	-52	2.7	1.6	$3.4\cdot10^{-11}$	6.0
20863	01-316 01:32:08	259	2	2	21	8	6	6	13	15	11	0	0	4	31	5	0	1	1	1	5	95.1	-0.1	141.637	60	155	24	2.3	1.9	$2.5\cdot10^{-11}$	10.5
20867	01-332 14:25:42	259	2	2	238	14	22	14	14	9	0	1	1	59	27	5	0	1	1	1	6	96.4	-0.1	160.228	115	156	-20	2.0	1.9	$1.1\cdot10^{-09}$	10.5
20877	02-002 19:59:10	259	2	4	107	24	22	14	15	6	0	1	1	19	19	5	0	1	1	1	6	99.5	0.0	107.169	300	48	24	2.0	1.9	$4.1\cdot10^{-09}$	10.5
20890	02-015 08:17:10	8	2	4	20	30	53	26	14	13	0	1	1	11	4	5	0	1	1	1	6	100.9	0.0	33.272	62	149	23	2.0	1.9	$1.2\cdot10^{-07}$	10.5
20891	02-015 13:28:34	8	3	3	45	22	25	12	11	11	9	0	1	42	0	5	0	1	1	1	6	100.9	0.0	31.075	27	130	47	4.2	1.6	$3.2\cdot10^{-10}$	6.0
20892	02-016 22:44:31	8	2	2	234	11	4	12	14	13	0	1	1	45	28	5	0	1	1	1	6	101.2	0.0	14.523	121	148	-24	2.0	1.9	$5.3\cdot10^{-11}$	10.5
20893	02-017 02:38:04	8	3	4	0	24	29	21	15	9	5	0	1	46	1	5	0	1	1	1	6	101.2	0.0	12.217	999	999	999	6.4	3.1	$2.2\cdot10^{-10}$	58.7
20897	02-017 07:56:35	8	3	4	236	29	29	19	11	11	5	0	1	46	0	5	0	1	1	1	6	101.2	0.0	9.006	118	149	-22	2.3	1.9	$1.5\cdot10^{-08}$	10.5
20899	02-017 08:39:03	8	3	4	227	24	27	25	15	11	9	0	1	9	0	5	0	1	1	1	6	101.2	0.0	8.586	131	144	-31	3.9	1.6	$7.6\cdot10^{-10}$	6.0
20900	02-017 10:46:26	22	3	2	125	9	29	5	12	10	7	0	1	26	1	5	0	1	1	1	6	101.3	0.0	7.384	274	42	3	4.5	1.9	$8.1\cdot10^{-11}$	10.5
20902	02-017 18:03:14	259	2	4	78	26	4	9	6	15	15	0	1	25	0	5	0	1	1	1	6	101.3	0.0	5.741	340	71	50	19.0	1.9	$3.3\cdot10^{-13}$	10.5
20903	02-018 03:22:22	22	2	2	224	11	11	6	12	13	10	0	0	5	31	5	0	1	1	1	6	101.4	0.0	10.567	135	142	-34	4.5	1.9	$8.8\cdot10^{-12}$	10.5
20904	02-018 03:43:36	22	3	2	178	8	49	4	13	14	8	0	1	26	1	5	0	1	1	1	6	101.4	0.0	10.787	200	72	-49	2.3	1.9	$1.3\cdot10^{-09}$	10.5
20905	02-018 05:29:46	8	2	2	185	8	14	5	13	14	5	0	0	43	1	5	0	1	1	1	6	101.4	0.0	11.885	190	83	-53	2.7	1.6	$4.8\cdot10^{-11}$	6.0
20907	02-019 03:40:25	8	2	3	40	17	15	13	12	0	13	0	1	26	1	5	0	1	1	1	6	101.4	0.0	24.398	34	136	43	2.0	1.9	$6.6\cdot10^{-10}$	10.5
20997	02-143 00:49:36	22	2	2	185	9	5	10	12	15	11	0	0	5	31	5	0	1	1	1	6	110.6	0.3	343.589	190	88	-53	4.5	1.9	$2.3\cdot10^{-12}$	10.5
21041	02-270 02:38:21	22	2	2	15	12	8	12	13	15	0	1	1	14	31	5	0	1	1	1	6	121.4	0.5	216.955	69	182	17	2.3	1.9	$6.7\cdot10^{-11}$	10.5
21046	02-292 00:55:21	22	3	3	13	22	29	12	15	9	6	0	1	46	1	5	0	1	1	1	6	123.4	0.5	135.606	72	191	15	2.0	1.9	$9.2\cdot10^{-09}$	10.5
21075	02-308 16:48:59	22	3	3	13	23	27	25	15	9	8	0	1	35	31	5	0	1	1	1	6	125.1	0.6	14.372	72	191	15	6.4	3.1	$1.4\cdot10^{-10}$	58.7

No.	IMP. DATE	TEV	CLN	AR	SEC	IA	EA	CA	IT	ET	EIT	EIC	ICC	PA	PET	EVD	ICP	ECP	CCP	PCP	HV	LON	LAT	D_{Jup}	ROT	S_{LON}	S_{LAT}	V	VEF	M	MEF
21076	02-308 16:48:59	22	3	2	107	9	50	4	14	14	8	0	1	26	1	5	0	1	1	1	6	125.1	0.6	14.372	300	86	24	2.0	1.9	$4.1 \cdot 10^{-09}$	10.5
21078	02-308 20:00:06	22	3	2	244	9	14	12	13	14	7	0	1	4	12	5	0	1	1	1	6	125.1	0.6	12.002	107	191	-13	2.7	1.6	$5.7 \cdot 10^{-11}$	6.0
21079	02-308 22:28:43	259	3	2	239	12	21	14	13	12	9	0	1	38	0	5	0	1	1	1	6	125.2	0.6	10.014	114	190	-19	2.3	1.9	$3.7 \cdot 10^{-10}$	10.5
21080	02-308 22:51:23	259	2	3	98	23	15	26	15	15	0	1	1	40	31	5	0	1	1	1	6	125.2	0.6	9.698	312	91	33	2.0	1.9	$1.6 \cdot 10^{-09}$	10.5
21081	02-308 22:51:52	259	3	4	27	29	30	27	12	12	5	0	1	46	1	5	0	1	1	1	6	125.2	0.6	9.691	52	186	30	2.0	1.9	$3.1 \cdot 10^{-08}$	10.5
21082	02-308 22:52:53	259	3	4	240	29	30	25	12	12	9	0	1	46	1	5	0	1	1	1	6	125.2	0.6	9.676	113	190	-17	2.0	1.9	$3.1 \cdot 10^{-08}$	10.5
21085	02-309 02:22:17	22	3	2	235	11	21	18	13	12	8	0	1	40	0	5	0	1	1	1	6	125.2	0.6	6.530	120	189	-23	2.3	1.9	$3.1 \cdot 10^{-10}$	10.5
21087	02-309 02:44:49	2	2	3	52	22	27	8	13	15	15	0	1	23	3	5	0	1	1	1	6	125.2	0.6	6.164	17	160	51	2.5	1.6	$2.5 \cdot 10^{-09}$	6.0
21088	02-309 03:10:28	2	2	2	245	11	13	9	6	15	15	0	1	8	5	5	0	1	1	1	6	125.2	0.6	5.740	105	191	-12	9.5	5.0	$1.2 \cdot 10^{-12}$	282.4
21089	02-309 03:21:48	2	3	3	234	21	25	22	15	15	7	0	1	44	0	5	0	1	1	1	6	125.2	0.6	5.550	121	188	-24	2.5	1.6	$1.5 \cdot 10^{-09}$	6.0
21090	02-309 04:13:33	104	2	3	232	22	25	22	15	15	0	1	1	42	9	5	0	1	1	1	6	125.2	0.6	4.665	124	187	-26	2.5	1.6	$1.8 \cdot 10^{-09}$	6.0
21091	02-309 04:30:41	2	1	2	66	9	9	22	15	4	0	1	0	44	27	5	0	1	1	1	6	125.2	0.6	4.366	357	133	55	2.0	1.9	$9.0 \cdot 10^{-11}$	10.5
21093	02-309 05:05:18	2	2	3	82	21	22	20	14	10	0	1	1	46	27	5	0	1	1	1	6	125.2	0.6	3.759	335	106	48	2.0	1.9	$2.4 \cdot 10^{-09}$	10.5
21095	02-309 05:19:00	2	2	3	25	22	23	3	11	13	12	0	0	46	4	5	0	1	1	1	6	125.2	0.6	3.519	55	187	28	2.3	1.9	$1.9 \cdot 10^{-09}$	10.5
21097	02-309 05:29:23	2	1	2	26	8	14	2	15	15	0	1	0	44	14	5	0	1	1	1	6	125.2	0.6	3.339	53	186	29	2.1	1.6	$1.3 \cdot 10^{-10}$	6.0
21098	02-309 05:34:43	2	3	4	24	24	3	12	15	15	10	0	1	6	3	5	0	1	1	1	6	125.2	0.6	3.247	56	187	27	2.0	1.9	$2.8 \cdot 10^{-10}$	10.5
21099	02-309 05:36:36	2	2	2	221	9	21	7	11	12	15	0	1	17	2	5	0	1	1	1	6	125.2	0.6	3.215	139	181	-38	7.2	1.9	$5.0 \cdot 10^{-12}$	10.5
21100	02-309 05:37:35	2	2	4	234	28	30	25	12	11	0	1	1	22	11	5	0	1	1	1	6	125.2	0.6	3.198	121	188	-24	3.9	1.6	$2.1 \cdot 10^{-09}$	6.0
21102	02-309 05:39:32	2	1	2	237	9	13	20	14	15	15	0	0	11	6	5	0	1	1	1	6	125.2	0.6	3.165	117	189	-21	2.1	1.6	$1.3 \cdot 10^{-10}$	6.0
21104	02-309 05:39:32	2	2	3	217	22	10	3	15	15	15	0	1	17	5	5	0	1	1	1	6	125.2	0.6	3.165	145	177	-41	2.0	1.9	$6.3 \cdot 10^{-10}$	10.5
21107	02-309 05:42:19	2	1	2	212	8	6	18	13	6	15	0	0	7	6	5	0	1	1	1	6	125.2	0.6	3.117	152	172	-45	2.3	1.9	$2.5 \cdot 10^{-11}$	10.5
21108	02-309 05:43:01	2	2	4	30	24	21	24	13	14	0	1	1	49	31	5	0	1	1	1	6	125.2	0.6	3.106	48	184	33	2.0	1.9	$3.5 \cdot 10^{-09}$	10.5
21109	02-309 05:43:01	2	2	3	190	21	13	5	15	13	0	1	1	42	31	5	0	1	1	1	6	125.2	0.6	3.106	183	133	-54	2.0	1.9	$8.2 \cdot 10^{-10}$	10.5
21110	02-309 05:45:57	2	3	4	244	30	57	24	13	15	5	0	1	46	0	5	0	1	1	1	6	125.2	0.6	3.056	107	191	-13	2.0	1.9	$2.4 \cdot 10^{-07}$	10.5
21112	02-309 05:49:51	2	2	3	26	19	9	4	15	14	0	1	1	46	27	5	0	1	1	1	6	125.2	0.6	2.991	53	186	29	2.0	1.9	$3.4 \cdot 10^{-10}$	10.5
21113	02-309 05:50:50	2	2	4	32	30	57	27	13	15	0	1	1	26	6	5	0	1	1	1	6	125.2	0.6	2.975	45	183	35	2.0	1.9	$2.4 \cdot 10^{-07}$	10.5
21114	02-309 05:51:49	2	2	3	45	23	25	18	15	15	0	1	1	46	9	5	0	1	1	1	6	125.2	0.6	2.958	27	170	47	2.5	1.6	$2.2 \cdot 10^{-09}$	6.0
21116	02-309 05:53:46	2	2	3	40	21	24	13	13	12	6	0	1	17	19	5	0	1	1	1	6	125.2	0.6	2.926	34	176	43	2.5	1.6	$1.3 \cdot 10^{-09}$	6.0
21117	02-309 05:53:46	2	1	2	22	8	18	18	15	1	0	1	0	41	8	5	0	1	1	1	6	125.2	0.6	2.926	59	188	25	2.0	1.9	$2.3 \cdot 10^{-10}$	10.5
21118	02-309 05:54:45	2	2	3	24	21	24	19	13	15	0	1	1	23	15	5	0	1	1	1	6	125.2	0.6	2.910	56	187	27	2.5	1.6	$1.3 \cdot 10^{-09}$	6.0
21119	02-309 05:56:43	2	2	3	71	23	21	11	14	15	15	0	1	23	2	5	0	1	1	1	6	125.2	0.6	2.878	350	124	54	2.0	1.9	$3.0 \cdot 10^{-09}$	10.5
21120	02-309 05:56:43	2	1	2	221	9	7	3	15	15	0	1	0	11	31	5	0	1	1	1	6	125.2	0.6	2.878	139	181	-38	2.0	1.9	$6.5 \cdot 10^{-11}$	10.5
21121	02-309 05:57:40	2	3	4	224	26	9	26	9	1	10	0	1	17	1	5	0	1	1	1	6	125.2	0.6	2.862	135	183	-35	7.2	1.9	$1.2 \cdot 10^{-11}$	10.5
21122	02-309 05:59:38	2	2	3	148	20	21	8	14	15	0	1	1	46	31	5	0	1	1	1	6	125.2	0.6	2.831	242	86	-22	2.0	1.9	$1.8 \cdot 10^{-09}$	10.5
21123	02-309 05:59:38	2	2	2	36	12	7	3	15	3	13	0	0	19	3	5	0	1	1	1	6	125.2	0.6	2.831	39	179	39	2.0	1.9	$1.1 \cdot 10^{-10}$	10.5
21124	02-309 06:00:36	2	2	4	229	26	30	26	12	12	0	1	1	18	9	5	0	1	1	1	6	125.2	0.6	2.815	128	186	-29	2.5	1.6	$7.3 \cdot 10^{-09}$	6.0
21127	02-309 06:03:06	2	2	2	196	9	15	6	11	0	15	0	1	18	4	5	0	1	1	1	6	125.2	0.6	2.775	174	145	-54	7.2	1.9	$2.6 \cdot 10^{-12}$	10.5
21128	02-309 06:05:04	2	1	2	12	13	11	25	15	3	0	1	0	41	28	5	0	1	1	1	6	125.2	0.6	2.744	73	191	14	2.0	1.9	$2.4 \cdot 10^{-10}$	10.5
21130	02-309 06:08:01	2	2	4	42	24	28	28	12	14	0	1	1	20	10	5	0	1	1	1	6	125.2	0.6	2.698	31	174	44	2.5	1.6	$4.1 \cdot 10^{-09}$	6.0
21131	02-309 06:09:00	2	2	3	29	23	26	25	15	10	6	0	1	9	7	5	0	1	1	1	6	125.2	0.6	2.683	49	185	32	4.9	2.1	$2.9 \cdot 10^{-10}$	14.3
21133	02-309 06:09:58	2	2	4	30	27	27	25	11	11	0	1	1	21	12	5	0	1	1	1	6	125.2	0.6	2.668	48	184	33	2.3	1.9	$8.1 \cdot 10^{-09}$	10.5
21135	02-309 06:16:48	2	2	3	226	20	22	12	13	12	8	0	1	12	7	5	0	1	1	1	6	125.2	0.6	2.565	132	184	-33	2.5	1.6	$7.8 \cdot 10^{-10}$	6.0
21137	02-309 06:16:48	2	2	2	38	8	12	13	15	14	0	1	1	44	20	5	0	1	1	1	6	125.2	0.6	2.565	37	178	41	2.5	1.6	$4.5 \cdot 10^{-11}$	6.0
21138	02-309 06:17:47	2	2	4	43	28	28	25	12	12	0	1	1	62	15	5	0	1	1	1	6	125.2	0.6	2.551	30	172	45	2.0	1.9	$2.0 \cdot 10^{-08}$	10.5
21139	02-309 06:17:47	2	2	3	226	20	21	19	14	13	0	1	1	25	20	5	0	1	1	1	6	125.2	0.6	2.551	132	184	-33	2.0	1.9	$1.8 \cdot 10^{-09}$	10.5
21140	02-309 06:17:47	2	2	2	213	12	11	14	15	12	0	1	1	46	22	5	0	1	1	1	6	125.2	0.6	2.551	150	173	-45	2.0	1.9	$2.0 \cdot 10^{-10}$	10.5
21141	02-309 06:18:44	2	2	3	31	22	8	10	13	3	9	0	1	5	5	5	0	1	1	1	6	125.2	0.6	2.537	46	183	34	2.0	1.9	$4.5 \cdot 10^{-10}$	10.5
21143	02-309 06:18:44	2	2	2	230	12	20	3	14	14	13	0	0	37	6	5	0	1	1	1	6	125.2	0.6	2.537	127	186	-28	2.0	1.9	$5.7 \cdot 10^{-10}$	10.5
21144	02-309 06:19:43	2	2	2	198	13	21	3	15	14	14	0	0	4	15	5	0	1	1	1	6	125.2	0.6	2.523	172	149	-53	2.0	1.9	$8.1 \cdot 10^{-10}$	10.5
21145	02-309 06:20:42	2	1	2	32	9	11	4	13	12	15	0	0	20	3	5	0	1	1	1	6	125.2	0.6	2.508	45	183	35	5.2	1.9	$4.1 \cdot 10^{-12}$	10.3
21146	02-309 06:20:42	2	2	4	44	30	56	26	13	15	0	1	1	26	6	5	0	1	1	1	6	125.2	0.6	2.508	28	171	46	2.0	1.9	$2.0 \cdot 10^{-07}$	10.5
21147	02-309 06:20:42	2	3	3	173	21	5	7	14	1	10	0	1	13	5	5	0	1	1	1	6	125.2	0.6	2.508	207	105	-46	2.0	1.9	$2.2 \cdot 10^{-10}$	10.5
21148	02-309 06:21:40	2	2	4	51	26	27	15	14	15	3	1	1	52	5	5	0	1	1	1	6	125.2	0.6	2.495	18	161	51	2.0	1.9	$1.3 \cdot 10^{-08}$	10.5
21149	02-309 06:22:20	2	3	2	207	9	20	20	14	15	14	0	1	8	4	5	0	1	1	1	6	125.2	0.6	2.485	159	165	-49	2.0	1.9	$3.5 \cdot 10^{-10}$	10.5
21150	02-309 06:22:20	2	2	3	163	23	14	7	15	15	0	1	1	46	31	5	0	1	1	1	6	125.2	0.6	2.485	221	94	-38	2.0	1.9	$1.4 \cdot 10^{-09}$	10.5

No.	IMP. DATE	TEV	CLN	AR	SEC	IA	EA	CA	IT	ET	EIT	EIC	ICC	PA	PET	EVD	ICP	ECP	CCP	PCP	HV	LON	LAT	D_{Jup}	ROT	S_{LON}	S_{LAT}	V	VEF	M	MEF
21151	02-309 06:23:19	2	2	2	30	9	13	5	15	15	10	0	1	6	5	5	0	1	1	1	6	125.2	0.6	2.471	48	184	33	2.1	1.6	$1.3\cdot10^{-10}$	6.0
21152	02-309 06:24:20	2	2	3	67	23	6	28	14	3	15	0	1	17	5	5	0	1	1	1	6	125.2	0.6	2.457	356	132	55	2.0	1.9	$3.9\cdot10^{-10}$	10.5
21153	02-309 06:25:19	2	2	4	245	26	14	5	15	10	14	0	1	27	1	5	0	1	1	1	6	125.2	0.6	2.444	105	191	-12	2.0	1.9	$2.3\cdot10^{-09}$	10.5
21154	02-309 06:25:19	2	1	2	209	8	9	12	15	15	0	1	0	43	31	5	0	1	1	1	6	125.2	0.6	2.444	156	168	-48	2.0	1.9	$7.5\cdot10^{-11}$	10.5
21155	02-309 06:26:25	2	2	2	185	13	0	13	15	15	0	1	1	0	31	5	0	1	1	1	6	125.2	0.6	2.429	190	124	-53	2.0	1.9	$7.4\cdot10^{-10}$	10.5
21156	02-309 06:27:46	2	2	4	206	27	28	21	14	14	0	1	1	62	18	5	0	1	1	1	6	125.2	0.6	2.410	160	163	-50	2.0	1.9	$1.8\cdot10^{-08}$	10.5
21157	02-309 06:28:25	2	2	2	181	12	7	15	15	0	0	1	1	43	28	5	0	1	1	1	6	125.2	0.6	2.402	195	117	-51	2.0	1.9	$1.1\cdot10^{-10}$	10.5
21158	02-309 06:28:40	2	2	4	242	25	26	19	11	12	0	1	1	58	10	5	0	1	1	1	6	125.2	0.6	2.398	110	191	-15	2.3	1.9	$5.1\cdot10^{-09}$	10.5
21159	02-309 06:29:27	2	1	2	237	8	10	18	15	14	0	1	0	43	31	5	0	1	1	1	6	125.2	0.6	2.388	117	189	-21	2.5	1.6	$3.3\cdot10^{-11}$	6.0
21160	02-309 06:29:27	2	2	3	0	21	11	11	14	15	0	1	1	18	29	5	0	1	1	1	6	125.2	0.6	2.388	999	999	999	2.0	1.9	$5.9\cdot10^{-10}$	10.5
21161	02-309 06:29:41	2	2	4	183	25	21	13	15	14	0	1	1	24	31	5	0	1	1	1	6	125.2	0.6	2.385	193	120	-52	2.0	1.9	$4.0\cdot10^{-09}$	10.5
21162	02-309 06:30:30	2	2	2	162	11	6	4	12	11	10	0	0	10	28	5	0	1	1	1	6	125.2	0.6	2.374	222	94	-37	4.5	1.9	$3.9\cdot10^{-12}$	10.5
21163	02-309 06:30:38	2	2	3	211	22	23	18	12	12	0	0	0	61	14	5	0	1	1	1	6	125.2	0.6	2.372	153	170	-46	2.0	1.9	$3.5\cdot10^{-09}$	10.5
21164	02-309 06:31:12	2	1	2	223	9	4	4	15	15	0	1	0	7	29	5	0	1	1	1	6	125.2	0.6	2.365	136	182	-36	2.0	1.9	$3.9\cdot10^{-11}$	10.5
21165	02-309 06:31:43	5	3	4	218	30	12	22	14	4	10	0	1	11	1	5	0	1	1	1	6	125.2	0.6	2.358	143	178	-40	2.0	1.9	$3.0\cdot10^{-09}$	10.5
21166	02-309 06:32:28	2	2	2	159	10	6	3	15	15	0	1	1	5	31	5	0	1	1	1	6	125.2	0.6	2.349	226	91	-34	2.0	1.9	$6.4\cdot10^{-11}$	10.5
21167	02-309 06:32:41	2	2	3	246	22	23	10	12	12	0	1	1	27	15	5	0	1	1	1	6	125.2	0.6	2.346	104	192	-11	2.0	1.9	$3.5\cdot10^{-09}$	10.5
21169	02-309 06:33:45	2	3	4	212	30	49	27	14	15	12	0	1	25	1	5	0	1	1	1	6	125.2	0.6	2.333	152	172	-45	2.0	1.9	$6.1\cdot10^{-08}$	10.5
21171	02-309 06:34:38	2	2	3	48	21	20	14	14	13	0	1	1	18	18	5	0	1	1	1	6	125.2	0.6	2.322	23	166	49	2.0	1.9	$1.7\cdot10^{-09}$	10.5
21172	02-309 06:34:46	2	2	4	21	30	14	20	14	13	15	0	1	28	4	5	0	1	1	1	6	125.2	0.6	2.320	60	189	24	2.0	1.9	$4.2\cdot10^{-09}$	10.5
21174	02-309 07:30:05	259	2	2	217	11	29	11	11	10	15	0	1	26	1	5	0	1	1	1	6	125.2	0.6	1.992	145	177	-41	7.2	1.9	$2.5\cdot10^{-11}$	10.5
21175	02-309 07:30:23	259	2	3	31	20	15	19	14	0	14	0	1	25	3	5	0	1	1	1	6	125.2	0.6	1.992	46	183	34	2.0	1.9	$9.5\cdot10^{-10}$	10.5
21176	02-309 07:30:23	259	3	2	43	11	20	8	15	15	14	0	1	27	5	5	0	1	1	1	6	125.2	0.6	1.992	30	172	45	2.0	1.9	$4.8\cdot10^{-10}$	10.5
21178	02-309 07:30:23	259	3	4	57	27	12	24	14	6	13	0	1	27	5	5	0	1	1	1	6	125.2	0.6	1.992	10	151	54	2.0	1.9	$1.9\cdot10^{-09}$	10.5
21179	02-309 07:30:31	259	2	3	168	20	15	13	14	15	0	1	1	10	29	5	0	1	1	1	6	125.2	0.6	1.993	214	99	-42	2.0	1.9	$9.5\cdot10^{-10}$	10.5
21180	02-309 07:30:40	259	3	4	212	24	25	11	11	14	12	0	1	60	3	5	0	1	1	1	6	125.2	0.6	1.993	152	172	-45	2.3	1.9	$3.7\cdot10^{-09}$	10.5
21181	02-309 07:30:40	259	2	3	254	23	28	20	15	8	7	0	1	46	0	5	0	1	1	1	6	125.2	0.6	1.993	93	192	-1	7.3	3.9	$1.1\cdot10^{-10}$	128.4
21183	02-310 00:44:19	259	3	2	90	8	50	14	14	14	8	0	1	25	1	5	0	1	1	1	6	125.3	0.6	16.303	323	97	41	2.0	1.9	$3.4\cdot10^{-09}$	10.5
21202	02-329 06:20:41	259	3	4	235	24	28	26	15	12	11	0	1	44	0	5	0	1	1	1	6	126.7	0.6	148.699	120	189	-23	2.5	1.6	$4.1\cdot10^{-09}$	6.0
21207	03-030 00:00:00	95000	3	4	239	28	30	20	12	13	5	0	1	46	1	5	0	1	1	1	6	131.7	0.7	318.493	114	207	-16	2.5	1.6	$9.7\cdot10^{-09}$	6.0
21208	03-030 00:14:23	95000	3	4	6	25	30	24	15	12	5	0	1	35	31	5	0	1	1	1	6	131.7	0.7	318.508	82	210	9	2.5	1.6	$6.2\cdot10^{-09}$	6.0
21210	03-066 18:14:23	1020	3	4	17	24	29	13	15	12	6	0	1	46	1	5	0	1	1	1	6	134.6	0.8	357.009	66	209	22	2.5	1.6	$4.8\cdot10^{-09}$	6.0
21211	03-066 18:14:23	1020	2	2	41	11	23	7	13	15	7	0	0	43	1	5	0	1	1	1	6	134.6	0.8	357.009	32	195	47	2.3	1.9	$4.4\cdot10^{-10}$	10.5
21212	03-066 18:15:50	1020	3	2	234	13	24	10	13	15	6	0	1	44	1	5	0	1	1	1	6	134.6	0.8	357.010	121	205	-22	2.3	1.9	$7.3\cdot10^{-10}$	10.5
21213	03-067 15:07:11	1560	3	2	13	10	21	18	13	13	11	0	1	37	0	5	0	1	1	1	6	134.6	0.8	357.592	72	210	17	2.3	1.9	$2.7\cdot10^{-10}$	10.5
21214	03-067 15:08:38	1560	3	2	240	15	23	23	14	12	11	0	1	41	1	5	0	1	1	1	6	134.6	0.8	357.593	113	207	-15	2.0	1.9	$1.5\cdot10^{-09}$	10.5
21215	03-069 15:00:00	260	2	3	32	22	22	22	11	8	0	1	1	46	23	5	0	1	1	1	6	134.8	0.8	358.875	45	202	38	2.3	1.9	$1.6\cdot10^{-09}$	10.5
21216	03-069 15:00:00	260	3	2	4	15	26	14	13	15	6	0	1	3	31	5	0	1	1	1	6	134.8	0.8	358.875	84	210	7	2.3	1.9	$1.4\cdot10^{-09}$	10.5
21218	03-264 02:12:38	259	3	2	16	10	21	18	14	13	9	0	1	42	0	5	0	1	1	1	6	150.4	1.0	17.003	68	209	21	2.0	1.9	$4.9\cdot10^{-10}$	10.5
21219	03-264 10:49:32	259	2	2	11	10	4	3	12	1	10	0	0	37	31	5	0	1	1	1	6	150.5	1.0	10.372	75	210	15	4.5	1.9	$2.4\cdot10^{-12}$	10.5
21220	03-264 12:24:22	259	3	4	205	24	27	20	15	10	9	0	1	46	0	5	0	1	1	1	6	150.5	1.0	8.938	162	177	-46	4.9	2.1	$3.9\cdot10^{-10}$	14.3
21222	03-264 14:54:04	8	2	3	188	20	23	6	15	15	15	0	1	20	4	5	0	1	1	1	6	150.5	1.0	6.424	186	148	-50	2.5	1.6	$9.3\cdot10^{-10}$	6.0
21224	03-264 15:01:08	8	3	4	137	28	30	25	12	13	7	0	1	6	1	5	0	1	1	1	6	150.5	1.0	6.295	257	101	-7	2.5	1.6	$9.7\cdot10^{-09}$	6.0
21225	03-264 15:15:18	8	3	3	33	21	26	25	15	8	7	0	1	46	1	5	0	1	1	1	6	150.5	1.0	6.033	44	202	39	7.3	3.9	$5.3\cdot10^{-11}$	128.4
21226	03-264 15:29:27	8	3	3	229	21	24	26	15	15	8	0	1	43	0	5	0	1	1	1	6	150.5	1.0	5.767	128	202	-27	2.5	1.6	$1.3\cdot10^{-09}$	6.0
21229	03-264 15:43:36	8	3	2	16	11	22	21	13	15	8	0	1	41	1	5	0	1	1	1	6	150.5	1.0	5.495	68	209	21	2.3	1.9	$3.7\cdot10^{-10}$	10.5
21230	03-264 16:40:13	8	1	2	254	10	10	3	13	15	15	0	0	13	6	5	0	1	1	1	6	150.5	1.0	4.346	93	210	0	2.3	1.9	$6.7\cdot10^{-11}$	10.5
21231	03-264 17:01:27	8	2	2	31	8	13	11	15	13	15	0	1	13	5	5	0	1	1	1	6	150.5	1.0	3.884	46	203	37	3.9	1.6	$1.1\cdot10^{-11}$	6.0
21232	03-264 17:15:36	8	2	4	135	29	15	25	13	0	7	0	1	17	1	5	0	1	1	1	6	150.5	1.0	3.565	260	101	-5	2.0	1.9	$4.0\cdot10^{-09}$	10.5
21233	03-264 17:15:36	8	3	3	191	22	28	6	15	8	13	0	1	26	1	5	0	1	1	1	6	150.5	1.0	3.565	181	153	-51	7.3	3.9	$9.1\cdot10^{-11}$	128.4
21234	03-264 17:22:41	8	3	2	210	13	14	6	15	9	14	0	1	24	2	5	0	1	1	1	6	150.5	1.0	3.401	155	185	-44	2.0	1.9	$3.9\cdot10^{-10}$	10.5
21235	03-264 17:29:46	8	2	3	250	21	12	5	13	7	13	0	0	46	2	5	0	1	1	1	6	150.5	1.0	3.235	98	210	-4	2.0	1.9	$7.0\cdot10^{-10}$	10.5
21236	03-264 17:29:46	8	3	2	224	14	14	4	13	14	8	0	1	24	2	5	0	1	1	1	6	150.5	1.0	3.235	135	199	-32	2.3	1.9	$2.5\cdot10^{-10}$	10.5
21238	03-264 17:36:50	8	3	4	195	30	57	26	14	15	5	0	1	26	2	5	0	1	1	1	6	150.5	1.0	3.066	176	161	-50	2.0	1.9	$2.4\cdot10^{-07}$	10.5
21239	03-264 17:36:50	8	3	3	237	21	25	12	13	15	12	0	1	26	1	5	0	1	1	1	6	150.5	1.0	3.066	117	206	-19	2.5	1.6	$1.5\cdot10^{-09}$	6.0

No.	IMP. DATE	TEV	CLN	AR	SEC	IA	EA	CA	IT	ET	EIT	EIC	ICC	PA	PET	EVD	ICP	ECP	CCP	PCP	HV	LON	LAT	D_{Jup}	ROT	S_{LON}	S_{LAT}	V	VEF	M	MEF
21240	03-264 17:36:50	8	3	2	166	14	26	5	15	15	14	0	1	25	1	5	0	1	1	1	6	150.5	1.0	3.066	217	117	-38	2.0	1.9	$2.2 \cdot 10^{-09}$	10.5
21241	03-264 17:43:55	8	3	4	241	24	12	12	14	6	6	0	1	49	1	5	0	1	1	1	6	150.5	1.0	2.894	111	208	-14	2.0	1.9	$1.2 \cdot 10^{-09}$	10.5
21242	03-264 17:43:55	8	2	2	246	12	22	5	15	14	15	0	1	18	5	5	0	1	1	1	6	150.5	1.0	2.894	104	209	-8	2.0	1.9	$8.0 \cdot 10^{-10}$	10.5
21243	03-264 17:50:59	8	3	4	186	30	56	25	14	14	7	0	1	26	1	5	0	1	1	1	6	150.5	1.0	2.720	188	144	-50	2.0	1.9	$2.0 \cdot 10^{-07}$	10.5
21244	03-264 17:50:59	8	3	2	33	14	24	8	14	12	13	0	1	13	10	5	0	1	1	1	6	150.5	1.0	2.720	44	202	39	2.0	1.9	$1.6 \cdot 10^{-09}$	10.5
21246	03-264 17:59:01	22	3	2	239	9	22	5	14	12	13	0	1	37	8	5	0	1	1	1	6	150.5	1.0	2.518	114	207	-16	2.0	1.9	$4.9 \cdot 10^{-10}$	10.5
21248	03-264 17:59:01	22	3	4	4	24	28	25	15	10	5	0	1	46	14	5	0	1	1	1	6	150.5	1.0	2.518	84	210	7	4.9	2.1	$4.6 \cdot 10^{-10}$	14.3
21249	03-264 17:59:01	22	3	3	44	21	22	5	13	14	8	0	1	49	6	5	0	1	1	1	6	150.5	1.0	2.518	28	191	49	2.0	1.9	$2.4 \cdot 10^{-09}$	10.5
21250	03-264 17:59:01	22	3	4	172	27	11	18	9	3	10	0	1	27	2	5	0	1	1	1	6	150.5	1.0	2.518	208	123	-42	7.2	1.9	$1.9 \cdot 10^{-11}$	10.5

Table 6: Slopes α of power law fits to the measured dust flux profiles and Io's dust production.

Orbit	Distance (R_J)	Time interval	α	Dust Production ($kg\,s^{-1}$)
G1	48 – 15	96-175 to 96-179	–1.9	0.1 – 2
G2	128 – 20	96-214 to 96-250	–4.3	0.2 – 5
C3	113 – 20	96-284 to 96-310	–1.9	0.2 – 10
E4	49 – 20	96-349 to 96-352	–0.7	3 – 20
E6	38 – 15	97-048 to 97-051	–1.6	0.01 – 0.07
G7	59 – 20	97-087 to 97-093	–3.5	0.1 – 5
G8	48 – 20	97-123 to 97-127	–5.4	0.2 – 3
C9	50 – 20	97-173 to 97-177	–2.0	0.07 – 1
C10	55 – 20	97-256 to 97-260	–1.7	0.1 – 5
E11	57 – 20	97-304 to 97-309	–3.7	0.1 – 1
E12	50 – 20	97-344 to 97-348	–2.1	0.05 – 0.7
E14	48 – 20	98-083 to 98-087	–6.1	0.05 – 0.3
E16	39 – 20	98-198 to 98-200	–7.3	0.01 – 0.5
E17	44 – 20	98-265 to 98-268	–1.4	0.05 – 0.5
E18	47 – 33	98-321 to 98-323	–5.6	0.05 – 0.5
E19	48 – 20	99-027 to 99-030	–0.6	0.05 – 0.5
E26	15 – 30	00-005 to 00-006	–5.3	0.01 – 0.05
G28	22 – 167	00-143 to 00-168	–1.8	0.1 – 3
G28	270 – 290	00-227 to 00-252	–	10 – 1000
G29	290 – 172	00-253 to 00-335	+10.4	0.1 – 500
G29	20 – 216	01-365 to 01-070	–2.1	0.01 – 1
I32	22 – 93	01-290 to 01-300	+0.2	0.005 – 0.5
I33	61 – 348	02-023 to 02-164	–1.1	0.05 – 5
A34	348 – 22	02-164 to 02-308	–0.4	0.05 – 1

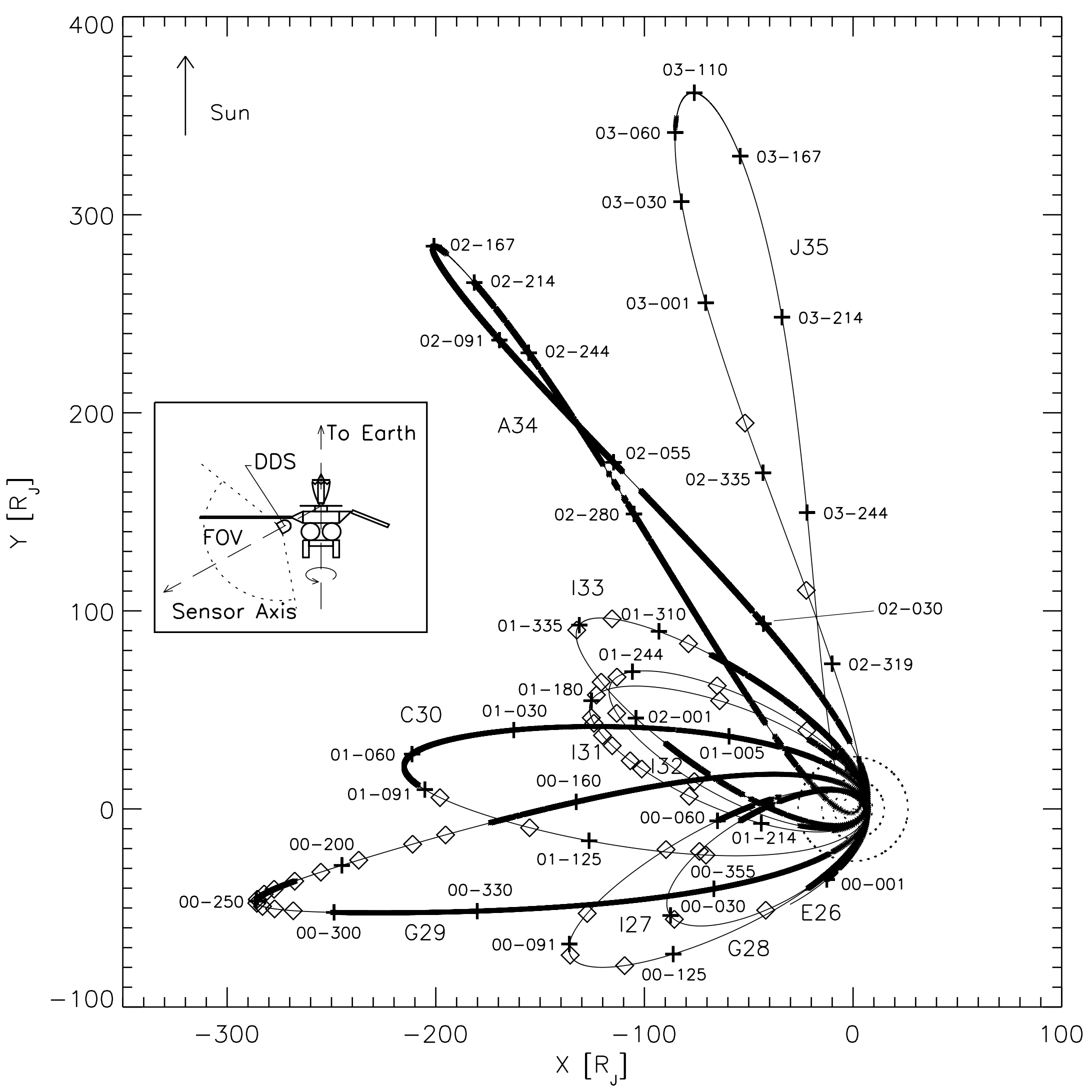

Figure 1: Galileo's trajectory in the jovian system from 2000 to 2003 in a Jupiter-centric coordinate system (thin solid line). Crosses mark the spacecraft position at approximately 30 day intervals (days of year are indicated). Periods when RTS data were obtained are shown as thick solid lines, MROs are marked by diamonds. Galileo's orbits are labelled 'E26', 'I27', 'G28', 'G29', 'C30', 'I31', 'I32', 'I33', 'A34' and 'J35'. Sun direction is to the top and the Sun and Earth directions coincide to within 10°. The orbits of the Galilean moons are indicated (dotted lines). The sketch of the Galileo spacecraft shows the dust detector (DDS), its geometry of dust detection and its field-of-view (FOV). The spacecraft antenna usually pointed towards Earth and the spacecraft made about 3 revolutions per minute.

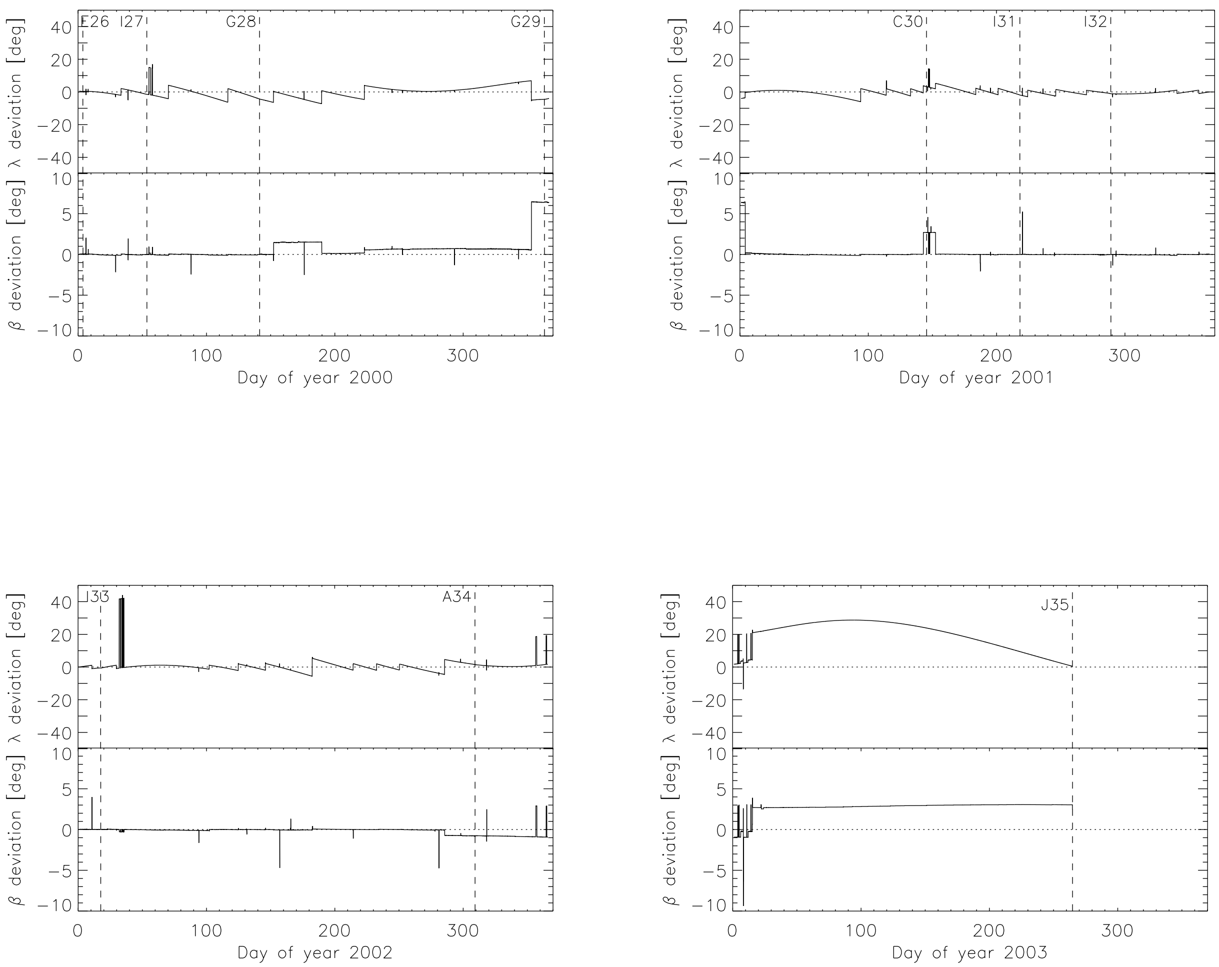

Figure 2: Spacecraft attitude: deviation of the antenna pointing direction (i. e. negative spin axis) from the Earth direction. The angles are given in ecliptic longitude (λ) and latitude (β, equinox 1950.0). Dashed vertical lines indicate satellite flybys (E26-A34) or Galileo's Jupiter impact (J35). Sharp spikes are associated with imaging observations with Galileo's cameras or orbit trim maneuvers with the spacecraft thrusters.

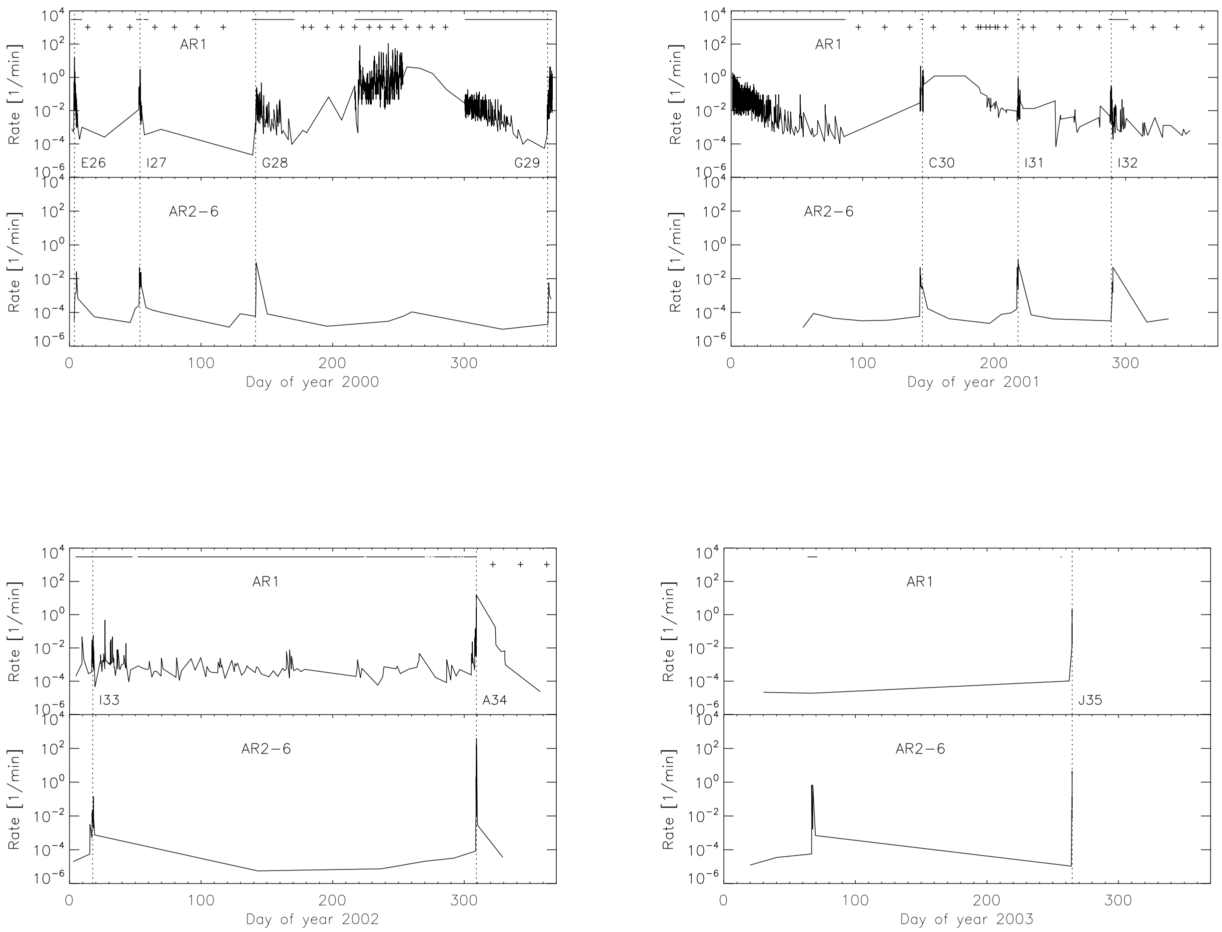

Figure 3: Dust impact rate detected in 2000-2003. For each year the top panel shows the impact rate in AR1 and the bottom panel that for the higher amplitude ranges AR2-6. Only data for classes 2 and 3 are shown. Dotted lines indicate satellite flybys (E26-A34) or Galileo's Jupiter impact (J35). Perijove passages occurred within two days of the moon closest approaches. These curves are plotted from the number of impacts with the highest time resolution which is available only in electronic form. No smoothing was applied to the data. In the top panels (AR1), time intervals with continuous RTS coverage are indicated by horizontal bars, memory readouts (MROs) are marked by crosses.

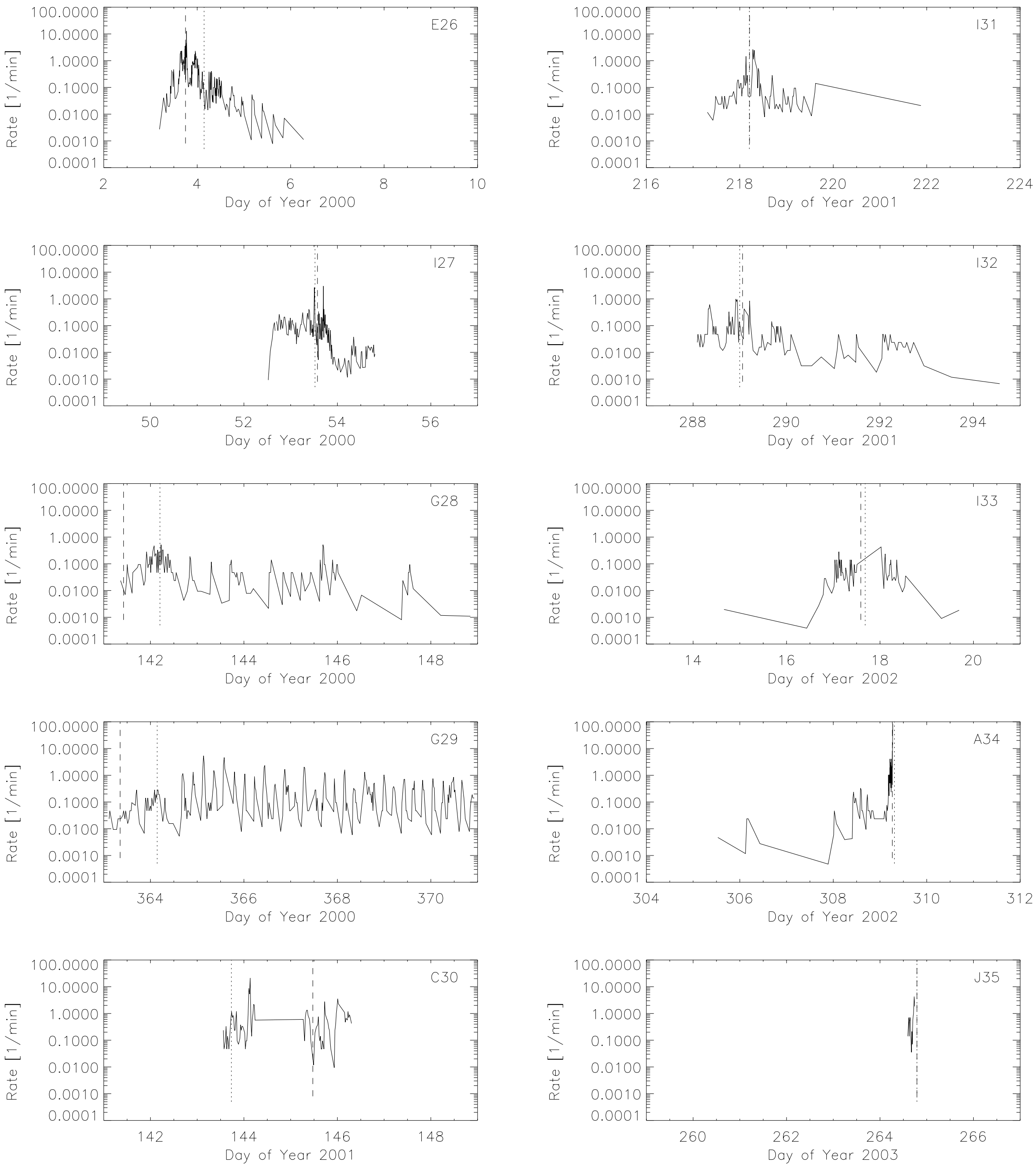

Figure 4: Dust impact rate detected in the inner jovian system in higher time resolution. An 8-day interval is shown in each panel. Only data for AR1 (classes 2 and 3) are shown. Dotted lines indicate perijove passages of Galileo, dashed lines satellite closest approaches (E26-A34) or Jupiter impact (J35).

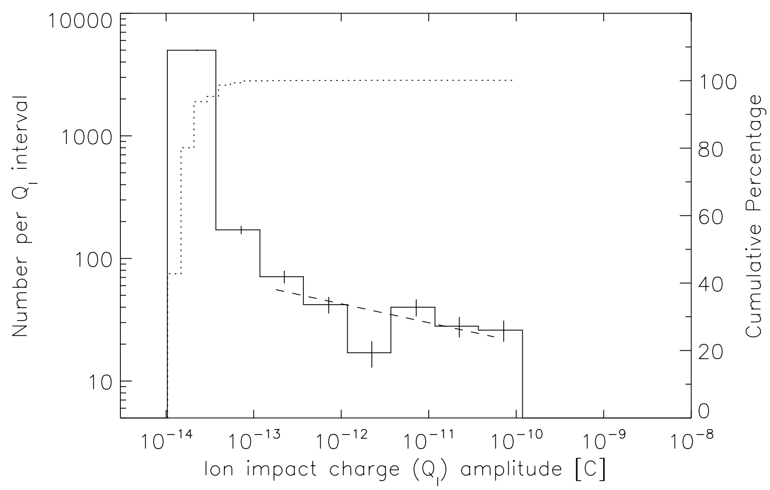

Figure 5: Amplitude distribution of the impact charge $Q_{\rm I}$ for the 5389 dust particles detected in 2000-2003. The solid line indicates the number of impacts per charge interval, whereas the dotted line shows the cumulative distribution. Vertical bars indicate the $\sqrt{n}$ statistical fluctuation. A power law fit to the data with $Q_{\rm I} > 10^{-13}\,{\rm C}$ (big particles, AR2-4) is shown as a dashed line (Number $N \sim Q_{\rm I}^{-0.15}$).

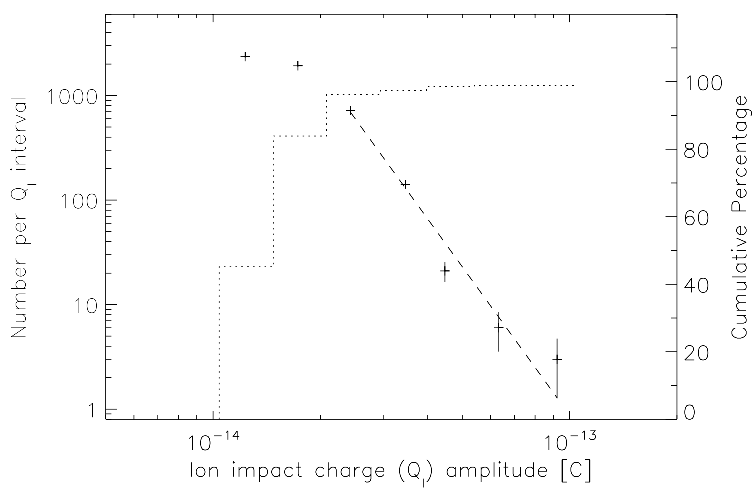

Figure 6: Same as Figure 5 but for the 5165 small particles in the lowest amplitude range (AR1) only. A power law fit to the data with $2 \times 10^{-14}\,{\rm C} < {\rm Q_I} < 10^{-13}\,{\rm C}$ is shown as a dashed line (Number $N \sim Q_{\rm I}^{-4.72}$).

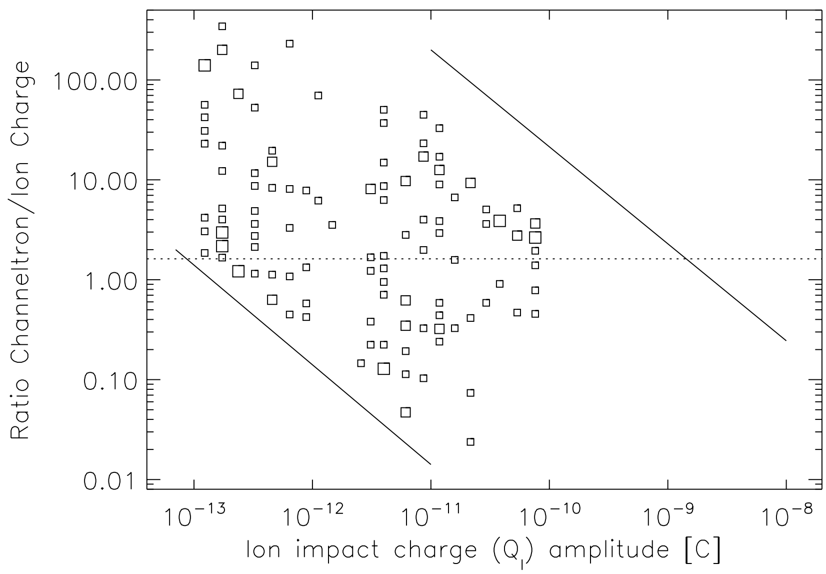

Figure 7: Channeltron amplification factor $A = Q_C/Q_I$ as a function of impact charge Q_I for big particles (AR2-6) detected in 2000-2003. Only impacts measured with a channeltron high voltage setting HV $= 6$ are shown. The solid lines indicate the sensitivity threshold (lower left) and the saturation limit (upper right) of the channeltron. Squares indicate dust particle impacts, and the area of the squares is proportional to the number of events (the scaling of the squares is the same as in Papers VI and VIII). The dotted horizontal line shows the mean value of the channeltron amplification $A = 1.62$ calculated from 65 impacts in the ion impact charge range 10^{-12} C $< Q_I < 10^{-10}$ C.

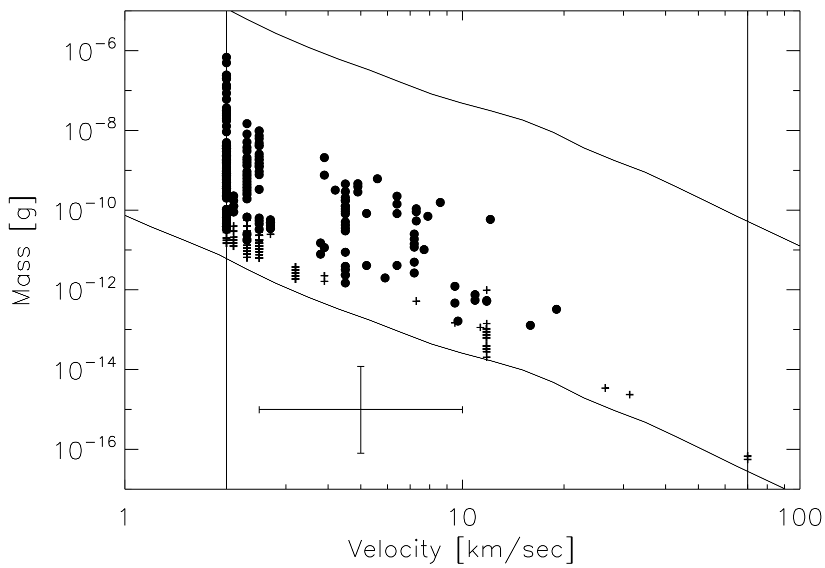

Figure 8: Masses and impact speeds of all 5389 impacts recorded in 2000-2003. The lower and upper solid lines indicate the threshold and saturation limits of the detector, respectively, and the vertical lines indicate the calibrated velocity range. A sample error bar is shown that indicates a factor of 2 error for the velocity and a factor of 10 for the mass determination. Note that all particles are most likely much faster and smaller than implied by this diagram (see text for details). Plus signs show particles in AR1 while filled circles refer to particles in AR2-4. No impacts were measured in AR5 or AR6.

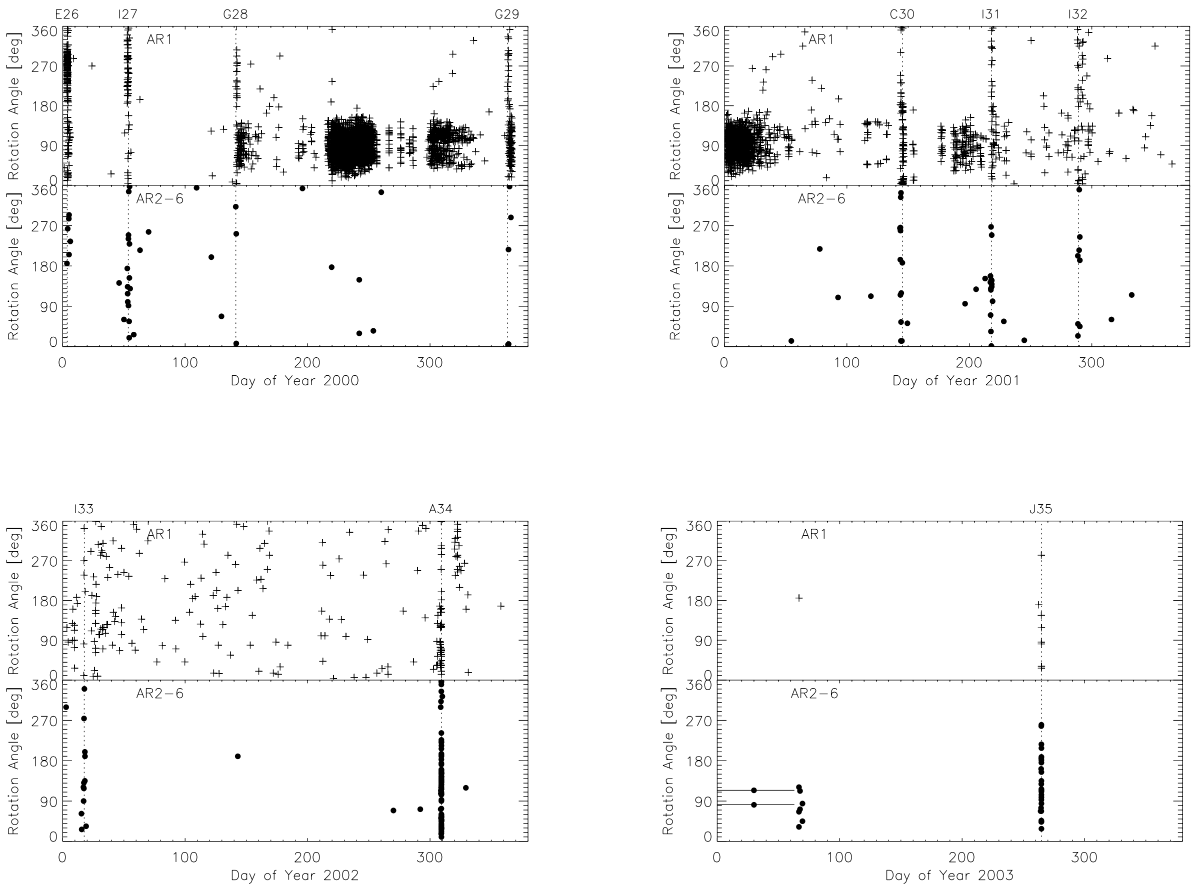

Figure 9: Rotation angle vs. time for two different mass ranges. Upper panel: small particles, AR1; lower panel: big particles, AR2-4. See Section 2 for an explanation of the rotation angle. Vertical dotted lines indicate Galileo's satellite encounters (E26-A34) or the spacecraft impact into Jupiter (J35). No impacts were measured in AR5 or AR6. The uncertainty in the determination of the impact time is usually much smaller than the symbol sizes, except for two impacts in 2003 which have a very large uncertainty (indicated by two horizontal bars).

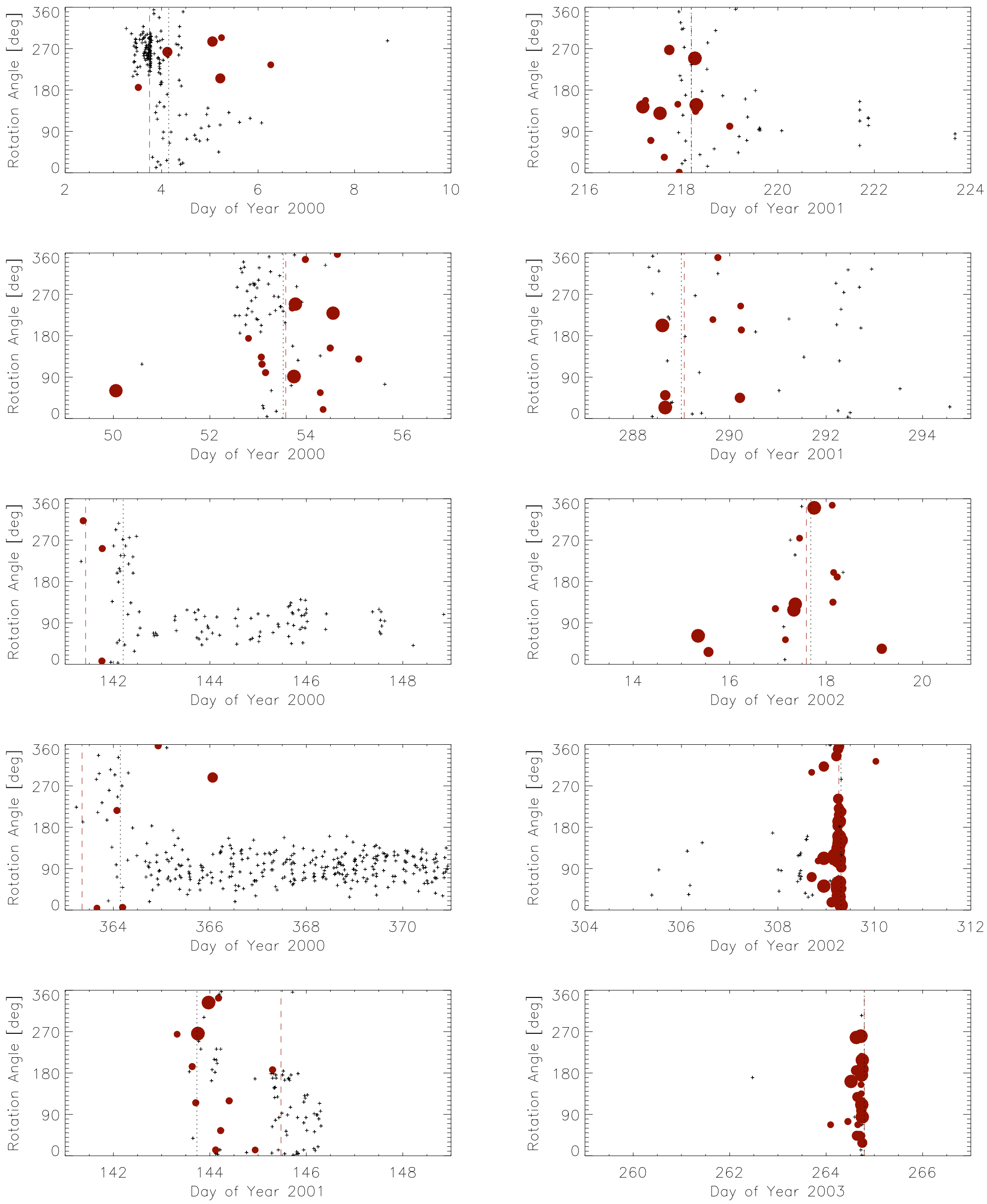

Figure 10: Rotation angle detected by the dust instrument in the inner jovian system in higher time resolution. Only dust data for classes 2 and 3 are shown. Crosses denote impacts in AR1, filled circles those in AR2-4, with the circle size indicating the amplitude range. Dotted lines indicate perijove passages of Galileo, dashed lines satellite closest approaches (E26-A34) or Jupiter impact (J35).

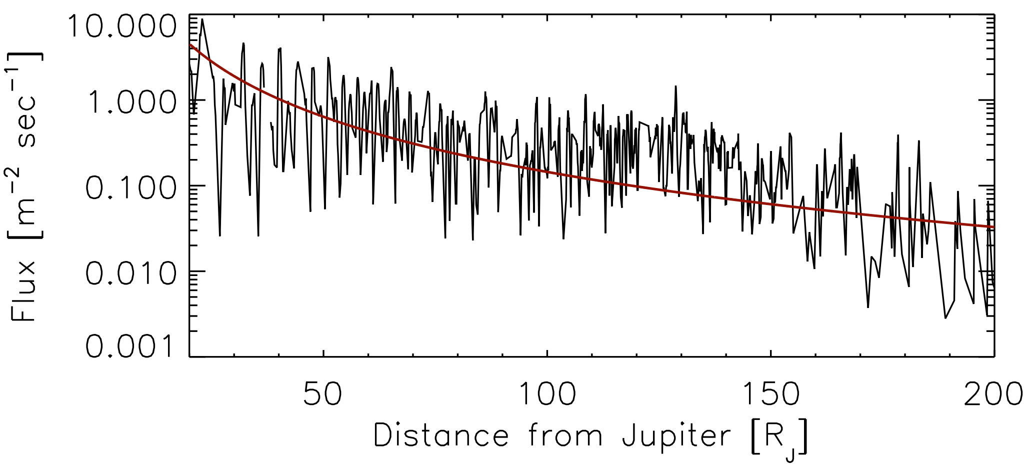

Figure 11: Dust flux measured during Galileo's G29 orbit. The data were smoothed with a 2-hour boxcar average. A power law fit with slope −2.14 is shown. See text for details.

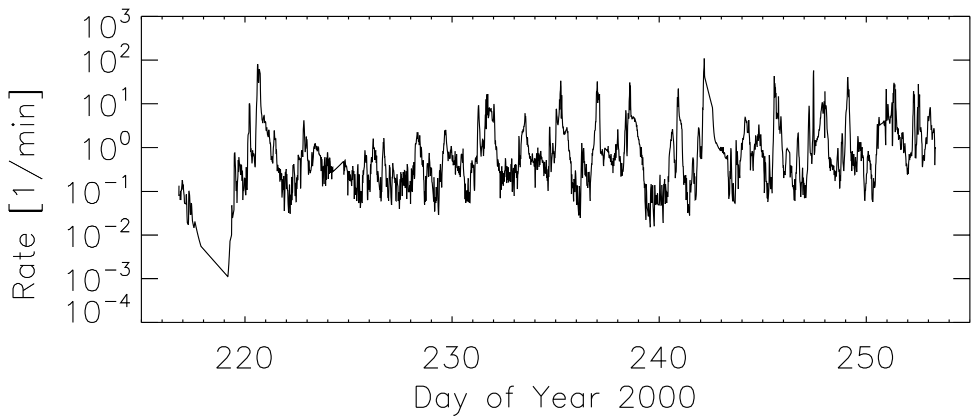

Figure 12: Impact rate of jovian dust stream particles (AC21 and AC31) measured during Galileo's G28 orbit at approximately 280 R_J from Jupiter (no smoothing applied).

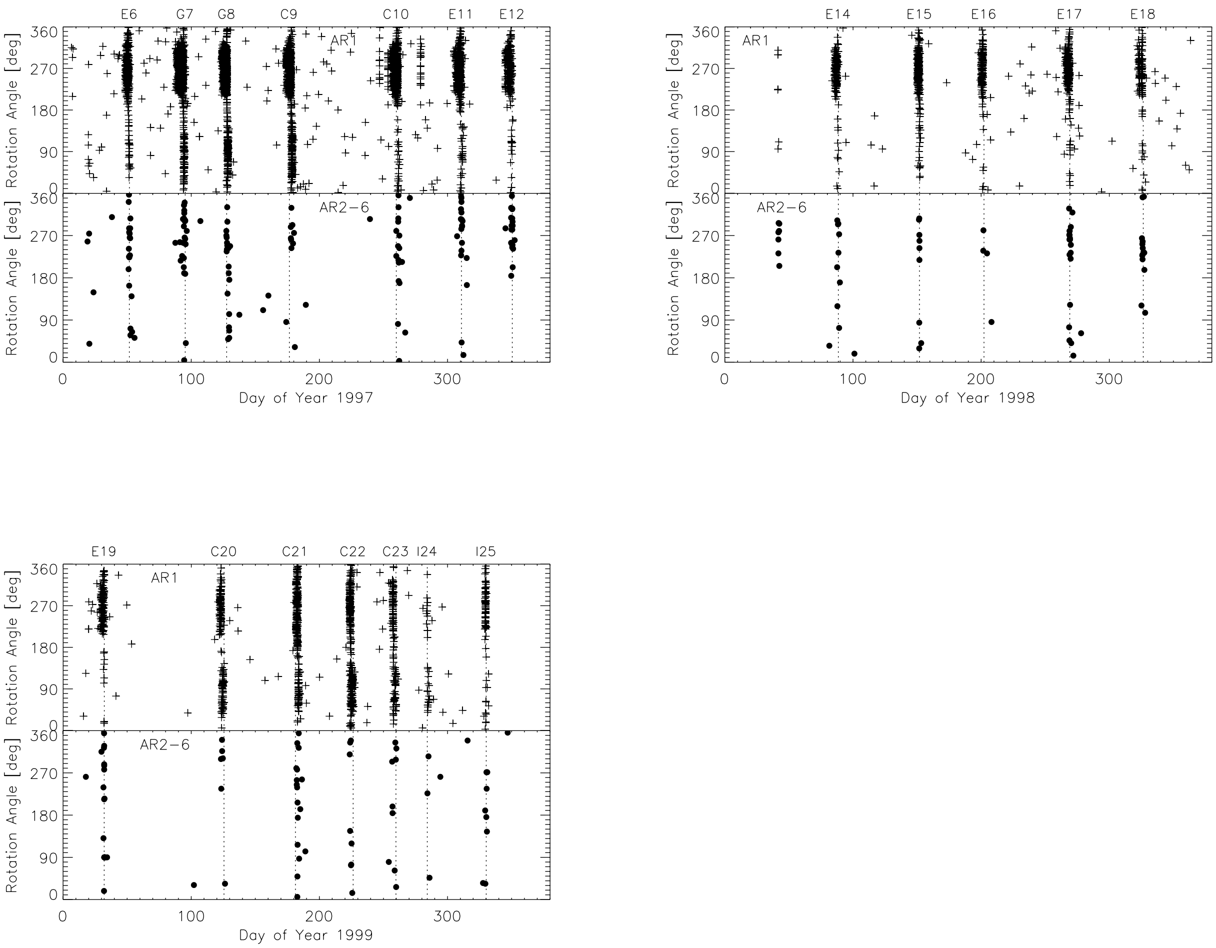

Figure 13: Correction for Paper VIII: rotation angle vs. time for two different mass ranges for the time interval 1997-1999. Upper panel: small particles, AR1 (Io dust stream particles); lower panel: big particles, AR2-4. Vertical dotted lines indicate Galileo's satellite encounters.